

A model of the pressure dependence of the  
enantioselectivity of *Candida rugosa* lipase  
towards ( $\pm$ )-menthol

Entwicklung eines Modells zur Druckabhängigkeit  
der Enantioselektivität der *Candida rugosa* Lipase  
gegenüber ( $\pm$ )-Menthol

VON DER FAKULTÄT GEO- UND BIOWISSENSCHAFTEN DER UNIVERSITÄT  
STUTTGART ZUR ERLANGUNG DER WÜRDE EINES DOKTORS DER  
NATURWISSENSCHAFTEN (DR. RER. NAT.) GENEHMIGTE ABHANDLUNG

VORGELEGT VON

**ULRICH KAHLOW**

AUS MÜNCHEN

HAUPTBERICHTER: PROF. DR. ROLF D. SCHMID

MITBERICHTER: PROF. ROBIN GHOSH

TAG DER MÜNDLICHEN PRÜFUNG: 27.02.2002

2002

INSTITUT FÜR TECHNISCHE BIOCHEMIE DER UNIVERSITÄT STUTTGART

Hiermit versichere ich, daß ich die Arbeit selbstständig verfaßt und keine anderen als die angegebenen Quellen und Hilfsmittel verwandt habe.

Even if there is only one possible unified theory, it is just a set of rules and equations. What is it that breathes fire into the equations and makes a universe for them to describe? The usual approach of science of constructing a mathematical model cannot answer the questions of why there should be a universe for the model to describe. Why does the universe go to all the bother of existing?

Stephen W. Hawking, *A Brief History of Time: From the Big Bang to Black Holes*,  
Bantam, NY, 1988, p 174

**DANKSAGUNG**

Prof. Rolf D. Schmid danke ich für die Überlassung des Themas, die anregenden Diskussionen und die großzügige Förderung meiner Arbeit.

Prof. Dr. Uwe T. Bornscheuer und Dr. habil. Jürgen Pleiss danke ich für die ausgezeichnete Betreuung während der vergangenen Jahre.

Herrn Prof. Ghosh danke ich für die Durchsicht und Begutachtung dieser Arbeit.

Dr. Holger Scheib gilt mein besonderer Dank für die anregenden Diskussionen und seine andauernde Hilfe - auch während der sogenannten schlechteren Zeiten.

Den Arbeitsgruppenleitern Genetik, Dr. Jutta Schmitt, und Fermentation, Dipl.-Ing. (FH) Gaby Neumann, danke ich für die hervorragende Betreuung meiner Experimente in den jeweiligen Labors.

Besonderer Dank an folgende Mitarbeiter für ihre ständige Unterstützung und immer währende Hilfe: Markus Fischer, Christian Gentner, Petra Traub, Ulrike Schmid, Markus Enzelberger, Frank Zocher, Sandra Vorlová, Erik Henke, Stefan Minning.

Allen ehemaligen und jetzigen Mitgliedern der Bioinformatik-Gruppe und der Biokatalyse-Gruppe danke ich für das tolle und menschliche Klima, bei der Arbeit und nach Dienstschluß.

Allen Mitarbeitern des ITB gilt mein Dank für die schöne und produktive Zeit der vergangenen Jahre.

Im Besonderen möchte ich mich bei Frau Erika Denzel aus dem Arbeitskreis von Dipl. Ing. Nils Langer an dem Institut für Lebensmitteltechnologie der Universität Hohenheim für die Bestimmung des Wassergehaltes der kommerziell erhältlichen Lipasepräparation aus *Candida rugosa* bedanken.

Diese Arbeit wurde durch das BMBF unterstützt.

Einen ganz persönlichen Dank an die Menschen, die mich während der ganzen Jahre unterstützt und als Freund wertgeschätzt haben.

Meiner Familie danke ich von ganzem Herzen für den Respekt für meine Entscheidung, Ihre Unterstützung, unermüdliche Hilfe und Liebe.



## Abstract

Transesterification of ( $\pm$ )-menthol using propionic acid anhydride and *Candida rugosa* lipase was performed in chloroform and water at different pressures (1, 10, 50, and 100 bar) to study the pressure dependence of enantioselectivity  $E$ . As a result,  $E$  significantly decreased with increasing pressure from  $E=55$  (1 bar) to  $E=47$  (10 bar),  $E=37$  (50 bar), and  $E=9$  (100 bar).

In order to rationalize the experimental findings, molecular dynamics simulations of *Candida rugosa* lipase were carried out. Analyzing the lipase geometry at 1, 10, 50, and 100 bar revealed a cavity in the *Candida rugosa* lipase. The cavity leads from a position on the surface distinct from the substrate binding site to the core towards the active site and is limited by F415 and the catalytic H449. In the crystal structure of the *Candida rugosa* lipase, this cavity is filled with 6 water molecules. The number of water molecules in this cavity gradually increased with increasing pressure: 6 molecules in the simulation at 1 bar, 10 molecules at 10 bar, 12 molecules at 50 bar, and 13 molecules at 100 bar. Likewise, the volume of the cavity progressively increased from about 1864 Å<sup>3</sup> in the simulation at 1 bar to 2529 Å<sup>3</sup> at 10 bar, 2526 Å<sup>3</sup> at 50 bar, and 2617 Å<sup>3</sup> at 100 bar. At 100 bar, one water molecule slipped between F415 and H449, displacing the catalytic histidine side chain and thus opening the cavity to form a continuous water channel. The rotation of the side chain leads to a decreased distance between the H449-N $\epsilon$  and the (+)-menthyl-alcohol-oxygen (non-preferred enantiomer) in the acyl enzyme intermediate, a factor determining the enantioselectivity of the lipase.

While the geometry of the preferred enantiomer is similar in all simulations, the geometry of the non-preferred enantiomer gets gradually more reactive. This observation correlates with the gradually decreasing enantioselectivity  $E$ .

## ZUSAMMENFASSUNG

### Zielsetzung

Gegenstand dieser Arbeit war die Untersuchung der Druckabhängigkeit der Enantioselektivität der lipase-katalysierten Trennung racemischen Menthols. Als biologischer Katalysator wurde die Lipase aus *Candida rugosa* verwendet. Während in einem biokatalytischen Teil eine mit steigendem Druck abnehmende Enantioselektivität  $E$  beobachtet wurde, konnte hierzu in einem zweiten computergestützten Teil ein Modell dieser Druckabhängigkeit erarbeitet werden.

### Biokatalytische Untersuchung

(-)-Menthol ist ein industriell sehr wichtiger Geruchsstoff. Ursprünglich aus dem Öl der *Mentha arvensis* extrahiert, wird er heute zum größten Teil auf chemischem Wege hergestellt. Für die enantiomerenreine Darstellung von (-)-Menthol entwickelte z.B. Haarmann & Reimer, der Marktführer für (-)-Menthol, einen chemischen Prozeß, der besonders durch seine Trennung der Enantiomeren besticht (siehe Abbildung 1).

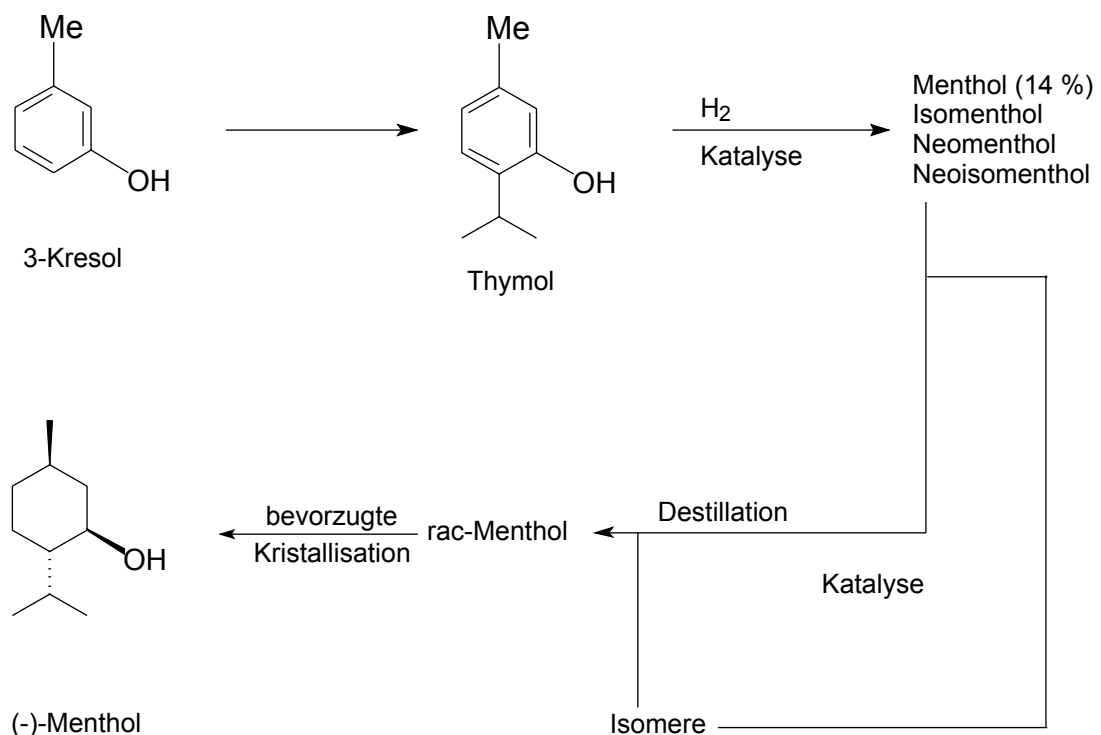


Abbildung 1 Darstellung enantiomerenreinen (-)-Menthols.

Bei diesem Prozeß wird die Trennung des ( $\pm$ )-Menthols über die bevorzugte Kristallisation der Diastereomeren von Menthylbenzoat erreicht. Dies wird erst dann möglich, wenn zu dem Medium kleine Mengen reiner Kristalle der entsprechenden Diastereomeren als Kristallisationskeime zugefügt werden. Takasago, nach Haarmann & Reimer der zweitgrößte Produzent von (-)-Menthol, geht von Myrcen aus und verfolgt eine Syntheseroute über Diethylgeranylamin, Zitronellalenamin und Zitronellal, um schließlich zu (-)-Menthol zu gelangen.

Die Verwendung biologischer Katalysatoren eröffnet neben der recht aufwendigen chemischen Trennung zusätzliche Möglichkeiten der Enantiomerentrennung. Im Falle von Lipasen (E.C. 3.1.1.3), einer Klasse hydrolytischer Enzyme, ergeben sich mehrere enzymatische Reaktionen zur Trennung der Mentholenantiomere (siehe Figure 3, Seite 4), die in der Literatur beschrieben sind. Grundsätzlich stehen hierzu drei mögliche Wege zur Verfügung:

- Hydrolyse eines Esters
- Synthese eines Esters
- Esterübertragung auf eine Säure

Zur Untersuchung der Enantioselektivität der lipase-katalysierten Trennung racemischen Menthols wurde als Beispielreaktion die Veresterung von (-)-Menthol mit Propionsäureanhydrid gewählt, da diese Reaktion in Screeningversuchen die besten Werte der Enantioselektivität bzw. die höchste Reaktionsgeschwindigkeit zeigte. Bei der Veresterung von Menthol mit Propionsäureanhydrid entsteht zunächst Propionsäure (siehe Abbildung 2) und schließlich Wasser (siehe Abbildung 3). Das Anhydrid lag in leichtem Überschuß (Menthol:Propionsäureanhydrid = 1:1.2) vor.

Für die Untersuchung der Veresterung von Menthol mit Propionsäureanhydrid wurde folgender Versuchsansatz gewählt:

- 100 mg Menthol (156,27 g/mol; 640  $\mu$ mol)
- 100 mg Propionsäureanhydrid (130,14 g/mol; 768 mol)
- 500 mg Lipase Amano AY
- 10 ml Chloroform
- kleine Magnetrührfische

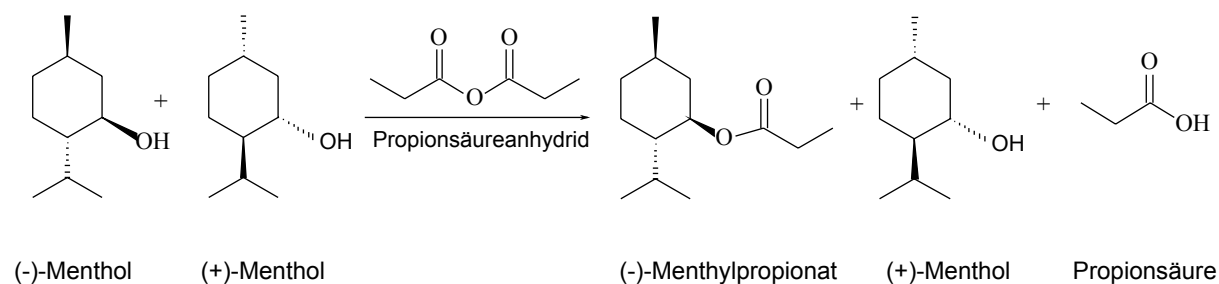


Abbildung 2 Veresterung racemischen Menthols. In der Grundreaktion entsteht neben (+)-Menthol und Propionsäure (-)-Menthylpropionat.

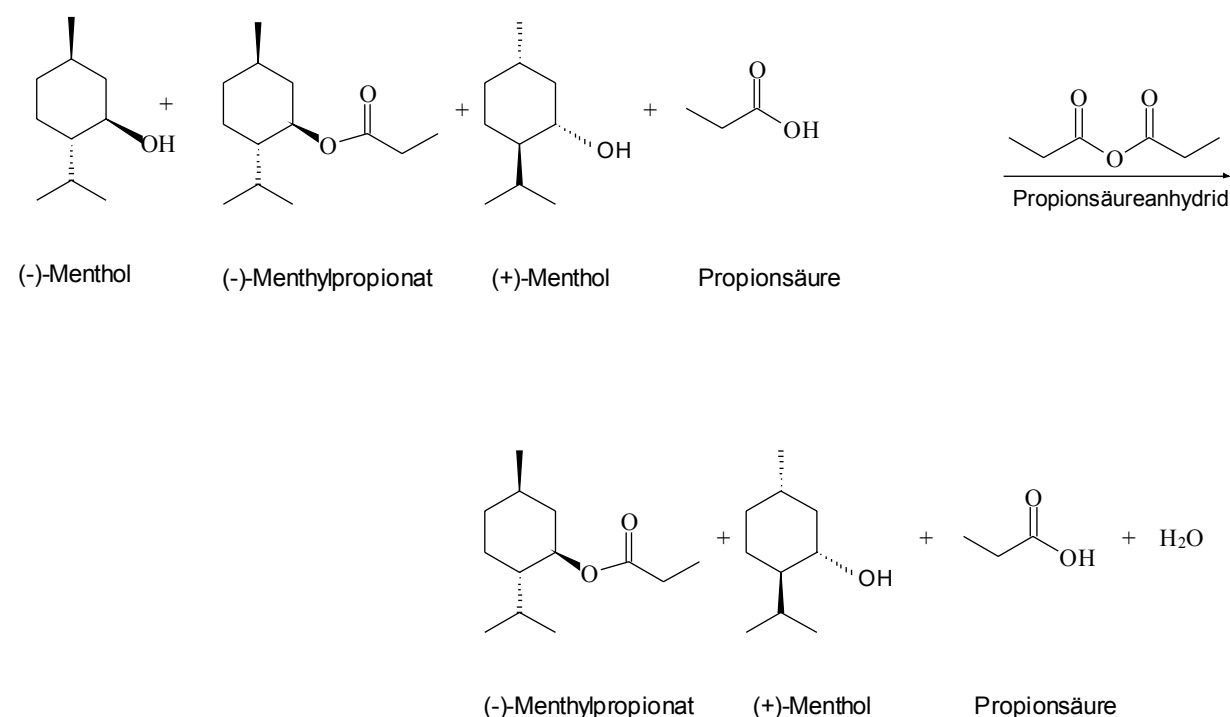


Abbildung 3 Veresterung von Menthol. In einer Nebenreaktion wird Wasser bei der Veresterung von (-)-Menthol mit Propionsäure gebildet.

Die lipase-katalysierte Trennung racemischen Menthols mit Propionsäureanhydrid wurde im Labor bei verschiedenen Drücken (1 bar, 10 bar, 50 bar, 100 bar) durchgeführt. Der Druck wurde über eine Kolbenpumpe aufgebaut, die üblicherweise zur Extraktion von Bodenproben mittels überkritischem CO<sub>2</sub> genutzt wird.

Die Reaktionskomponenten wurden jeweils vor Versuchsbeginn in der Probenkammer homogen gelöst (siehe Abbildung 4). Bei geschlossenem Einlaßventil wurde in der Kolbenpumpe der Druck (1 bar, 10 bar, 50 bar, 100 bar) aufgebaut. Anschließend wurde bei geschlossenem Auslaßventil das Einlaßventil

geöffnet und die Probe entsprechend unter Druck gesetzt. Die Regelung der Temperatur erfolgte über ein Wasserbad, in welchem sich die Probenkammer befand. Das Wasserbad wurde zusätzlich mit 300 rpm geschüttelt.

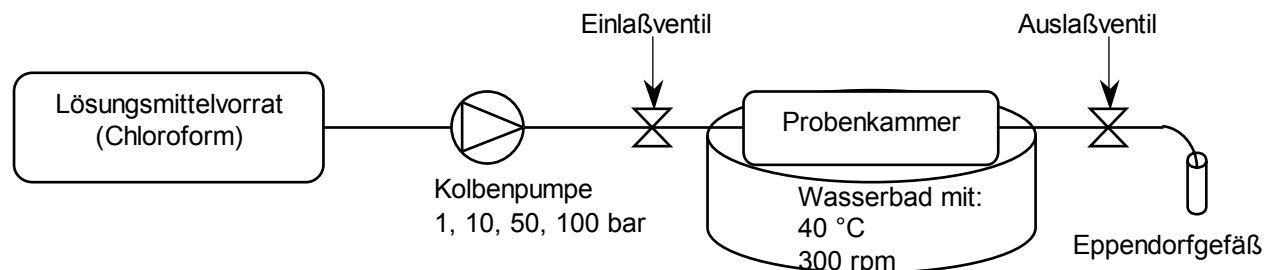


Abbildung 4 Schematischer Versuchsaufbau der Veresterung racemischen Menthols mit Propionsäureanhydrid.

Um systematische Druckverluste auszugleichen, wurde das Einlaßventil während des Versuches nicht geschlossen, so daß isobare Versuchsbedingungen gegeben waren.

Als Ergebnis wurde eine Druckabhängigkeit der Enantioselektivität der lipase-katalysierten Trennung racemischen Menthols festgestellt und quantifiziert (siehe Tabelle 1).

Zeit [h]	Druck [bar]	Umsatz [%]	Enantioselektivität E	Standardabweichung $\sigma$
24	1	28	55	1.5
24	10	20	47	2.1
48	50	24	37	1.5
48	100	15	9	0.4

Tabelle 1 Druckabhängigkeit der Enantioselektivität der lipase-katalysierten Trennung racemischen Menthols.

*Computerunterstützte Untersuchung*

In einem zweiten Teil wurde ein Modell zur beobachteten Druckabhängigkeit der lipase-katalysierten Trennung racemischen Menthols erarbeitet. Hierzu wurde die offene Form der Lipase aus *Candida rugosa*, deren Raumstruktur bereits ermittelt wurde, benutzt (pdb-Eintrag 1LPM; siehe Anhang 8.1). Um die Experimente des biokatalytischen Teiles dieser Arbeit möglichst exakt auf dem Computer abzubilden, wurden molekular-dynamische (MD) Simulationen der Lipase bei 1 bar Umgebungsdruck sowohl in Wasser als auch in Chloroform durchgeführt (siehe Abbildung 5). Zusätzlich wurde bei der Simulation der Lipase in Chloroform der Umgebungsdruck von 1 bar auf 10 bar, 50 bar und zuletzt 100 bar erhöht.

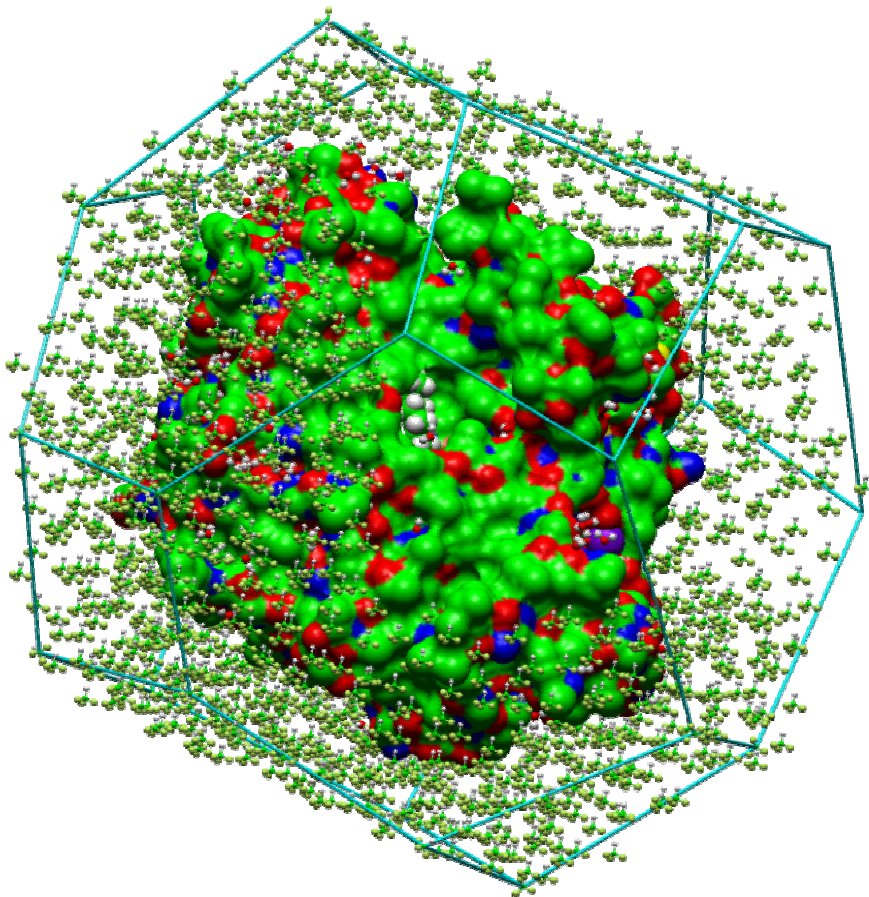


Abbildung 5 Simulationseinheit der Lipase aus *Candida rugosa* in Chloroform mit Kristallwasser und Ionen. Der Inhibitor ist in CPK dargestellt, die Lipase selbst als molekulare Oberfläche, Kristallwasser und Chloroform als "Balls-and-Sticks". Die Lipase befindet sich in einer sog. "truncated octahedral box".

Die Simulationen wurden mit dem Computerprogrammpaket GROMOS96 durchgeführt. Grundsätzlich wurden die MD-Simulationen in sog. „truncated octahedral boxes“ berechnet (siehe Abbildung 5). Diese Boxen wurden dann mit dem Lösungsmittel (Wasser bzw. Chloroform) gefüllt. Die Befüllung einer Simulationsbox geschah über wiederholtes Einfügen vorberechneter und equilibrierter Boxen des gewünschten Lösungsmittels, die jeweils 216 Moleküle enthielten. Der an seinen Ecken abgeschnittene Oktaeder ähnelt geometrisch einer Kugel und ist derart gestaltet, daß er eine nur relative dünne Lösungsmittelschicht kugelförmig um das Molekül herum zuläßt, aber trotzdem, und dies steht im Gegensatz zu einer Kugel, ohne entstehende Zwischenräume aneinandergelegt werden kann. So können diese Boxen virtuell im Raum vervielfacht werden, obwohl nur die Atome innerhalb einer Box berechnet werden müssen. Damit verringert sich erstens der Rechenaufwand für ein einzelnes Molekül erheblich und des weiteren wird so eben nicht nur ein Molekül berechnet, sondern eine Lösung des Moleküls simuliert.

Die komplette Simulationszelle bestand nun aus den folgenden Teilen:

- 1 Molekül Lipase (CRL)
- 244 Moleküle Kristallwasser
- 17 Natrium-Ionen
- 2289 Moleküle Chloroform

Nachdem das System bei 1 bar Umgebungsdruck equilibriert war, wurde in der Simulation mit Chloroform als Lösungsmittel schrittweise der Simulationsdruck erhöht. Dazu wurden die jeweils ersten 50 ps der Simulation bei einem gegebenen Druck zur Equilibrierung des Systems genutzt. Anschließend daran wurde sowohl die Simulation bei diesem Druck fortgeführt, als auch in einer neuen molekulardynamischen Simulation der Druck auf die nächste Stufe erhöht, so daß zuletzt dasselbe System 400 ps bei 1 bar, 350 ps bei 10 bar, 300 ps bei 50 bar und 250 ps bei 100 bar simuliert wurde.

Zur Auswertung der molekulardynamischen Simulationen wurden aus den jeweils letzten 50 ps bei den vier verschiedenen Drücken mittlere Strukturen gebildet. In diese wurde jeweils der tetrahedrale Übergangszustand des (+)- bzw. (-)-Menthylesters in das aktive Zentrum der Lipase gedockt und nach einer Energieminimierung geometrisch ausgewertet. Dabei ergab sich eine

Druckabhängigkeit des Abstandes zwischen dem Substratester-Alkohol-Sauerstoff-Atom und dem  $\epsilon$ -Stickstoffatom des Histidin449 im aktiven Zentrum (siehe Tabelle 2).

Simulierter Druck [bar]	Abstand zwischen His449-N $\epsilon$ und (-)-Menthyl-Alkohol-O [ $\text{\AA}$ ]	(+)-Menthyl- Alkohol-O [ $\text{\AA}$ ]	Differenz der Abstände [ $\text{\AA}$ ]
1	3.0	4.6	1.6
10	2.9	4.5	1.6
50	2.9	3.9	1.0
100	2.6	3.3	0.7

Tabelle 2 Geometrische Auswertung der mit dem tetrahedralen Übergangszustand des (+)- bzw. (-)-Menthylesters gedockten und energieminierten mittleren Strukturen bei 1 bar, 10 bar, 50 bar und 100 bar.

Der Abstand zwischen dem  $\epsilon$ -Stickstoffatom des Histidin449 und dem Alkoholsauerstoffatom des (-)-Menthol ändert sich kaum mit zunehmendem Druck, während der entsprechende Abstand für das (+)-Menthol beträchtlich abnimmt (siehe Tabelle 2). Gerade dieser Abstand aber ist essentiell für den reibungslosen Ablauf des Mechanismus der katalytischen Triade (siehe Figure 54, Seite 99).

Außerdem richtet sich zwischen 10 bar und 50 bar schlagartig die Geometrie der Esterbindung des ersten tetrahedralen Übergangszustandes für den (+)-Menthylester in Richtung des katalytisch aktiven Histidins H449 aus, so daß das Estersauerstoffatom im gebundenen (+)-Menthylester ab einem Druck von 50 bar genau so ausgerichtet ist, wie im gebundenen (-)-Menthylester (siehe Table 15 und Figure 57 bis Figure 60, Seiten 106, 107).

Für die Umsetzung von (+)-Menthol, dem langsamer reagierenden Enantiomer, mit der Lipase aus *Candida rugosa* bei 1 bar Umgebungsdruck wurde von Kazlauskas et al. eine Verdrehung des Imidazolringes des Histidin449 um  $60^\circ$  gefunden (siehe Figure 8, Seite 12). Diese Verdrehung bewirkt zum Einen eine deutliche Vergrößerung des Abstandes zwischen dem  $\epsilon$ -Stickstoffatom des Histidin449 und dem Sauerstoffatom des (+)-Menthol und zum Anderen ist auch das freie Elektronenpaar des Estersauerstoffatomes nicht mehr optimal auf das Histidin



hinausgerichtet. Zusammen mit dem Verlust einer Wasserstoffbrückenbindung führt dies im Ende zu einem wesentlich schlechteren Ablauf der Katalyse.

Mit steigendem Umgebungsdruck wird nun also einerseits der Unterschied der jeweiligen Abstände des Alkoholsauerstoffatoms des tetrahedralen Übergangszustandes des (+)- und (-)-Menthylesters zu dem  $\epsilon$ -Stickstoffatom des Histidin449 immer kleiner. Andererseits wird das freie Elektronenpaar des (+)-Menthylestersauerstoffatoms, analog zum (-)-Menthylestersauerstoffatom, in Richtung des H449-N $\epsilon$  ausgerichtet. Damit sinkt im gleichen Maße auch die Fähigkeit der Lipase, zwischen (+)- und (-)-Menthol zu unterscheiden. Dies wirkt sich in einem Absinken der Enantioselektivität aus (siehe Tabelle 1) aus.

Als Grund für die Änderung der Geometrie des aktiven Zentrums mit steigendem Druck wurde eine wassergefüllte Vertiefung der Lipase aus *Candida rugosa* identifiziert. Die wassergefüllte Vertiefung ist im Grundzustand, bei 1 bar Umgebungsdruck, mit 6 Wassermolekülen gefüllt. Mit zunehmendem Druck wird immer mehr Wasser in die Vertiefung gedrängt, so daß sich in dieser bei 10 bar 10 Wassermoleküle, bei 50 bar 12 Wassermoleküle und schließlich bei 100 bar 13 Wassermoleküle befinden. Bei 100 bar fällt außerdem auf, daß sich die Vertiefung soweit geöffnet hat, daß ein offener, wassergefüllter Kanal entstanden ist, der sich zum aktiven Zentrum hin öffnet (siehe Abbildung 6).

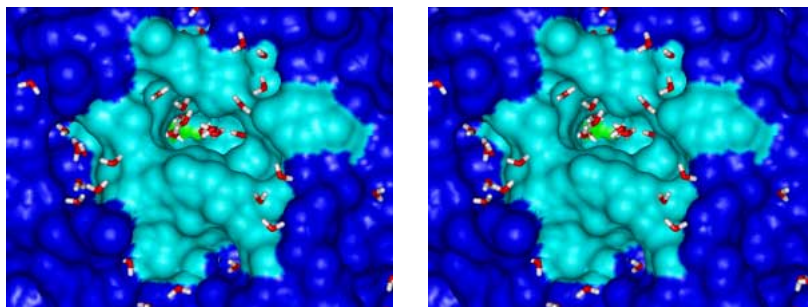


Abbildung 6 Stereobild des Wasserkanals in der simulierten Struktur der *Candida rugosa* Lipase in Chloroform als Lösungsmittel bei 100 bar. Die gezeigte Konformation stellt eine Momentaufnahme bei 250 ps dar. Der Kanal ist offen.

*Fazit*

Durch die Aufteilung dieser Arbeit in einen biokatalytischen und einen computergestützten, theoretischen Teil war es möglich, sich dem Problem der Druckabhängigkeit der enzymatischen Reaktion von zwei unabhängigen Seiten her zu nähern. Für beide Teile wurde auf die Einhaltung möglichst derselben Reaktionsbedingungen geachtet. Sowohl das Lösungsmittel, als auch der Wassergehalt und die verwandten Drücke waren in beiden Untersuchungen identisch. Sowohl im biokatalytischen als auch im theoretischen Teil wurde eine Druckabhängigkeit der Lipase erkannt und daraus ein Modell der Druckabhängigkeit der Enantioselektivität der lipase-katalysierten Trennung racemischen Menthols entwickelt.

**TABLE OF CONTENTS**

<b>1. Introduction</b>	<b>1</b>
<b>1.1. Biocatalysis</b>	<b>1</b>
1.1.1. Menthol	1
1.1.2. Lipases	4
1.1.2.1. Application of lipases	5
1.1.2.2. Evolution of the $\alpha/\beta$ hydrolase fold enzymes and related proteins	6
1.1.2.3. Structure and function of lipases	7
1.1.2.4. The mechanism of the catalytic triad	10
1.1.2.5. Substrate binding	11
1.1.2.6. Interfacial activation	13
1.1.3. Stereoselectivity	14
<b>1.2. Pressure</b>	<b>15</b>
1.2.1. NMR	15
1.2.2. Molecular Modeling	15
1.2.3. Pressure denaturation of proteins	16
<b>1.3. Introduction to molecular modeling</b>	<b>17</b>
1.3.1. Quantum mechanical methods	17
1.3.2. Molecular mechanics methods	18
1.3.3. Application of molecular modeling to proteins	19
<b>2. Purpose</b>	<b>20</b>
<b>3. Materials and Methods</b>	<b>21</b>
<b>3.1. Chemicals</b>	<b>21</b>
<b>3.2. Enzymes</b>	<b>21</b>
<b>3.3. Equipment</b>	<b>22</b>
<b>3.4. Hardware</b>	<b>23</b>
<b>3.5. Software</b>	<b>23</b>
<b>3.6. Biocatalytic methods</b>	<b>24</b>
3.6.1. Experimental setup	24
3.6.2. Sample reaction	25
3.6.3. Enzyme activity (pH-stat assay)	26
3.6.4. Water content (Karl-Fischer titration)	26
3.6.5. Enantiomeric excess (gas chromatography)	26

<b>3.7. Molecular dynamics simulation methods</b>	<b>27</b>
3.7.1. The GROMOS96 Force Field	27
3.7.2. Periodic boundary conditions in GROMOS96	29
3.7.3. Energy minimization	30
3.7.4. Molecular dynamics algorithm in GROMOS96 (Leap frog Algorithm)	32
3.7.5. Setup of the MD simulations of <i>Candida rugosa</i> lipase in GROMOS96	33
3.7.6. Reformatting coordinates	37
3.7.6.1. PROCS2	37
3.7.6.2. PROPDF	38
3.7.7. Building a topology	39
3.7.8. Generating coordinates	44
3.7.8.1. PROGCH	44
3.7.8.2. PROGWH	44
3.7.8.3. PROBOX	45
3.7.8.4. PROION	46
3.7.9. Calculating Molecular dynamics simulations	48
3.7.10. Analyzing molecular dynamics simulations	53
3.7.10.1. PROAVX	53
3.7.10.2. PROCOX	54
<b>4. Results</b>	<b>55</b>
<b>4.1. Biocatalysis</b>	<b>55</b>
4.1.1. Screening for the sample reaction	55
<b>4.2. Computer modeling</b>	<b>68</b>
<b>5. Discussion</b>	<b>94</b>
<b>5.1. Biocatalysis</b>	<b>94</b>
<b>5.2. Modeling</b>	<b>95</b>
5.2.1. Molecular dynamics simulations of biological systems	95
5.2.2. Analysis of the molecular dynamics simulations – effects on CRL-structure	97
<b>6. Outlook</b>	<b>108</b>
<b>7. References</b>	<b>109</b>
<b>8. Appendix</b>	<b>119</b>
<b>8.1. pdb entry 1LPM.pdb</b>	<b>119</b>
<b>8.2. Coordinate file in GROMOS96 format (lpmcoord6.dat)</b>	<b>127</b>
<b>8.3. Molecular topology for the <i>Candida rugosa</i> lipase</b>	<b>132</b>

**ABBREVIATIONS**lipases:

CRL	<i>Candida rugosa</i> lipase
DLH	dienlacton hydrolase
HAL	haloalkan dehalogenase
CPW	carboxypeptidase II
AchE	acetylcholinesterase
GLP	<i>Geotrichum candidum</i> lipase
RML	<i>Rhizomucor miehei</i> lipase
CBPA	carboxypeptidase A
HPL	human pancreatic lipase

amino acids:

A, Ala	alanine
C, Cys	cysteine
D, Asp	aspartate
E, Glu	glutamate
F, Phe	phenylalanine
G, Gly	glycine
H, His	histidine
I, Ile	isoleucine
K, Lys	lysine
L, Leu	leucine
M, Met	methionine
N, Asn	asparagine
P, Pro	proline
Q, Gln	glutamine
R, Arg	arginine
S, Ser	serine
T, Thr	threonine
V, Val	valine
W, Trp	tryptophane
Y, Tyr	tyrosine

computer modelling:

MD, md	molecular dynamics
aa	aminoacid
Nu, nu	nucleophile
Sm, sm	small residue
X, x	some residue
rmsd	root mean square deviation
$r_{\text{gyr}}$	radius of gyration
spc	simple point charge
mtbb	molecular topology building block
$V^{\text{phys}}(\mathbf{r}, \mathbf{s})$	totale potential energy
$V^{\text{bon}}(\mathbf{r}, \mathbf{s})$	contribution of bonded energy to potential energy
$V^{\text{bond}}(\mathbf{r}, \mathbf{s})$	bond-stretching energy
$V^{\text{angle}}(\mathbf{r}, \mathbf{s})$	bond-angle bending energy
$V^{\text{har}}(\mathbf{r}, \mathbf{s})$	harmonic improper dihedral-angle bending energy
$V^{\text{trig}}(\mathbf{r}, \mathbf{s})$	trigonometric dihedral-angle torsion energy
$V^{\text{nonb}}(\mathbf{r}, \mathbf{s})$	contribution of non-bonded energy to potential energy
$b_n$	bond length of bond n
$\Theta_n$	bond angle value of bond angle n
$\xi_n, \varphi_n$	dihedral angle value of dihedral angle n
t	time
r	position
v	velocity

further abbreviations:

ee <sub>P</sub>	enantiomeric excess of the product
ee <sub>S</sub>	enantiomeric excess of the substrate
c	conversion
E	enantioselectivity
E <sub>kin</sub>	kinetic energy
E <sub>pot</sub>	potential energy
rpm	revolutions per minute
U, Unit	unit in mmole/minute
Da	dalton

## FIGURES

### Zusammenfassung in deutscher Sprache

Abbildung 1	Darstellung enantiomerenreinen (-)-Menthols. _____	VI
Abbildung 2	Veresterung racemischen Menthols. In der Grundreaktion entsteht neben (+)-Menthol und Propionsäure (-)-Menthylpropionat. _____	VIII
Abbildung 3	Veresterung von Menthol. In einer Nebenreaktion wird Wasser bei der Veresterung von (-)-Menthol mit Propionsäure gebildet. _____	VIII
Abbildung 4	Schematischer Versuchsaufbau der Veresterung racemischen Menthols mit Propionsäureanhydrid. _____	IX
Abbildung 5	Simulationseinheit der Lipase aus <i>Candida rugosa</i> in Chloroform mit Kristallwasser und Ionen. Der Inhibitor ist in CPK dargestellt, die Lipase selbst als molekulare Oberfläche, Kristallwasser und Chloroform als "Balls-and-Sticks". Die Lipase befindet sich in einer sog. "truncated octahedral box". _____	X
Abbildung 6	Stereobild des Wasserkanals in der simulierten Struktur der <i>Candida rugosa</i> Lipase in Chloroform als Lösungsmittel bei 100 bar. Die gezeigte Konformation stellt eine Momentaufnahme bei 250 ps dar. Der Kanal ist offen. _____	XIII

### Thesis in english language

Figure 1	Menthol, (+)-(1S, 2R, 5S)-menthol, (-)-(1R, 2S, 5R)-menthol. _____	2
Figure 2	The Haarmann & Reimer process for the synthesis of optically pure (-)-menthol. _____	3
Figure 3	Lipase catalyzed ester hydrolysis, synthesis and transfer reactions. _____	4
Figure 4	Schematic diagram of the $\alpha\beta$ -hydrolase fold (Ollis, Cheah et al. 1992). _____	7
Figure 5	Schematic drawing of the C-terminal half of DHL (Ollis, Cheah et al. 1992) with the $\beta$ -strands 5 to 8 and the $\alpha$ -helices C to F. _____	9
Figure 6	Schematic drawing of the mechanism of the catalytic triad in lipases. _____	10
Figure 7	Kazlauskas rule for the prediction of the enantioselectivity of lipases towards secondary alcohols (Cygler, Grochulski et al. 1994). _____	11
Figure 8	Structure of the (-)-1R- and (+)-1S-menthyl-hexylphosphonates in the active site of the <i>Candida rugosa</i> lipase, respectively (Kazlauskas 1994). _____	12
Figure 9	Molecular surface of the <i>Candida rugosa</i> lipase in the open and the closed form, respectively. The active site is shown in red, the lid in blue. _____	13
Figure 10	Schematic drawing of the experimental setup. _____	24
Figure 11	Kinetic resolution of racemic ( $\pm$ )-menthol with propionic acid anhydride. _____	25

Figure 12	Bond-stretching ( $V^{\text{bond}}$ ) and bond-angle bending ( $V^{\text{angle}}$ ) interaction contribution to the potential energy. The actual bond length of the bond $n$ between atoms with sequence numbers $i$ and $j$ is denoted by $b_n$ . The actual bond-angle value of the bond angle between atoms with sequence numbers $i, j$ and $k$ is denoted by $\theta_0$ . _____	28
Figure 13	Improper dihedral-angle bending (out of plane) ( $V^{\text{har}}$ ) interaction contribution to the total potential energy. The actual dihedral angle value of the dihedral angle between atoms with sequence numbers $i, j, k$ and $l$ is denoted by $\xi_n$ . For example, the atoms C-CA-N-O in an amino acid residue are kept near a planar configuration by defining an improper dihedral with $\xi_0 = 0^\circ$ . _____	28
Figure 14	Trigonometric dihedral-angle torsion (improper torsional bending) ( $V^{\text{rig}}$ ) contribution to the total potential energy. The actual dihedral angle value of the dihedral angle between atoms with sequence numbers $i, j, k$ and $l$ is denoted by $\phi_n$ . $\delta_n$ and $m_n$ are restricted to 0 or $\Pi$ . For example, improper torsional terms are commonly used to keep a benzene ring planar. _	28
Figure 15	Non-bonded van der Waals and electrostatic interaction ( $V^{\text{nonb}}$ ) contribution to the total potential energy. The first part of the formula corresponds to the Lennard-Jones potential (van der Waals interaction), the second part of the formula represents the Coulomb potential (electrostatic interaction). _____	29
Figure 16	The truncated octahedron as a box shape resembling a sphere. It fills all space by translation operation of the central box in three dimensions (Leach 1996). _____	30
Figure 17	Energy minimization as opposed to molecular dynamics simulations, illustrated on an energy profile. Energy minimizations are only capable of finding the next local energy minimum, whereas molecular dynamics simulations can skip local energy minima and find the global energy minimum. _____	31
Figure 18	Integration scheme of the leap-frog algorithm for calculating Newton's equation of motion. _____	32
Figure 19	Setup of the simulation assembly of the open form of the <i>Candida rugosa</i> lipase for molecular dynamics simulation. _____	34
Figure 20	Trend of the potential and kinetic energy during the energy minimization. _____	35
Figure 21	Trend of the potential and kinetic energy during the heating phase. _____	35
Figure 22	N-terminal end of CRL as generated in the first step by PROGMT. _____	40
Figure 23	Manual fix of the N-terminus of the CRL. Newly added atoms are shown with a red background, atoms edited are shown with a blue border. _____	40
Figure 24	C-terminal end of CRL as generated in the first step by PROGMT. _____	41
Figure 25	Manual fix of the C-terminus of the CRL. Newly added atoms are shown with a red background, atoms edited are shown with a blue border. _____	41
Figure 26	Esterification of menthol by <i>Candida rugosa</i> lipase. Dependency of the esterification on the chain length. The hydrophobic fatty acid used for esterification has a maximum at C18. ____	63
Figure 27	Chromatogram of the biotransformation sample after 48 hours at 100 bar. _____	65



- Figure 28 Experimentally determined dependence of the enantioselectivity of *Candida rugosa* lipase towards the esterification of ( $\pm$ )-menthol with propionic acid anhydride. For conversion rates  $c = 15\% - 30\%$ , the enantioselectivity significantly decreased with increasing pressure. Standard deviations were calculated for each  $E$ -value for 6 independent measurements
- applying equation  $\sigma_E = \sqrt{\frac{\sum (E_i - \bar{E})^2}{n - 1}}$  \_\_\_\_\_ 66
- Figure 29 Volume of the simulation assembly during the molecular dynamics simulations in water and chloroform. The conformation at 100 ps in water was taken as a starting structure for the molecular dynamics simulation in chloroform at 1 bar. Starting structures for the simulation at elevated pressures were the configurations obtained after 50 ps of simulation at previous, lower, pressure (depicted by the arrows). \_\_\_\_\_ 69
- Figure 30 Volume-Surface-Ratio of the *Candida rugosa* lipase simulated in different solvents compared to the crystal structure 1LPM. \_\_\_\_\_ 70
- Figure 31 Averaged number of hydrogen bonds of the active site residues and F415 during each molecular dynamics simulation at different pressures. \_\_\_\_\_ 70
- Figure 32 Radius of gyration during the molecular dynamics simulations in water at 1 bar and in chloroform at 1 bar, 10 bar, 50 bar, and 100 bar. The conformation at 100 ps in water was taken as starting structure for the molecular dynamics simulation in chloroform at 1 bar. \_\_\_\_\_ 72
- Figure 33 rms during the molecular dynamics simulations in water at 1 bar and in chloroform at 1 bar, 10 bar, 50 bar, and 100 bar. The conformation at 100 ps in water was taken as starting structure for the molecular dynamics simulation in chloroform at 1 bar. \_\_\_\_\_ 73
- Figure 34 Percentage of amino acid residues of the *Candida rugosa* lipase in the most favored regions of the ramachandran plot simulated in different solvents compared to the crystal structure 1LPM. \_\_\_\_\_ 74
- Figure 35 Ramachandran plot for the *Candida rugosa* crystal structure 1LPM. \_\_\_\_\_ 75
- Figure 36 Percentage of amino acid residues of the *Candida rugosa* lipase in the additional allowed regions of the ramachandran plot simulated in different solvents compared to the crystal structure 1LPM. \_\_\_\_\_ 76
- Figure 37 Ramachandran plot for the *Candida rugosa* lipase simulated in water as solvent. \_\_\_\_\_ 77
- Figure 38 Percentage of amino acid residues of the *Candida rugosa* lipase in the generously allowed regions of the ramachandran plot simulated in different solvents compared to the crystal structure 1LPM. \_\_\_\_\_ 78
- Figure 39 Ramachandran plot for the *Candida rugosa* lipase simulated in chloroform as solvent at 1 bar. \_\_\_\_\_ 79
- Figure 40 Percentage of amino acid residues of the *Candida rugosa* lipase in the disallowed regions of the ramachandran plot simulated in different solvents compared to the crystal structure 1LPM. \_\_\_\_\_ 80
- Figure 41 Ramachandran plot for the *Candida rugosa* lipase simulated in chloroform as solvent at 10 bar. \_\_\_\_\_ 81
- Figure 42 Ramachandran plot for the *Candida rugosa* lipase simulated in chloroform as solvent at 50 bar. \_\_\_\_\_ 83

Figure 43	<i>Ramachandran plot for the Candida rugosa lipase simulated in chloroform as solvent at 100 bar.</i>	85
Figure 44	<i>Calculation of the angle (N-O)<sup>+</sup>. The tetrahedral intermediate of the (+)-menthylester was docked into the energy minimized structures of the Candida rugosa lipase simulated at different pressures.</i>	87
Figure 45	<i>Correlation between biotransformation (experimentally determined E-value) and molecular dynamics simulation. The correlation for the distance of H449-Nε to F415-Cφ and the E-values was 97.5 %. For the differences in distance of H449-Nε to (±)-menthyl-O and the E-values, the correlation was 91.5 %. The correlation was calculated by the following equation:</i>	88
Figure 46	<i>Number of buried and accessible residues in the proposed water channel in the molecular dynamics simulations at varying pressures.</i>	90
Figure 47	<i>Location of the water molecule 631 throughout the molecular dynamics simulations at various pressures. The positions of water molecule 631, shown in blue, were taken from every 50 ps of the molecular dynamics simulations at various pressures, whereas the active site residues and F415, shown in red, were from the configuration after 250 ps at 100 bar. Left sample of positions of water molecule 631: occupied at pressures 1 bar, 10 bar, 50 bar, and for the first 50 ps of the simulation at 100 bar. Right sample of positions of water molecule 631: occupied after 50 ps of the simulation at 100 bar.</i>	91
Figure 48	<i>Stereo view of the water channel in the crystal structure of Candida rugosa lipase, 1LPM. The channel is closed. The hydrogen atoms of the water molecules were calculated.</i>	92
Figure 49	<i>Stereo view of the water channel in the simulated structure of Candida rugosa lipase with explicit water as solvent at 1 bar. The conformation shown is a snapshot at 400 ps. The channel is closed.</i>	92
Figure 50	<i>Stereo view of the water channel in the simulated structure of the Candida rugosa lipase with explicit chloroform as solvent and 244 essential water molecules at 1 bar. The conformation shown is a snapshot at 400 ps. The channel is closed.</i>	93
Figure 51	<i>Stereo view of the water channel in the simulated structure of the Candida rugosa lipase with explicit chloroform as solvent 244 essential water molecules at 100 bar. The conformation shown is a snapshot at 250 ps. The channel is open.</i>	93
Figure 52	<i>Fluctuations averaged over all Cα-atoms in the last 50 ps of each molecular dynamics simulation at 1 bar, 10 bar, 50 bar, and 100 bar, respectively.</i>	97
Figure 53	<i>Structure of the (1S)- and (1R)-menthyl-hexylphosphonates in the active site of Candida rugosa lipase, respectively (Kazlauskas 1994).</i>	99
Figure 54	<i>Schematic drawing of the mechanism of the catalytic triad in lipases</i>	99
Figure 55	<i>Schematic diagram of a folding energy landscape. Denatured molecules at the top of the funnel might fold to the native state by a myriad of different routes, some of which involve transient intermediates (local energy minima) whereas others involve significant kinetic traps (misfolded states). For proteins that fold without populating intermediates, the surface of the funnel would be smooth. Reproduced from (Schultz 2000).</i>	101

- Figure 56 *Pressure induced displacement of the H449 side chain in the active site of Candida rugosa lipase. The lipase structure was averaged over the last 50 ps of the 100 bar simulation with the coordinates of the 13 water molecules in the water channel taken from the snapshot at 250 ps (colored by atom: green (C), red (O), blue (N), white (H)). The (+)-menthylester was docked as tetrahedral intermediate to the averaged structure and energy minimized. For comparison, the crystal structure (1LPM) is shown in gray; it contains only 6 water molecules in the water channel.* \_\_\_\_\_ 103
- Figure 57 *The tetrahedral intermediate of (-)-menthylester (blue: isopropyl moiety oriented to the right side) and (+)-menthylester (red: isopropyl moiety oriented to the left side) docked to the averaged structure of the molecular dynamics simulation at 1 bar. The distance between H449-N $\epsilon$  and the alcohol oxygen is marked by arrows (blue: (-), red: (+)).* \_\_\_\_\_ 106
- Figure 58 *The tetrahedral intermediate of (-)-menthylester (blue: isopropyl moiety oriented to the right side) and (+)-menthylester (red: isopropyl moiety oriented to the left side) docked to the averaged structure of the molecular dynamics simulation at 10 bar. The distance between H449-N $\epsilon$  and the alcohol oxygen is marked by arrows (blue: (-), red: (+)).* \_\_\_\_\_ 106
- Figure 59 *The tetrahedral intermediate of (-)-menthylester (blue: isopropyl moiety oriented to the right side) and (+)-menthylester (red: isopropyl moiety oriented to the left side) docked to the averaged structure of the molecular dynamics simulation at 50 bar. The distance between H449-N $\epsilon$  and the alcohol oxygen is marked by arrows (blue: (-), red: (+)).* \_\_\_\_\_ 107
- Figure 60 *The tetrahedral intermediate of (-)-menthylester (blue: isopropyl moiety oriented to the right side) and (+)-menthylester (red: isopropyl moiety oriented to the left side) docked to the averaged structure of the molecular dynamics simulation at 100 bar. The distance between H449-N $\epsilon$  and the alcohol oxygen is marked by arrows (blue: (-), red: (+)).* \_\_\_\_\_ 107

## TABLES

## Zusammenfassung in deutscher Sprache

<i>Tabelle 1</i>	<i>Druckabhängigkeit der Enantioselektivität der lipase-katalysierten Trennung racemischen Menthols.</i>	<i>IX</i>
<i>Tabelle 2</i>	<i>Geometrische Auswertung der mit dem tetrahedralen Übergangszustand des (+)- bzw. (-)-Menthylesters gedockten und energieminierten mittleren Strukturen bei 1 bar, 10 bar, 50 bar und 100 bar.</i>	<i>XII</i>

## Thesis in english language

<i>Table 1</i>	<i>Main sources of (-)-menthol in 1992 (Leffingwell and Shakelford 1974; Hopp 1993).</i>	<i>1</i>
<i>Table 2</i>	<i>Rmsd values for the partial superimposition of the first 5 enzymes (Ollis, Cheah et al. 1992).</i>	<i>8</i>
<i>Table 3</i>	<i>Enzymes screened for stereoselective reaction</i>	<i>56</i>
<i>Table 4</i>	<i>Substrates screened with the enzymes listed in Table 3.</i>	<i>57</i>
<i>Table 5</i>	<i>Various immobilization methods tested for the stabilization of the enzymes screened in organic solvent.</i>	<i>58</i>
<i>Table 6</i>	<i>Conversion, conv, and E-values, E, for the screening with propionic acid anhydride as acyl donor. Lipases with an E-value greater than 20 are marked red. Screening was performed for 36 hours.</i>	<i>59</i>
<i>Table 7</i>	<i>Conversion, conv, and E-values, E, for the screening with acetic acid anhydride as acyl donor. Lipases with an E-value greater than 20 are marked red. Screening was performed for 36 hours.</i>	<i>60</i>
<i>Table 8</i>	<i>Conversion, conv, and E-values, E, for the screening with benzoic acid as acyl donor. The enantiomeric excess was not yet determinable after 108 hours.</i>	<i>61</i>
<i>Table 9</i>	<i>Conversion, conv, and E-values, E, for the screening with phenyl acetate as acyl donor. The enantiomeric excess was not determinable after 108 hours.</i>	<i>61</i>
<i>Table 10</i>	<i>Conversion, conv, and E-values, E, for the screening of the hydrolysis of menthyl acetate. Lipases with an E-value greater than 20 are marked red. Screening was performed for 36 hours.</i>	<i>62</i>
<i>Table 11</i>	<i>Conversion, conv, and E-values, E, for the Candida rugosa lipase immobilized on different carriers with propionic acid anhydride as acyl donor. Results with E-values greater than 20 are marked red. Screening was performed for 36 hours.</i>	<i>63</i>
<i>Table 12</i>	<i>Screening results with the best values for enantioselectivity.</i>	<i>64</i>

Table 13	<i>Kinetic parameters of the transesterification reaction at different pressures. Standard deviations were calculated for each E-value with 6 independent measurements.</i>	66
Table 14	<i>rmsd values of all backbone C<math>\alpha</math>-atoms from the crystal structure of <i>Candida rugosa</i> lipase averaged over the last 50 ps of each simulation production phase. In case of molecular dynamics simulation with explicit water as solvent, the last 15 ps were used for averaging.</i>	71
Table 15	<i>Geometrical analysis of the averaged and energy minimized structures of <i>Candida rugosa</i> lipase containing the manually docked tetrahedral intermediate of the (-)-and (+)-menthylester at increasing pressure. The angle (N-O)<sup>+</sup> was calculated using the scalar product of the vector from the H449-N<math>\epsilon</math> to its hydrogen atom and the sum of the vectors of the neighboring carbon atoms towards the (+)-menthyl ester oxygen atom. For the visualization of the calculation see also Figure 44. The distances listed in column 4 were taken from the averaged structure without docking of the transition state analogue.</i>	87
Table 16	<i>Properties of the proposed water channel as analyzed in the averaged structures without docking. The volume of the cavity was estimated with the C<math>\alpha</math>-atoms of three amino acid pairs, R518/N339, L435/F391, and F517/G341, respectively. Only the water molecules were counted in the last configuration of each molecular dynamics simulation. The volume was determined by measuring the distances between Arg518/Asn339, Leu435/Phe391 and Phe517/Glu341.</i>	89

## 1. INTRODUCTION

### 1.1. BIOCATALYSIS

#### 1.1.1. MENTHOL

(-)-menthol is one of the most important flavoring chemicals. Menthol is utilized largely in the hygiene (toothpaste) as well as the food (cigarettes, sweets) and cosmetics (bath, skin care products) industry. In 1992, about 6300 tons of (-)-menthol were produced (see Table 1).

The original way of synthesis of (-)-menthol is by freezing the oil of the *Mentha arvensis* and the subsequent crystallization of menthol. The crystals are then centrifuged and therefore the menthol crystals are separated from the supernatant, also called dementholized cornmint oil. Traces of *Mentha arvensis* oil often impart a slight peppermint aroma to the menthol.

Haarmann & Reimer and Takasago are the two dominant companies producing (-)-menthol by synthetic or semi-synthetic processes. This has led to only small fluctuations in the price of natural (-)-menthol compared to former times, when (-)-menthol was only produced by extraction.

Source	Tons
China	2,300
Haarmann & Reimer	1,600
India	750
Takasago	650
Others	650
Brazil/Paraguay	350
Total	6,300

Table 1 Main sources of (-)-menthol in 1992 (Leffingwell and Shakelford 1974; Hopp 1993).

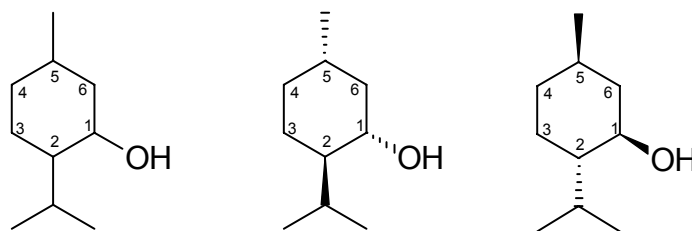


Figure 1 Menthol, (+)-(1S, 2R, 5S)-menthol, (-)-(1R, 2S, 5R)-menthol.

Menthol is a secondary alcohol (see Figure 1). It contains three stereocenters. The stereocenters are at C-atoms 1, 2 and 5 respectively. A racemic mixture of menthol contains (-)-(1R, 2S, 5R)-menthol and (+)-(1S, 2R, 5S)-menthol. Of these two forms, the (-)-menthol has the characteristic minty, fresh taste.

For the chemical synthesis, Haarmann & Reimer and Takasago established different processes.

Racemic menthol itself can not be resolved using distillation, filtering or other conventional methods of separation as enantiomers have the same physical properties (see chapter 1.1.3). Haarmann & Reimer, the market leader in synthetic (-)-menthol, utilizes the selective crystallization of menthyl benzoate diastereomers (see chapter 1.1.3), which can be induced by seeding the bulk with one of the diastereomers (see Figure 2). This process of producing (-)-menthol leads to more than 90% overall yield (Leffingwell and Shakelford 1974; Hopp 1993).

Takasago developed the synthesis of (-)-menthol starting from myrcene in the early 1980's. Using lithium as a catalyst, diethylamine is added to myrcene, which is, therefore, converted to diethylgeranylamine. Catalytical isomerization yields the chiral 3R-citronellal enamine with 96-99% enantiomeric excess. The enamine is then further hydrolyzed resulting in the formation of 3R-(+)-citronellal. In contrast to the fractional distillation from citronella oil, the citronellal produced in such a way has a higher optical purity. 3R-(+)-citronellal then is converted to (-)-menthol by cyclization in protonic media (Leffingwell and Shakelford 1974; Hopp 1993).

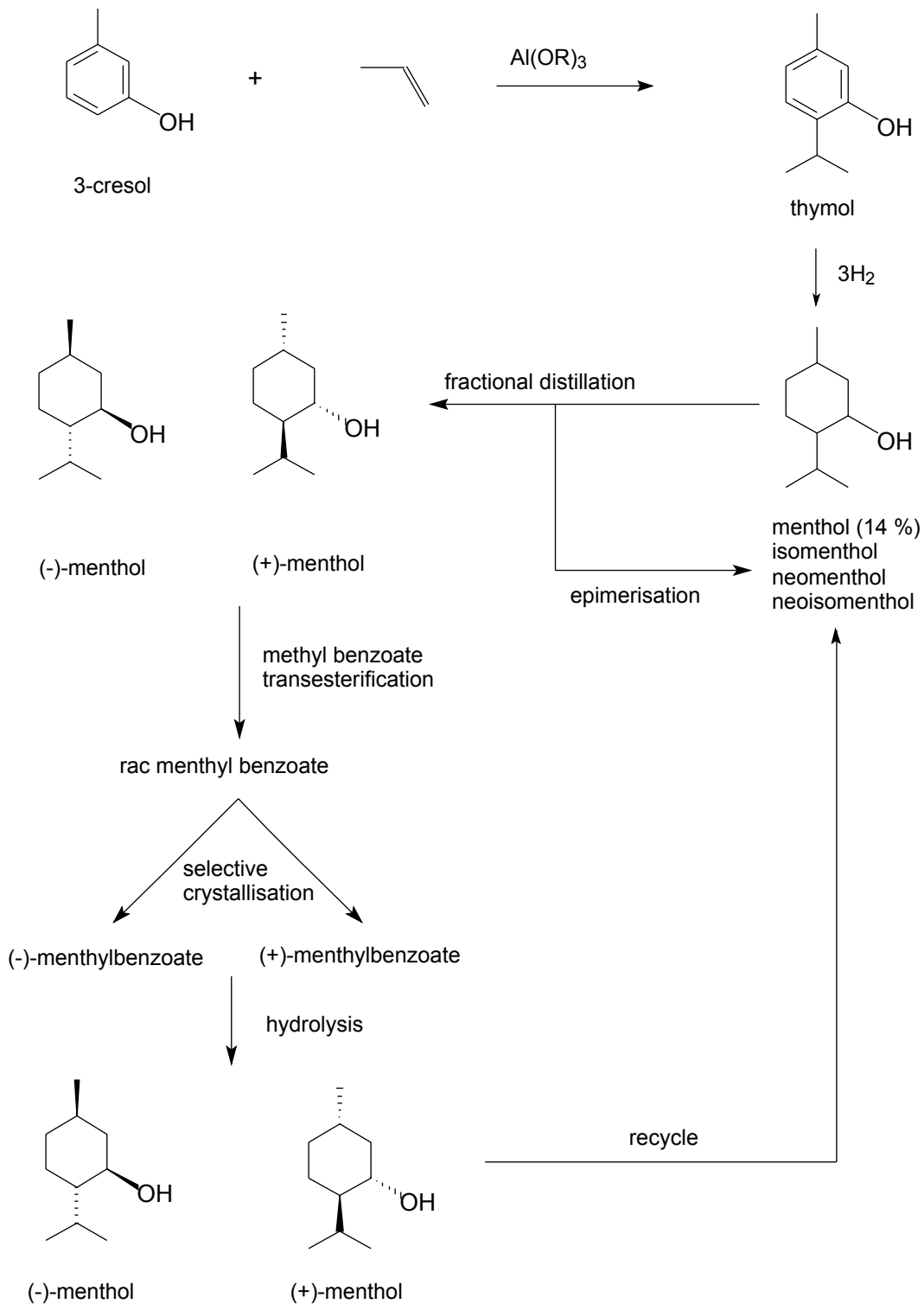


Figure 2 The Haarmann & Reimer process for the synthesis of optically pure (-)-menthol.

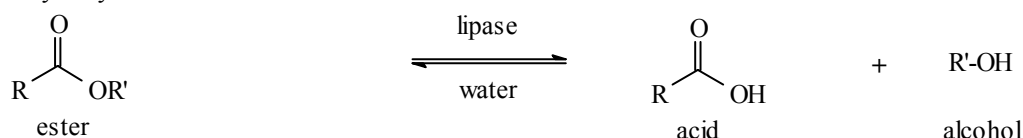
The use of biological catalysts provides further opportunities to separate ( $\pm$ )-menthol. In the presence of lipases (E.C. 3.1.1.3), a class of hydrolytic enzymes, hydrolysis, esterification or transesterification reactions can be used, to preferentially modify just one of the two enantiomers (see Figure 3).



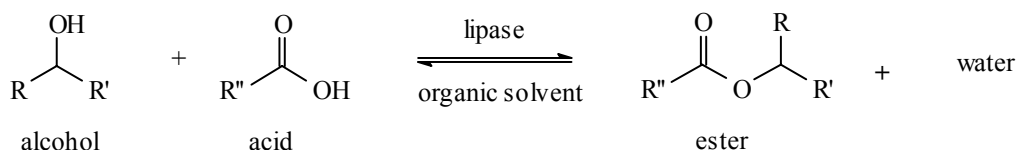
### 1.1.2. LIPASES

Lipases (E.C. 3.1.1.3) (Tipton 1994; Barrett 1995; Barrett 1996) belong to the family of the serine hydrolases and can be found in animals, plants and microorganisms (Borgstrom and Brockman 1984; Alberghina, Schmid et al. 1991; Schmid and Verger 1998; Bornscheuer and Kazlauskas 1999). They play an important role in the catabolism of triacylglycerides to di- and monoacylglycerides, free fatty acids and glycerol. Lipases stereoselectively catalyze hydrolysis as well as the reverse reaction, esterification and transesterification. The direction of the reaction can be influenced by the use of adequate solvent systems, aqueous or organic (see Figure 3).

#### 1. Hydrolysis

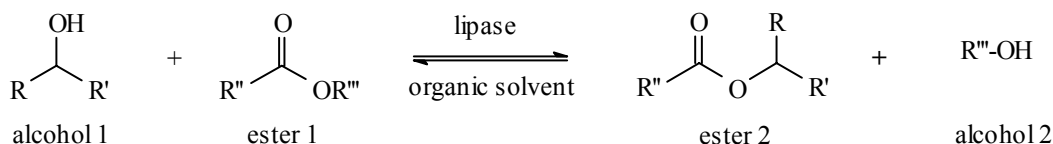


#### 2. Esterification

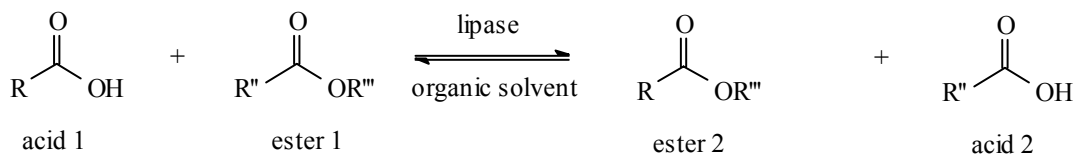


#### 3. Interesterification

##### a) Alcoholysis



##### b) Acidolysis



##### c) Interesterification

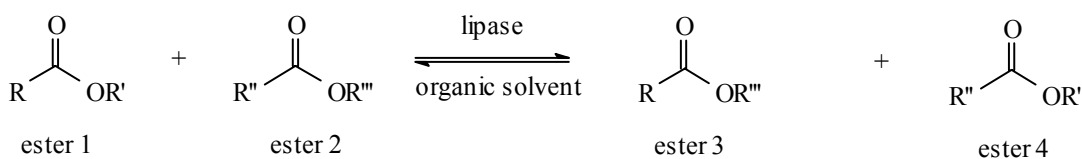


Figure 3 Lipase catalyzed ester hydrolysis, synthesis and transfer reactions.

The kinetic resolution of racemic secondary alcohols in organic solvent systems is a well studied application of lipases. Advantages of organic solvent systems are the high solubility of hydrophobic substrates or the ease of separation and reuse of the biocatalyst (Otero, Ballesteros et al. 1988; Narang, Barker et al. 1990; Otero, Robledo et al. 1995; Ivanov and Schneider 1997). Even supercritical fluids have been used as solvent, thus facilitating downstream processing (Marty, Chulalaksananukul et al. 1992; Beckman, Russell et al. 1995; Ikushima 1997). Intense research has been performed on the impact of various parameters on the stereoselectivity of lipases, such as immobilization, coating of lipases with surfactants, use of acid anhydrides as substrates or controlling stereoselectivity via the surface pressure of substrate monolayers (Rogalska, Ransac et al. 1990; Ransac, Rogalska et al. 1991; Rogalska, Ransac et al. 1991; Bianchi, Battistel et al. 1993; Bornscheuer, Herar et al. 1993; Rogalska, Cudrey et al. 1993; Rogalska, Ransac et al. 1993; Bornscheuer, Herar et al. 1995; Cygler, Grochulski et al. 1995; Kamiya, Goto et al. 1995; Stadler, Kovac et al. 1995; Yang, Cao et al. 1996; Koteshwar and Fadnavis 1997).

#### **1.1.2.1. APPLICATION OF LIPASES**

Lipases are used for a wide variety of biotransformations and in preparative organic synthesis (Kazlauskas and Bornscheuer 1998; Schmid and Verger 1998). Natural substrates of lipases are esters of cholesterol or glycerol but lipases are commonly used in the synthesis of precursors for agrochemicals, pharmaceuticals, herbicides, pesticides or other synthetic targets (Cygler, Grochulski et al. 1994; Kazlauskas 1994; Peters, van Aalten et al. 1996).

Furthermore, lipases can be used in washing agents. When utilized as supplements in detergents, they help to remove oil and grease. They not only have their impact during the washing process itself, but also thereafter, when they are attached to the clothing fiber and continue cleaving the remaining fat as well as prevent deposition of further fat. Especially useful is the stability of lipases towards high pH or temperature. Moreover, lipases are used in the food industry. Applied either as raw extract or as commercially available lipase, they are employed in the maturation of cheese. The refinement of lower order fatty acids can be accomplished using lipases. Cacao butter surrogate is produced by Unilever and Fuji Oil using lipases. Baby food or other special diets can be completed with essential fatty acids by transesterification reactions of lipases.

### 1.1.2.2. EVOLUTION OF THE $\alpha\beta$ HYDROLASE FOLD ENZYMES AND RELATED PROTEINS

Lipases differ widely in the number of amino acids in their primary sequences. For example, the *Candida rugosa* lipase contains more than 500 amino acids whereas, on the other side, the *Candida antarctica* lipase B contains less than 200 amino acids.

Nevertheless, some features are common to all lipases. The active site in all lipases is built up of the three amino acids serine, aspartate or glutamate and histidine, which are referred to as the catalytic triad. The three dimensional structure of all lipases follows a common motif, the  $\alpha\beta$  hydrolase fold (Ollis, Cheah et al. 1992).

Four groups of enzymes, whose active site comprise a catalytic triad can be distinguished:

- the  $\alpha\beta$  hydrolase fold enzymes
- the serine proteases
- the subtilisins
- the cysteine proteases

Except for the reaction mechanism, i.e. the serine O $\gamma$ , the acid carboxylate group and the imidazole ring of the catalytic histidine, there is no global similarity between these enzymes.

These four classes of enzymes are outstanding in several ways.

On the first hand, it is important to notice that convergent evolution led from different starting positions to four classes of enzymes, each of which having the same purpose; hydrolytic reactions in the biochemical catabolism. This clearly shows that hydrolytic reactions have are very central position in nature.

On the other hand, all  $\alpha\beta$  hydrolase fold enzymes have evolved by divergent evolution, starting from a common ancestor. Conserving only the active site and, therefore, the mechanism of reaction, the  $\alpha\beta$  hydrolase fold enzymes represent a class of enzymes with the broadest substrate spectrum compared to any other class of catalytic triad enzymes.

### 1.1.2.3. STRUCTURE AND FUNCTION OF LIPASES

The structure of several lipases have been well studied since 1990 (Cygler, Schrag et al. 1993) with the structure of the *Candida rugosa* lipase being available since 1993 (Grochulski, Li et al. 1993; Grochulski, Li et al. 1994). The  $\alpha\beta$  hydrolase fold is common to all lipases, and the catalytic triad consists of serine, aspartate or glutamate, and histidine (Ollis, Cheah et al. 1992). The catalytically active nucleophile, serine, is placed in the tip of a sharp loop, the nucleophilic elbow. While lipases have no general similarity, a consensus sequence common to all lipases is the amino acid sequence of the nucleophilic elbow, G-X-S-X-G-Sm, where Sm is a small residue.

#### *The $\alpha\beta$ -hydrolase fold*

A comparison of the structure of several hydrolytic enzymes containing a catalytic triad revealed a general structural motif: the  $\alpha\beta$ -hydrolase fold (Ollis, Cheah et al. 1992). The core of each enzyme consists of 8  $\beta$ -sheets connected by  $\alpha$ -helices (see Figure 4). Ollis et al. studied the acetylcholinesterase (AChE), carboxypeptidase II (CPW), dienlacton hydrolase (DLH), haloalkane dehalogenase (HAL) and *Geotrichum Candidum* lipase (GLP).

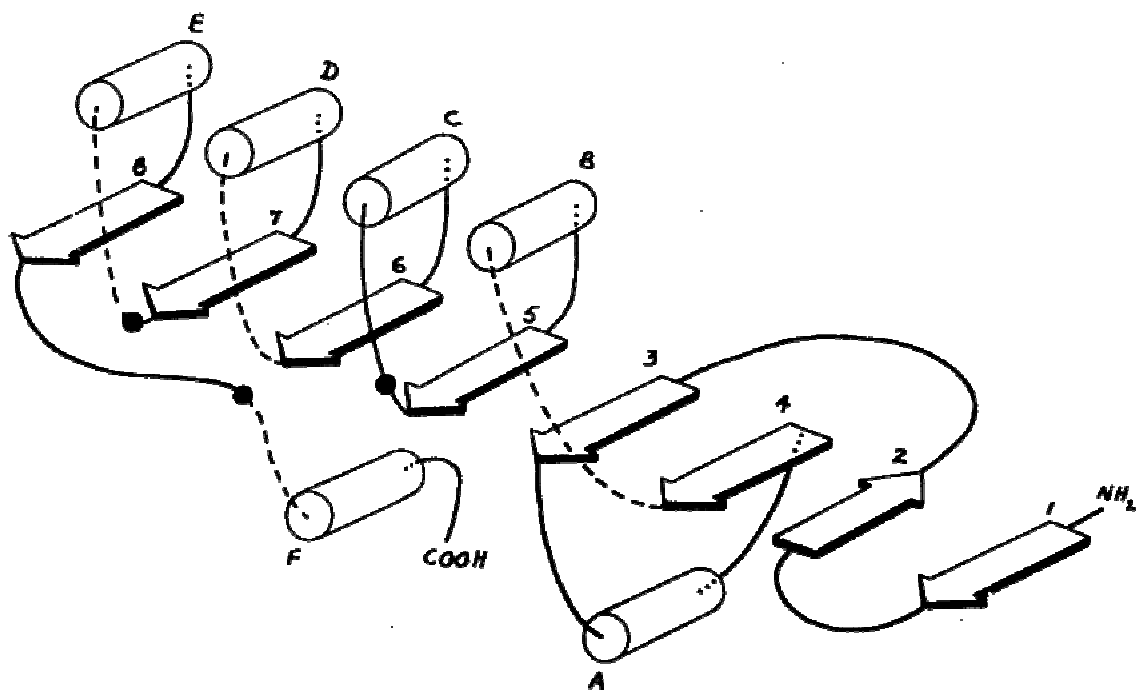


Figure 4 Schematic diagram of the  $\alpha\beta$ -hydrolase fold (Ollis, Cheah et al. 1992).

The experimentally determined structures of these enzymes were superimposed with a rmsd of 1.90 Å (AChE/GLP) to 3.04 Å (DLH/HAL). Rmsd values of about 3 Å per C $\alpha$ -atom are indicative for a similar three-dimensional structure, yet with some major differences. These are caused by a more or less distinct kink, which can be found between strands 5 and 6 of the  $\alpha\beta$ -hydrolase fold. A superposition of either strands two through five or strands six, seven and eight remarkably improves the quite ordinary rmsd values (see Table 2).

protein	superimposed strands	rmsd of corresponding C $\alpha$ -atoms				
		AchE	CPW	DLH	HAL	GLP
AChE	2-5	-	-	-	-	-
	6-8	-	-	-	-	-
	2-8	-	-	-	-	-
CPW	2-5	0.76	-	-	-	-
	6-8	1.01	-	-	-	-
	2-8	1.00	-	-	-	-
DLH	2-5	0.97	0.88	-	-	-
	6-8	0.84	1.08	-	-	-
	2-8	1.34	1.58	-	-	-
HAL	2-5	0.98	1.05	1.14	-	-
	6-8	0.88	1.04	0.89	-	-
	2-8	1.38	1.45	1.87	-	-
GLP	2-5	0.38	0.74	1.00	0.97	-
	6-8	0.44	1.00	0.88	0.86	-
	2-8	0.54	1.00	1.15	1.47	-

Table 2 Rmsd values for the partial superimposition of the first 5 enzymes (Ollis, Cheah et al. 1992).

The order of the catalytic triad amino acids in the primary sequence always is „nucleophile-acid-histidine“. All amino acids of the catalytic triad are positioned at the end of the C-terminus of a  $\beta$ -strand. The only exception is the histidine in AChE and GLP. The parallel  $\beta$ -sheet has a left-hand twist (see Figure 5). These peculiarities

permit an exact positioning of the amino acids of the catalytic triad with only small loops. Furthermore, the steric interference of the catalytic triad by the  $\beta$ -sheet is minimized.

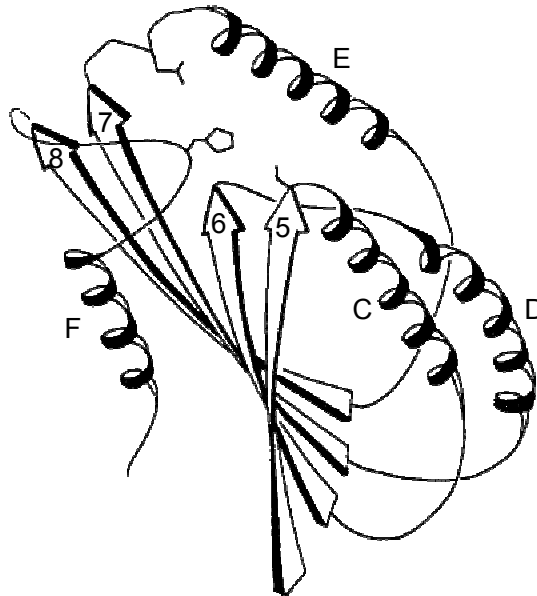


Figure 5 Schematic drawing of the C-terminal half of DHL (Ollis, Cheah et al. 1992) with the  $\beta$ -strands 5 to 8 and the  $\alpha$ -helices C to F.

#### *The nucleophile elbow:*

This loop contains the nucleophile, mostly serine, but also cysteine or aspartate are possible. It always is the central amino acid in a sharp  $\gamma$ -like turn between strand 5 and helix C. This motive (strand-nucleophile-helix) is one of the best conserved in the  $\alpha\beta$ -hydrolase fold. The amino acids „Nu-2“ and „Nu+2“ have to be glycine, „Nu+3“ has to be an amino acid with a small residue. The consensus sequence of the nucleophile elbow then is „G-X-Nu-X-G-Sm. In contrast, the same sequence for the trypsin-like proteases is „Sm-X-Nu-G-G“.

#### *The acid turn:*

The acid can either be aspartate or glutamine. It is located at the end of strand 7. The acid is common to two reverse turns being the last amino acid of the first and the first amino acid of the second turn.

#### *The histidine loop:*

The histidine loop is placed at the end of strand 8 and consists of the motif „turn-amino acid-histidine“. The histidine cannot be replaced by any other amino acid.

*Oxyanion hole:*

The oxyanion hole is located in a turn between strand 3 and helix A. The amides of the amino acid directly following the nucleophile and the amides in the turn are oriented into a nearby cavity.

**1.1.2.4. THE MECHANISM OF THE CATALYTIC TRIAD**

The reaction mechanism of the catalytic triad consists of two similar steps (see Figure 6) (Carter and Wells 1988).

In the first step, the amide nitrogens of two amino acids in the oxyanion hole polarize the substrate ester oxygen. The resulting oxyanion is stabilized by at least two hydrogen bonds. The nucleophilic serine O $\gamma$  attacks the positively charged carbonyl carbon of the substrate, forming the first tetrahedral transition state. The proton donated from the O $\gamma$  to the histidine imidazole ring is stabilized by the carboxy group of the catalytic acid. The proton is then donated to the scissile bond, cleaving the C-O bond between the tetrahedral carbon atom and the ester oxygen atom to release the alcohol and form the acyl-enzyme intermediate.

In the second step, the acyl-enzyme intermediate is hydrolyzed by water, analogous to the first step. The liberated acid leaves the enzyme.

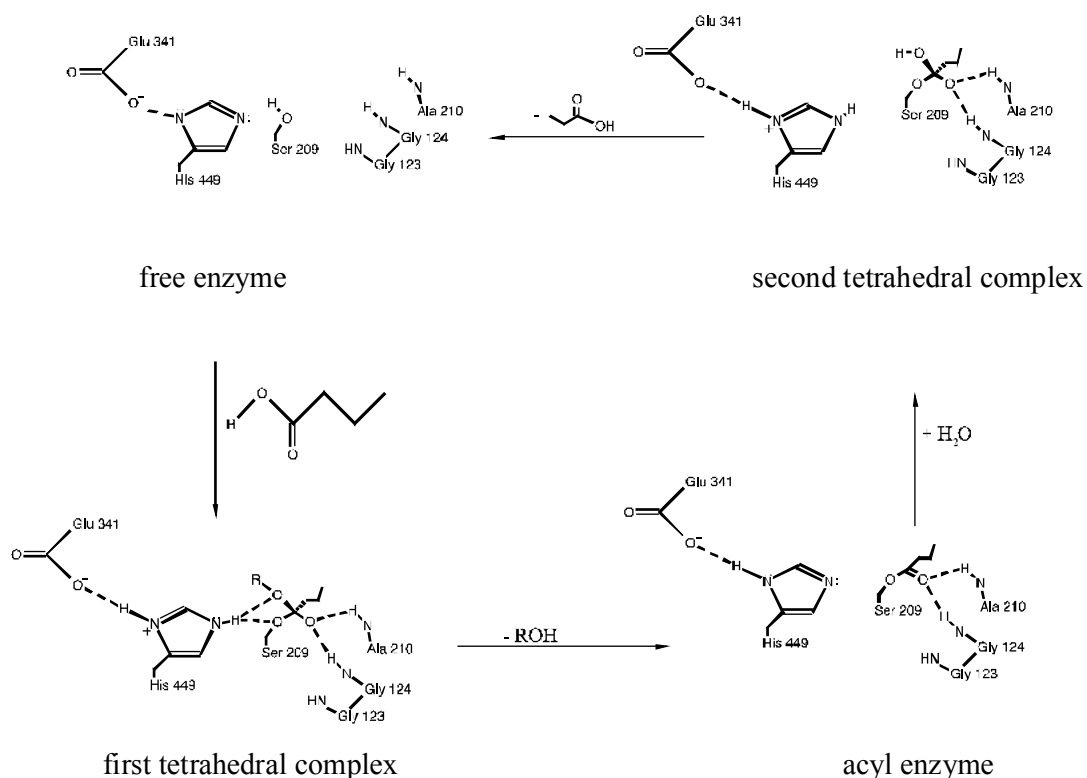


Figure 6 Schematic drawing of the mechanism of the catalytic triad in lipases.

### 1.1.2.5. SUBSTRATE BINDING

The binding of substrates is accomplished by three regions in the lipase, where the substrates can be fixed spatially oriented:

- a hydrophobic pocket
- a tunnel above  $\alpha$ -helix C
- the  $M_L$ -region above  $\beta$ -strand 5

The large substituent binds to the hydrophobic pocket, whereas the medium-sized substituent binds to the  $M_L$ -region. The acyl chain of the ester binds to the tunnel. Following a substrate mapping of lipases, Kazlauskas and coworkers developed a model to predict the enantioselectivity of lipases towards secondary alcohols (Kazlauskas, Weissfloch et al. 1991) (see Figure 7).

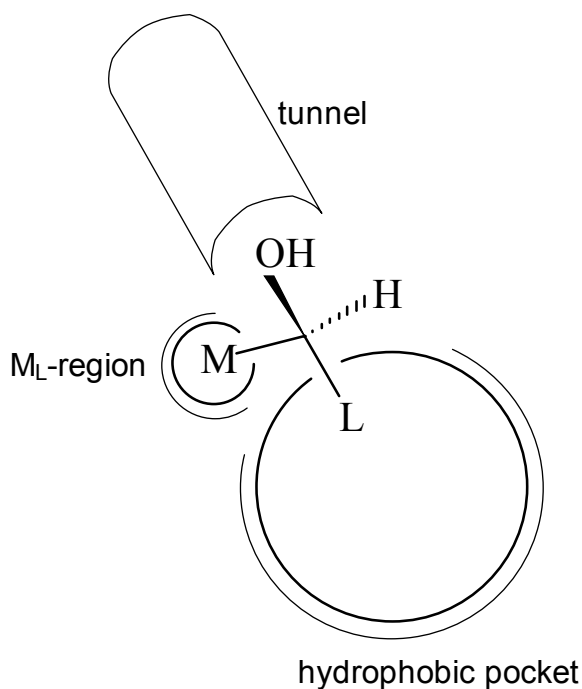


Figure 7 Kazlauskas rule for the prediction of the enantioselectivity of lipases towards secondary alcohols (Cygler, Grochulski et al. 1994).

When the hydroxyl group of the alcohol points forward out of the plane of the paper, only the enantiomer with the large substituent on the right side will be favored by the lipase.



*Binding of menthol to the active site:*

The collapse of the first tetrahedral transition state releases the alcohol from the substrate (see chapter 1.1.2.4). Thus, the enantioselectivity of a lipase towards the alcohol is determined during the formation or the collapse of the first tetrahedral intermediate, whichever step is slower. This tetrahedral intermediate can be mimicked by phosphonates. O-1R-menthyl-hexylphosphonate (mimicking the fast reacting enantiomer) and O-1S-menthyl-hexylphosphonate (mimicking the slow reacting enantiomer) covalently bind to the enzyme and, after crystallization, give a picture of the active site accommodating the fast reacting enantiomer as well as the slow reacting enantiomer. The isopropyl residue of the slow reacting (+)-1S-menthyl-hexylphosphonate turns away the imidazole ring of the catalytically active histidine by about 60°. Thereby, the substrate alcohol oxygen atom lies out of the hydrogen bonding distance and, therefore, cannot build the second hydrogen bond (see Figure 8).

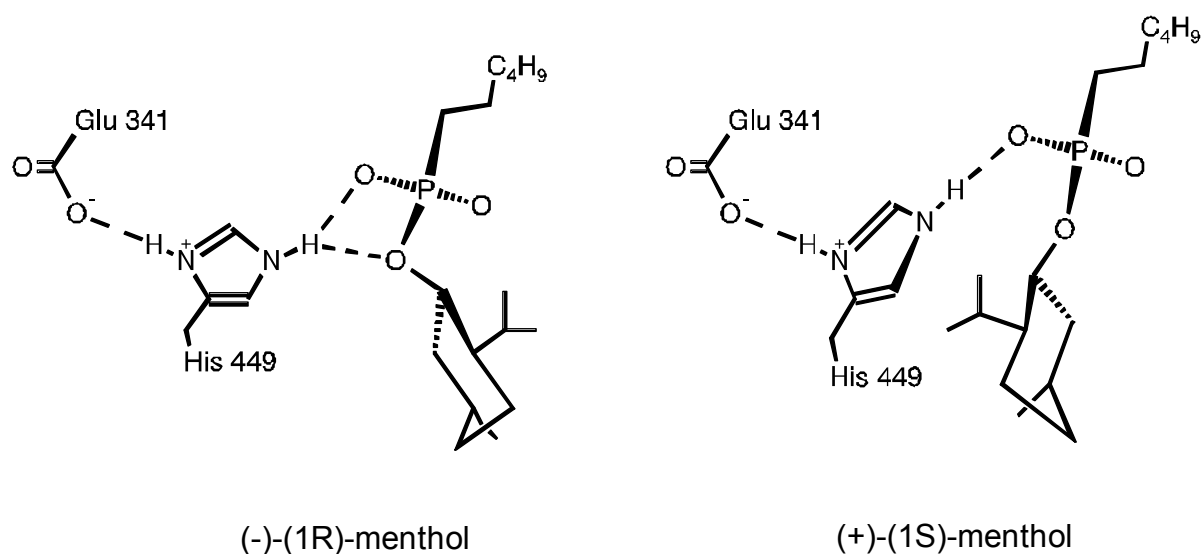


Figure 8      Structure of the (-)-1R- and (+)-1S-menthyl-hexylphosphonates in the active site of the *Candida rugosa* lipase, respectively (Kazlauskas 1994).

### 1.1.2.6. INTERFACIAL ACTIVATION

Lipases do not follow the Michaelis-Menten kinetics, but rather show a sigmoidal increase in reaction velocity with increasing substrate concentration. Thus, lipases seem to have to be activated before they can take part in biochemical reactions.

The water-soluble lipases take part in the catabolism of lipids. Thus, lipase reaction takes place at a water-oil interface. This led to a special mechanism of enzyme-substrate interaction, the interfacial activation. A lid, covering the active site of lipases in hydrophilic solvents, only opens at the water-oil interface, giving access to the active site for the substrates (see Figure 9). With no substrates present, the lid is closed and the enzyme is inactive. In the presence of substrates, a water-oil interface exists. This interface leads to the opening of the lid and the activation of the lipase. The lid consists of one or two amphiphilic  $\alpha$ -helices, depending on the lipase.

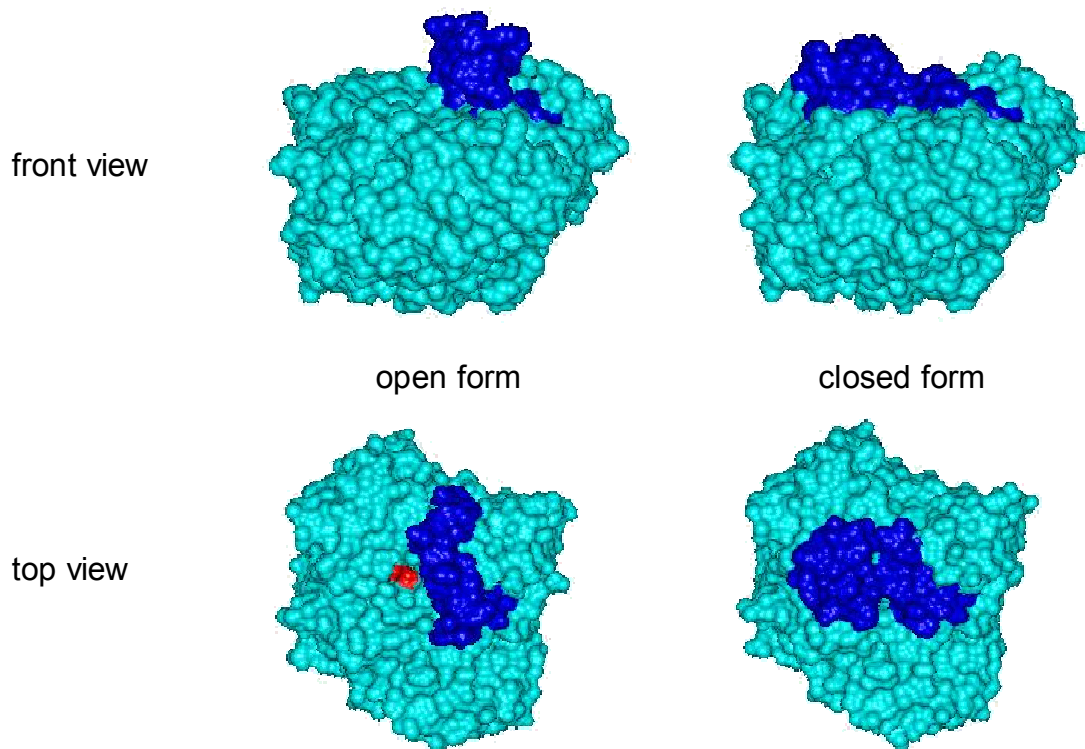


Figure 9 Molecular surface of the *Candida rugosa* lipase in the open and the closed form, respectively. The active site is shown in red, the lid in blue.

In lack of a lid, the *Pseudomonas aeruginosa* lipase and the *Fusarium solani* cutinase can not be activated at an interface.

### 1.1.3. STEREOSELECTIVITY

Stereoselectivity deals with the three dimensional structure of molecules. The isomerism due to differences in the spatial arrangement of atoms without any differences in connectivity or bond multiplicity between the isomers is referred to as stereoisomerism. Therefore, stereoisomers possess identical constitution, but differ in the arrangement of their atoms in space.

Generally, three kinds of stereoisomerism are distinguished:

- optical isomers
- *cis-trans* isomers
- conformation isomers

Enantiomers and diastereoisomers are counted among the optical isomers. Enantiomers are pairs of molecular entities which are mirror images of each other and non-superposable, whereas diastereoisomers (or diastereomers) are stereoisomers not related as mirror images. Diastereoisomers are characterized by differences in physical properties, and by some differences in chemical behavior towards achiral as well as chiral reagents.

*Cis-trans* isomers are stereoisomeric olefins or cycloalkanes (or hetero-analogues) which differ in the positions of atoms (or groups) relative to a reference plane: in the *cis*-isomer the atoms are on the same side, in the *trans*-isomer they are on opposite sides.

Conformation isomers are made up of the bisecting conformation (or eclipsing conformation) isomers and the envelope conformation isomers.

The preferential formation in a chemical reaction of one stereoisomer over another is referred to as stereoselectivity. When the stereoisomers are enantiomers, the phenomenon is called enantioselectivity and is quantitatively expressed by the enantiomeric excess; when they are diastereoisomers, it is called diastereoselectivity and is quantitatively expressed by the diastereoisomeric excess.

## 1.2. PRESSURE

To understand the effect of pressure on structure, dynamics, and activity of enzymes, NMR (Akasaka, Li et al. 1999; Li, Yamada et al. 1999; Inoue, Yamada et al. 2000; Kalbitzer, Görler et al. 2000) as well as molecular modeling studies (Kitchen, Reed et al. 1992; van Gunsteren and Brunne 1993; Paci and Marchi 1996; Floriano, Nascimento et al. 1998) have been carried out.

### 1.2.1. NMR

NMR revealed that, in general, helical and loop regions show higher compressibility and volume fluctuation than  $\beta$ -sheets (Akasaka, Li et al. 1999; Kalbitzer, Görler et al. 2000). Applying  $^{15}\text{N}/^1\text{H}$  2D-NMR exhibited that reversible structural changes in Ras guanine nucleotide dissociation stimulator (RasGDS) occur at pressures above 500 bar (Inoue, Yamada et al. 2000). These changes were mainly observed within cavity regions and putatively play a significant role in protein-protein interactions like receptor binding (Inoue, Yamada et al. 2000).

### 1.2.2. MOLECULAR MODELING

Molecular modeling studies have investigated the compressibility of proteins (Paci and Marchi 1996; Kharakoz 2000) or the pressure denaturation of proteins (Zipp and Kauzmann 1973; Hummer, Garde et al. 1998). Only very small changes in average protein structure and internal energy are observed in molecular dynamics simulations due to the low compressibility of proteins (Kitchen, Reed et al. 1992; van Gunsteren and Brunne 1993). Additionally, the compressibility of proteins depends on the activity of water (Kharakoz 2000). The compressibility of water surrounding hydrophobic groups on the other hand seems to be much larger than that of water hydrating charged groups or even bulk water (Kitchen, Reed et al. 1992). Therefore, the effect of pressure on proteins or solvents, is best described, at least at pressures up to 100 bar, with rather local than global effects. Increasing the pressure above 500 bar, protein unfolding seems to be driven to a large extent by increasing the exposed hydrophobic surface area of the protein (Kitchen, Reed et al. 1992; Hummer, Garde et al. 1998; Li, Yamada et al. 1999; Inoue, Yamada et al. 2000). The energy of elastic deformation, induced by creating an internal cavity is the beginning

of pressure denaturation. It can exceed the thermal motion energy (2.5 kJ/mole at room temperature) by an order of magnitude (Kharakoz 2000).

### 1.2.3. PRESSURE DENATURATION OF PROTEINS

In contrast to heat denaturation with a nonpolar molecule to be transferred from a nonpolar environment in the core of a protein towards its polar surface and, therefore, polar solvent, pressure denaturation can be understood as the transfer of water molecules into the protein (Hummer, Garde et al. 1998). Cavities in the protein structure are then filled with water molecules destabilizing the protein and, eventually, unfolding it.

Proteins can be denatured at pressures as low as 500 bar (Inoue, Yamada et al. 2000) or can remain active up to 10.000 bar (Kitchen, Reed et al. 1992). Pressure-denatured proteins retain more intact structural elements than heat denatured proteins (Zhang, Peng et al. 1995). In general, pressure denaturation is accompanied with increased hydrodynamic radius (Hummer, Garde et al. 1998). In 1987, for the first time Kauzmann et al. questioned the long established dogma that globular proteins are stabilized by a hydrophobic core (Kauzmann 1959).

To further examine the consequences of pressure on protein structure, various molecular dynamics approaches were performed. Floriano et al. carried out molecular dynamics simulations of metmyoglobin, an experimentally thoroughly studied protein (Zipp and Kauzmann 1973). The pressure scale to which the protein was exposed ranged from 1 bar to 12.000 bar over a time scale of 100 ps. Using the AMBER force field (Weiner, Kollman et al. 1984), periodic boundary conditions, and implicit water Nosè-Hoover dynamics were calculated (Floriano, Nascimento et al. 1998) (NPT ensemble: the number of particles, the pressure, and the energy are constant quantities). A decrease of  $\alpha$ -helical hydrogen bonds (from 81 at 1 bar to 21 at 12000 bar, respectively) indicated an overall loss of helical structure and, therefore, protein unfolding. The observed volume change was stable at about 4.6% for 1 to 6000 bar, and the rms-value was less than 2.0 Å for 1 to 1000 bar. However, it was found that the aromatic solvent accessibility significantly increased between 6000 and 7000 bar.

Kitchen and coworkers calculated different compressibilities of water molecules hydrating charged, polar, or nonpolar functional groups in low (111 bar) and high pressure molecular dynamics simulations (10274 bar) of basic pancreatic trypsin

inhibitor (BPTI) using the computer program IMPACT (Kitchen, Reed et al. 1992). Simulating the lipase from *Rhizomucor miehei in vacuum*, water, and methyl hexanote, Norin et al. studied the influence of different environments (Norin, Haeffner et al. 1994).

### **1.3. INTRODUCTION TO MOLECULAR MODELING**

Molecular modeling investigates molecular systems at the atomic level in order to understand their role in chemical and biological processes. This can be done using paper and pencil, mechanical models or computers. Today, several computer based methods of molecular modeling are at hand.

#### **1.3.1. QUANTUM MECHANICAL METHODS**

Quantum mechanics is based on solving the Schrödinger equation. In contrast to empirical force field methods, quantum mechanics explicitly represents the contribution of the electrons. The molecular orbital theory is the most prominent theory used in quantum mechanics. Other theoretical models used in quantum mechanics are the Hückel theory or the valence bond theory.

##### *Semi-empirical*

Semi-empirical methods use experimental data to simplify the solution of the Schrödinger equation. They use parameters derived on numerous experiments on appropriate model systems.

##### *Ab initio*

Ab initio methods only rely on mathematical approximations to exactly solve the Schrödinger equation. This is the most exact theoretical method, but as it requires exhaustive computational power, it is restricted to only small systems.

### 1.3.2. MOLECULAR MECHANICS METHODS

As soon as large molecules are to be investigated, quantum mechanics calculations get much too time-consuming.

Molecular mechanics methods are empirical, completely parameterized methods using force fields. The force fields in molecular mechanics are algebraic expressions, which describe how changes in the bond length or angles etc. affect the potential energy and are based upon experimental data (X-ray or NMR 3D structures, thermodynamics) and quantum mechanical methods. Atoms and bonds are treated as balls and springs, respectively. The potential energy of a molecule is represented as a function of geometric variables. As the movement of electrons is much faster compared to the movement of nuclei, the motions of the electrons and atomic nuclei can be treated separately. This is called the Born-Oppenheimer approximation. Although molecular mechanics cannot predict properties of molecular systems which depend on the electronic distribution in a molecule, contributions of the electrons are included into the parameters used. The interaction between molecules is described by quite simple analytical functions, derived from the classical mechanics. Hooke's law is used to describe the vibrational motion of a bond and the Van der Waals radius to account for atom-atom repulsions.

#### *Energy minimization*

Usually, the potential energy of a molecular system is a multidimensional function of the coordinates. It is represented by the potential energy surface, the hypersurface, which displays the change in energy with the coordinates. It is evident, that the hypersurface has one global and several local minima, each corresponding to a stable state of the system. Numerous minimization algorithms are known, all of which only can go downhill on the hypersurface. Therefore, only local minima can be found.

#### *Molecular dynamics method*

Molecular dynamics methods simulate the real motions of systems of atoms using Newton's equations of motion. The interaction potential is used to calculate the forces between atoms or molecules. The equations of motion are then used to compute the velocities and movements of the system. Starting with a set of coordinates and a subsequent energy minimization, only positions of, and forces on the atoms are known. To calculate velocities and new positions of the atoms, Newton's second law

is used. Therefore, time has to be taken into consideration explicitly and in very small time steps. Having calculated an adequate number of cycles, the equations of motion are integrated numerically and the molecular system can be animated with a simulated trajectory.

#### *Monte Carlo method*

In Monte Carlo simulations, configurations of the molecular systems are generated randomly in every step. Each configuration is assessed by its probability compared to only its direct predecessor. Lower energy states are accepted in any way, states with higher energies are accepted only if the Boltzmann factor of the energy difference is bigger than a randomly generated number.

### **1.3.3. APPLICATION OF MOLECULAR MODELING TO PROTEINS**

Molecular modeling techniques are applied to various problems in chemistry, pharmaceuticals or biology.

Molecular docking for example, tries to predict the structure of intermolecular complexes. The mode of action of protein inhibitors can be studied using molecular docking. This can be done either manually using an interactive simulation software or by automatic docking algorithms. On the other hand, new inhibitors or ligands can be designed to fit exactly into the binding site.

Applied to the biology, molecular modeling studies (Kazlauskas 2000) on the stereoselectivity of lipases for example, mostly perform conformational analysis (Uppenberg, Ohrner et al. 1995; Holmquist, Haeffner et al. 1996; Botta, Cernia et al. 1997; Yagnik, Littlechild et al. 1997), the rational design of the active site (Scheib, Pleiss et al. 1998; Scheib, Pleiss et al. 1999; Manetti, Mileto et al. 2000) or substrates (Stadler, Kovac et al. 1995; Tafi, van Almsick et al. 2000) or energy based evaluation of enantioselectivity (Haeffner, Norin et al. 1998).



## 2. PURPOSE

For the stereoselectivity of *Pseudomonas cepacia* lipase towards secondary alcohols, a quantitative model has been developed to predict the ranking of substrates by enantioselectivity (Schulz, Pleiss et al. 2000). According to this model, the distance between the catalytically active histidine and the substrate ester group of the non-preferred enantiomer correlates to the experimentally determined stereoselectivity. Schulz et al. found that low and high E-values correlate to small and large distances between the H286-N $\epsilon$  atom and substrate alcohol-oxygen atom, respectively.

In this work, the enantioselectivity of the *Candida rugosa* lipase is investigated. *Candida rugosa* lipase displays a broad substrate spectrum (Kazlauskas and Bornscheuer 1998) with the *Candida rugosa* lipase-catalyzed chiral resolution of ( $\pm$ )-menthol representing one of the most thoroughly studied reactions (Baratti, Buono et al. 1988; Salleh, Basri et al. 1993; Tseng, Kazlauskas et al. 1994; Kamiya and Goto 1997; Furukawa and Kawakami 1998). As a model reaction, esterification of racemic menthol with propionic acid anhydride in chloroform was investigated at 1, 10, 50, and 100 bar, respectively. A significant decrease in enantioselectivity of the lipase was observed for increasing pressure.

To date, no study has been reported providing a model for the pressure dependence of the enantioselectivity of *Candida rugosa* lipase.

In this work, molecular dynamics methods are applied to develop a model of the pressure dependence of *Candida rugosa* lipase-catalyzed enantioselectivity. In order to rationalize the findings in the biocatalytic part of this work, molecular dynamics simulations of the lipase were performed in organic solvent (2289 molecules of chloroform) containing 244 essential water molecules and 17 sodium ions applying the same pressures as in the experiment.

### 3. MATERIALS AND METHODS

#### 3.1. CHEMICALS

company name	chemical used
Fluka, Inc. Buchs / Switzerland	gum arabic potassium dihydrogen phosphate ( $\text{KH}_2\text{PO}_4$ ) <i>di</i> -sodium hydrogen phosphate ( $\text{Na}_2\text{HPO}_4$ ) sodium hydroxide ( $\text{NaOH}$ ) hydrogen chloride ( $\text{HCl}$ ) tributylin ( $\text{C}_{15}\text{H}_{26}\text{O}_6$ ) propionic acid anhydride ( $\text{C}_6\text{H}_{10}\text{O}_3$ )
Haarmann & Reimer, Inc. Holzminden / Germany	rac-menthol (+)-menthol (-)-menthol
Riedel-de Haen, Inc. Seelze / Germany	chloroform ( $\text{CHCl}_3$ ) acetone ( $\text{C}_3\text{H}_6\text{O}$ )

#### 3.2. ENZYMES

company name	enzyme used
Amano Enzyme, Inc. Nagoya / Japan	lipase Amano AY

### 3.3. EQUIPMENT

company name	equipment used
Riedel-de Haen	Karl-Fischer titration unit HYDRANAL <sup>®</sup> reagent
Metrohm	614 Impulsomat 620 pH-Meter 649 Stirrer 665 Dosimat
Amersham pharmacia biotech	REC 112 Recorder
Scientific Industries	vortex genie 2
Sartorius	balance basic, MC1 Research RC 210 D
Fisons Instruments	gas chromatograph mega 2 series A200 autosampler EL980 FID-detector
Chromatographie Service, GmbH	FS Cyclodex $\beta$ -I/P (length: 50m; inner diameter: 0,25mm; outer diameter: 0,38 mm)
ISCO, Inc.	supercritical fluid extractor model 500D syringe pump series D pump controller
Eppendorf, Inc.	eppendorf tubes, 2 ml Centrifuge 5417 C
Schott, Inc.	glass ware

company name	equipment used
Infors AG	HT OU Tron water bath
IKA Labortechnik	ETS-D4 fuzzy temperature controller RCT basic stirrer

### 3.4. HARDWARE

computer manufacturer	workstation	CPU	RAM
Digital	Alpha 433au	Alpha 21164	128 MB
Silicon Graphics	Indigo <sup>2</sup>	MIPS-R10000	128 MB
	Indy	MIPS-R4400	64 MB

### 3.5. SOFTWARE

application	software	www link
protein structures	PDB	<a href="http://www.rcsb.org/pdb">http://www.rcsb.org/pdb</a>
energy minimization	GROMOS96	<a href="http://www.c4.ethz.ch/gromos">http://www.c4.ethz.ch/gromos</a>
	sybyl 6.4	<a href="http://www.tripos.com">http://www.tripos.com</a>
molecular dynamics simulation	GROMOS96	<a href="http://www.c4.ethz.ch/gromos">http://www.c4.ethz.ch/gromos</a>
	sybyl 6.4	<a href="http://www.tripos.com">http://www.tripos.com</a>
docking	sybyl 6.4	<a href="http://www.tripos.com">http://www.tripos.com</a>
visualization	insightII	<a href="http://www.biosym.com">http://www.biosym.com</a>

application	software	www link
structure analysis	PROCHECK	<a href="http://www.biochem.ucl.ac.uk/~roman/procheck/procheck.html">http://www.biochem.ucl.ac.uk/~roman/procheck/procheck.html</a>
chromatography	Chrom-Card	<a href="http://ceinstruments.it">http://ceinstruments.it</a>

### 3.6. BIOCATALYTIC METHODS

#### 3.6.1. EXPERIMENTAL SETUP

The experimental setup for the chiral resolution of racemic ( $\pm$ )-menthol was as follows: 100 mg of ( $\pm$ )-menthol (640  $\mu$ mol) and 100 mg of propionic acid anhydride (768  $\mu$ mol) were mixed with 500 mg of Amano AY lipase in a 10 ml sample tube. For pressure regulation, an ISCO piston pump was used. The tube was placed in a water bath at 40°C and shaken at 300 rpm. Experiments were started as follows. First, the inlet as well as the outlet valves were closed and the corresponding pressure was built up with the piston pump. Subsequently, the inlet valve was opened in order to pressurize the sample tube. To account for the small systematic leak, the inlet valve remained open during the experiment. The water bath was then shaken with 300 rpm. Each experiment was terminated by closing the inlet valve and opening the outlet valve. The sample was collected in an Eppendorf tube (see Figure 10).

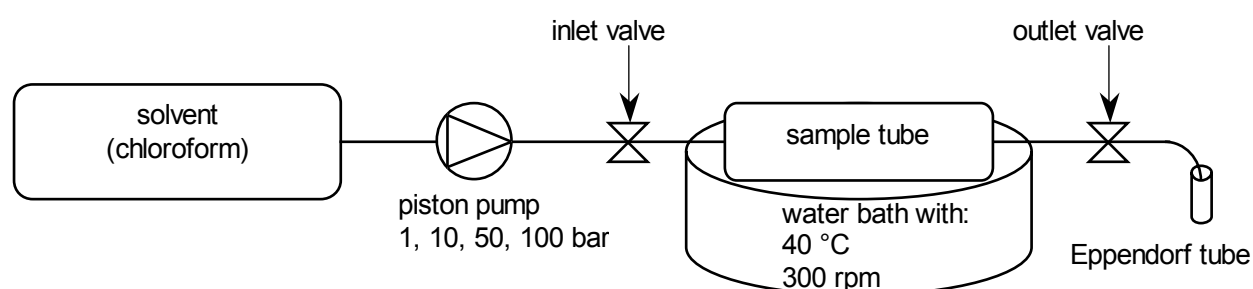


Figure 10 Schematic drawing of the experimental setup.

Due to the enhanced pressures under which the experiments were carried out, it was not possible to take samples during the experiment. Therefore, each biotransformation was set up as described and stopped after 24 and 48 hours, respectively. The samples were analyzed by gas chromatography with the

conversion rate held approximately constant at about 20 %. 0.5  $\mu\text{l}$  aliquots of the experimentally obtained biotransformation assay were sampled by gas chromatography. The data were collected 6-fold. For each data set, the enantioselectivity,  $E$ , was calculated with the enantiomeric excess of the product,  $ee_p$ , and the enantiomeric excess of the substrate,  $ee_s$ , from the following equations (Chen, Fujimoto et al. 1982; Chen, Wu et al. 1987):

$$E = \frac{\ln [(1-c)(1-ee_s)]}{\ln [(1-c)(1+ee_s)]} \quad \text{with:} \quad c = \frac{ee_s}{ee_s + ee_p}$$

### 3.6.2. SAMPLE REACTION

The reaction of lipase-catalyzed esterification of racemic ( $\pm$ )-menthol with propionic acid anhydride can be described as follows (see Figure 11):

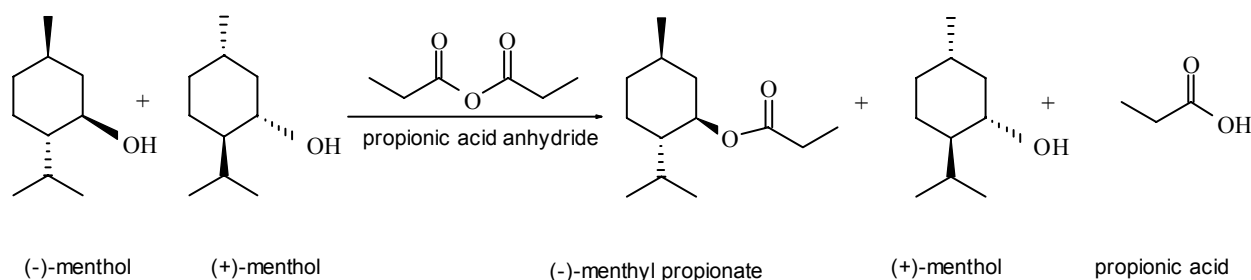


Figure 11 Kinetic resolution of racemic ( $\pm$ )-menthol with propionic acid anhydride.

In the main reaction, one molecule of (-)-menthol is esterified with propionic acid anhydride yielding (-)-menthylpropionate and propionic acid. However, if propionic acid is involved into the esterification of menthol, water can be formed as a byproduct. No molecular sieve was applied to prevent the production of water. The activity of the lipase was tested using a pH-stat assay (see chapter 3.6.3). The water content of the commercially available lipase preparation of the *Candida rugosa* lipase was estimated by Karl-Fischer titration (see chapter 3.6.4).

**3.6.3. ENZYME ACTIVITY (PH-STAT ASSAY)**

10 mg of the lipase preparation were dissolved in 1 ml 20 mM phosphate buffer, pH 7. The pH-stat was filled with 20 ml of assay solution A (2 % gum arabicum, 200 ml H<sub>2</sub>O, 3 ml tributyrin) with the pH adjusted to pH 7.2. After addition of 100 µl of the dissolved lipase preparation, pH was titrated with 0.01 M NaOH.

**3.6.4. WATER CONTENT (KARL-FISCHER TITRATION)**

Karl-Fischer titration was used to determine the water content in the commercially available lipase preparation. As any ambient moisture falsifies the results, it is essential to prevent additional moisture to adsorb or absorb to the sample. A sample is reacted with a Karl-Fischer reagent which contains iodine. Water present in the sample will react with the iodine and therefore continuously deplete the iodine. As long as iodine is present in the measured sample, the test will be sustained with current passing between two platinum electrodes. With no iodine present in the sample, no current will pass through the sample and the electrodes therefore will be depolarized and the test is complete. The corresponding potentiometric change is used to determine the titration end point and calculate the water concentration. The duration of the test indicates the water content.

The titration itself was done by Erika Denzel at the Institute for Food Technology, University of Hohenheim, research group of Dipl. Ing. Nils Langer.

**3.6.5. ENANTIOMERIC EXCESS (GAS CHROMATOGRAPHY)**

The analysis of the samples after 24 and 48 hours, respectively, was performed on a Fisons Instruments gas chromatograph using a FID with a β-cyclodex column. The chromatography column was heated to 125°C and held isotherm at 125°C for the measurement of (+)- and (-)-menthol and (+)- and (-)-menthyl propionate. The temperature of the injector as well as the detector was 200°C. The carrier gas used was hydrogen, make up gas was nitrogen.

### 3.7. MOLECULAR DYNAMICS SIMULATION METHODS

In order to reproduce the experimental setup in the biocatalysis section of this work (see Figure 10, Figure 11) as accurately as possible in the molecular modeling part, the simulation assembly contained the *Candida rugosa* lipase, 244 essential water molecules, 17 sodium ions and 2289 chloroform molecules. Due to the extremely large size of the simulated system of 17.320 atoms altogether, only molecular dynamics simulations were applicable to the task of studying the biocatalysis experiment using computer based simulation methods (see 1.3, page 17). Molecular dynamics simulations in this work were calculated using the program package GROMOS96. GROMOS96 is a script based program package for biomolecular simulations. Each program needs several input files. E.g. in the case of a molecular dynamics simulation of the molecular system XYZ, the shell script *jemXYZ.sh* is executed provided the parameter file *iemXYZ.dat*, the molecular topology file *XYZmta.dat*, the coordinate file *XYZcoord.dat*, the atomic reference positions file *XYZrefcoord.dat* and eventually the atomic restrained positions file *XYZrescoord.dat* are given all of which are referenced in the shell script file *jemXYZ.sh*.

#### 3.7.1. THE GROMOS96 FORCE FIELD

The standard physical interaction function in GROMOS96 has the following form:

$$V^{\text{phys}}(\mathbf{r};\mathbf{s}) = V^{\text{bon}}(\mathbf{r};\mathbf{s}) + V^{\text{nonbon}}(\mathbf{r};\mathbf{s})$$

with 
$$V^{\text{bon}}(\mathbf{r};\mathbf{s}) = V^{\text{bond}}(\mathbf{r};\mathbf{s}) + V^{\text{angle}}(\mathbf{r};\mathbf{s}) + V^{\text{har}}(\mathbf{r};\mathbf{s}) + V^{\text{trig}}(\mathbf{r};\mathbf{s})$$

Bonded ( $V^{\text{bon}}$ ) and non-bonded ( $V^{\text{nonb}}$ ) interaction terms contribute to the total potential energy ( $V^{\text{phys}}$ ) of a particle with coordinates  $\mathbf{r}$ , where the bonded interaction ( $V^{\text{bon}}$ ) consists of bond-stretching ( $V^{\text{bond}}$ ) (see Figure 12), bond-angle bending ( $V^{\text{angle}}$ ) (see Figure 12), harmonic improper dihedral-angle bending ( $V^{\text{har}}$ ) (see Figure 13) and trigonometric dihedral-angle torsion ( $V^{\text{trig}}$ ) and the non-bonded van der Waals and electrostatic interaction ( $V^{\text{nonb}}$ ) (see Figure 15) (van Gunsteren, Billeter et al. 1996).



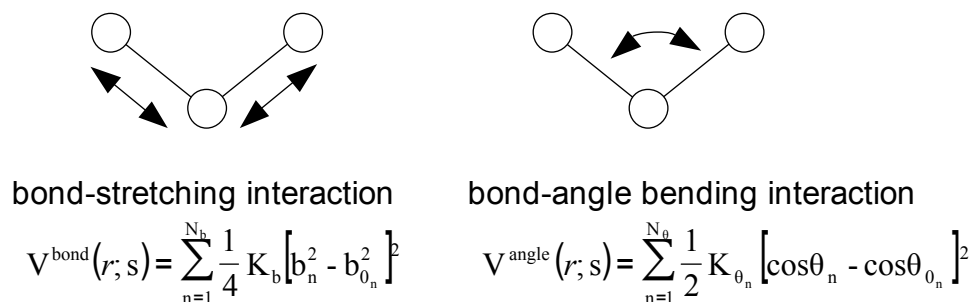
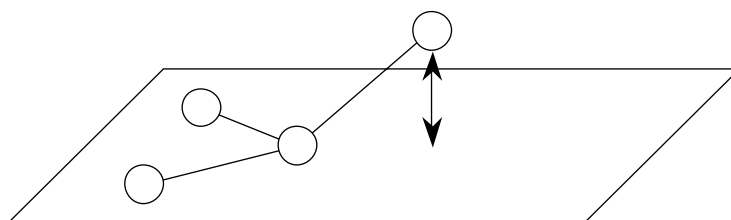


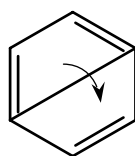
Figure 12 Bond-stretching ( $V^{\text{bond}}$ ) and bond-angle bending ( $V^{\text{angle}}$ ) interaction contribution to the potential energy. The actual bond length of the bond  $n$  between atoms with sequence numbers  $i$  and  $j$  is denoted by  $b_n$ . The actual bond-angle value of the bond angle between atoms with sequence numbers  $i$ ,  $j$  and  $k$  is denoted by  $\theta_n$ .



improper dihedral-angle bending interaction

$$V^{\text{har}}(r; s) = \sum_{n=1}^{N_\xi} \frac{1}{2} K_{\xi_n} [\xi_n - \xi_{0_n}]^2$$


Figure 13 Improper dihedral-angle bending (out of plane) ( $V^{\text{har}}$ ) interaction contribution to the total potential energy. The actual dihedral angle value of the dihedral angle between atoms with sequence numbers  $i$ ,  $j$ ,  $k$  and  $l$  is denoted by  $\xi_n$ . For example, the atoms C-CA-N-O in an amino acid residue are kept near a planar configuration by defining an improper dihedral with  $\xi_0 = 0^\circ$ .



improper torsional bending interaction

$$V^{\text{trig}}(r; s) = \sum_{n=1}^{N_\phi} K_{\phi_n} [1 + \cos(\delta_n) \cos(m_n \phi_n)]$$

Figure 14 Trigonometric dihedral-angle torsion (improper torsional bending) ( $V^{\text{trig}}$ ) contribution to the total potential energy. The actual dihedral angle value of the dihedral angle between atoms with sequence numbers  $i$ ,  $j$ ,  $k$  and  $l$  is denoted by  $\phi_n$ .  $\delta_n$  and  $m_n$  are restricted to 0 or  $\Pi$ . For example, improper torsional terms are commonly used to keep a benzene ring planar.



$$V^{\text{nonb}}(r, s) = \sum_{\text{nonbonded pairs}(i, j)} \left( \left\{ \left[ \frac{C_{12}(i, j)}{(r_{ij}^{4D})^6} - C_6(i, j) \right] \frac{1}{(r_{ij}^{4D})^6} \right\} + \left\{ \frac{q_i q_j}{4\pi\epsilon_0\epsilon_1} \left[ \frac{1}{r_{ij}^{4D}} - \frac{1/2 C_{\text{rf}} (r_{ij}^{3D})^2}{R_{\text{rf}}^3} - \frac{1 - 1/2 C_{\text{rf}}}{R_{\text{rf}}} \right] \right\} \right)$$

Figure 15 Non-bonded van der Waals and electrostatic interaction ( $V^{\text{nonb}}$ ) contribution to the total potential energy. The first part of the formula corresponds to the Lennard-Jones potential (van der Waals interaction), the second part of the formula represents the Coulomb potential (electrostatic interaction).

The GROMOS96 force field in its A-version has been developed for the simulation of proteins, nucleotides or sugars in aqueous or apolar solutions (van Gunsteren, Billeter et al. 1996).

### 3.7.2. PERIODIC BOUNDARY CONDITIONS IN GROMOS96

In order to study bulk properties of a molecular system at a reasonable computing cost, periodic boundary conditions can be imposed on the molecular dynamics simulation. A box of a given number of particles, replicated in all directions, gives a periodic array which resembles very much a bulk solution of the particles inside the box. Forces of a molecules counterpart in the neighboring virtual box are calculated as if the molecular system would extend beyond the actual box. There are various box shapes possible granted that they can be packed in all three dimensions without spacing.

Furthermore, in case of a solute surrounded by solvent, it is desirable to keep the solvent layer as small as possible. Globular proteins therefore would best be simulated in a spherical box which can be approximated by the truncated octahedral box (see Figure 16) available in GROMOS96.

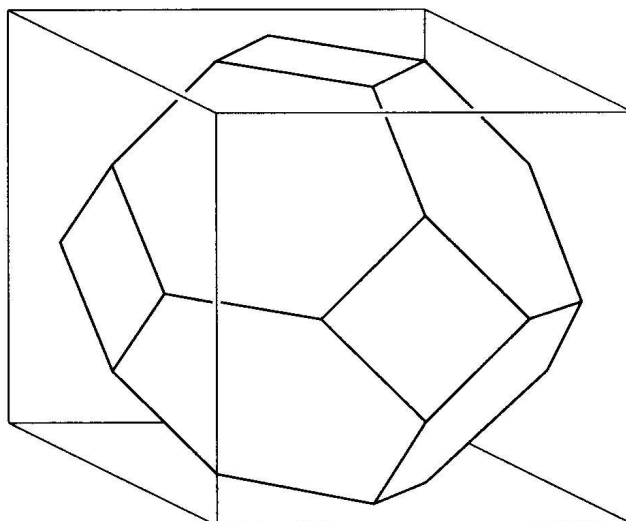


Figure 16 The truncated octahedron as a box shape resembling a sphere. It fills all space by translation operation of the central box in three dimensions (Leach 1996).

### 3.7.3. ENERGY MINIMIZATION

In most cases a pdb file (Bernstein, Koetzle et al. 1977) (see appendix 8.1) serves as the starting structure for a molecular dynamics simulation. Structures deposited in the pdb database are sets of coordinates either obtained by crystallography (over 80 %), by NMR (about 16 %) or, to a lesser extent, by theoretical modeling (2 %). The structures can be distorted by contacts between neighboring molecules in the crystal, by adding substrates, by adding hydrogen atoms which are not resolved by crystallography or further modification of the molecular system. Thus, the coordinates can contain unfavorable bond lengths, bond-angles or dihedrals which raise the potential energy of the molecular system and can, in the worst case, even lead to the abortion of the molecular dynamics simulation. Thus, energy minimization is used for obtaining a local minimum on the hypersurface for a molecular system (see chapter 1.3.2, page 18) (see Figure 17). In contrast, molecular dynamics simulations are used for obtaining the global energy minimum of a molecular system.

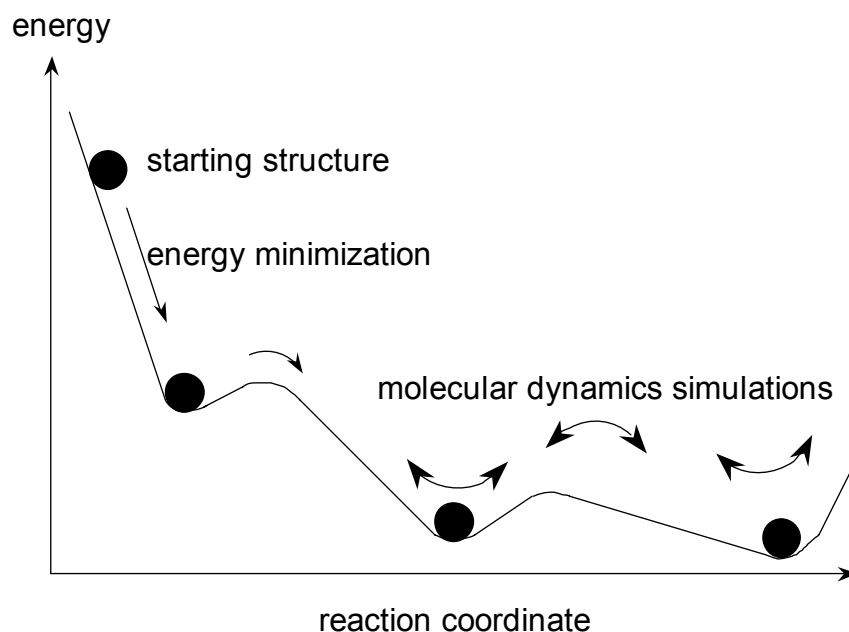


Figure 17 Energy minimization as opposed to molecular dynamics simulations, illustrated on an energy profile. Energy minimizations are only capable of finding the next local energy minimum, whereas molecular dynamics simulations can skip local energy minima and find the global energy minimum.

Various minimization algorithms are at hand for minimizing a molecular system which can be arranged into three general classes.

The direct search methods only utilize the energy function to find a local minimum. They converge very slowly.

The gradient methods utilize the energy function and its derivative to iteratively converge to the next minimum. Three subclasses of the gradient methods can be discerned. The steepest descents methods are the most simple and robust methods but they only perform well far from the minimum. The conjugate gradients methods utilize a local quadratic approximation to the function and are well suited for large systems like macromolecules. The variable metric or quasi-Newton methods utilize approximations to the inverse of the Hessian matrix of the second partial derivatives. They consume storage space and computing time and are therefore not suited for large systems.

The Second-order methods use the energy function, its derivative and the Hessian matrix. They too, like the quasi-Newton methods, are only applicable to small systems.

#### 3.7.4. MOLECULAR DYNAMICS ALGORITHM IN GROMOS96 (LEAP FROG ALGORITHM)

In order to integrate Newton's equation of motion, GROMOS96 applies the leap frog algorithm. Velocities at time  $t_n + \Delta t/2$  are calculated from the velocities at time  $t_n - \Delta t/2$  and accelerations at time  $t_n$ . Positions at time  $t_n + \Delta t$  are then calculated from the positions at time  $t_n$  and velocities at time  $t_n + \Delta t/2$ . Thus, velocities leap-frog over the positions (Leach 1996). Coupling to a temperature bath or a pressure bath can be applied, as well as distance constraints using the SHAKE method or periodic boundary conditions can be applied to the leap-frog algorithm.

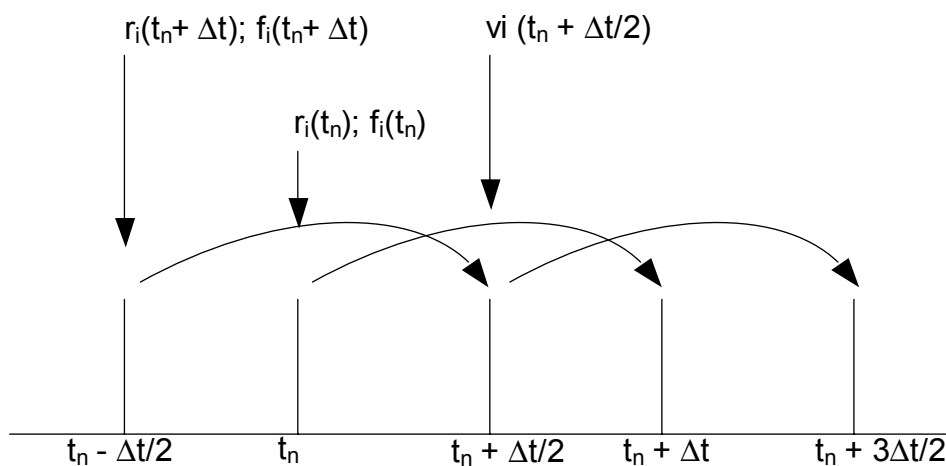


Figure 18 Integration scheme of the leap-frog algorithm for calculating Newton's equation of motion.

### 3.7.5. SETUP OF THE MD SIMULATIONS OF *CANDIDA RUGOSA* LIPASE IN GROMOS96

The starting conformation for the MD simulations was the crystal structure of the open form of *Candida rugosa* lipase (pdb-entry 1LPM; see appendix 8.1) (Cygler, Grochulski et al. 1994). Initially, the pdb file was edited to only hold the ATOM-part containing the solute and the HETATM-part containing the crystal water (marked blue in appendix 8.1). The inhibitor (-)-(1R)-menthyl hexyl phosphonate mimicking the fast reacting enantiomer (see chapter 1.1.2.5, Figure 8) was removed as well as the detergent N-acetyl-D-glucosamine. The file type was converted into GROMOS96 format (see appendix 8.2) using the program PROCS2 (see chapter 3.7.6.1). To fill free valences, the coordinate file was split into two parts with the first part containing the coordinates of the *Candida rugosa* lipase and the second part containing the coordinates of the essential water molecules. The programs PROGCH (see chapter 3.7.8.1) and PROGWH (see chapter 3.7.8.2) were used to fill the free valences for the *Candida rugosa* lipase and the essential water molecules, respectively. After generation of the hydrogen atoms, the two files were merged to contain the complete set of coordinates. Molecular topologies were calculated with the program PROGMT (see chapter 3.7.7). Essential water molecules were treated as being part of the solute. In order to neutralize the negatively charged system, 17 sodium ions were added by the program PROION (see 3.7.8.4). The program PROBOX (see 3.7.8.3) was used to fill a truncated octahedral box with the solute in its center either with water or with chloroform molecules as solvent. The sizes of the initial solvent boxes were 824 nm<sup>3</sup> for the molecular dynamics simulation with water as solvent and 880 nm<sup>3</sup> for the molecular dynamics simulation with chloroform as solvent. Molecular dynamics simulations were calculated using the program PROMD (see chapter 3.7.9). Specific snapshots of a configuration of the *Candida rugosa* lipase during the molecular dynamics simulations were converted to pdb-format with the program PROPDF (see chapter 3.7.6.2) and visualized with the program insightII (biosym). The analysis of the molecular dynamics simulation was done with the programs PROAVX (see chapter 3.7.10.1) and PROCOCX (see chapter 3.7.10.2) (see Figure 19).

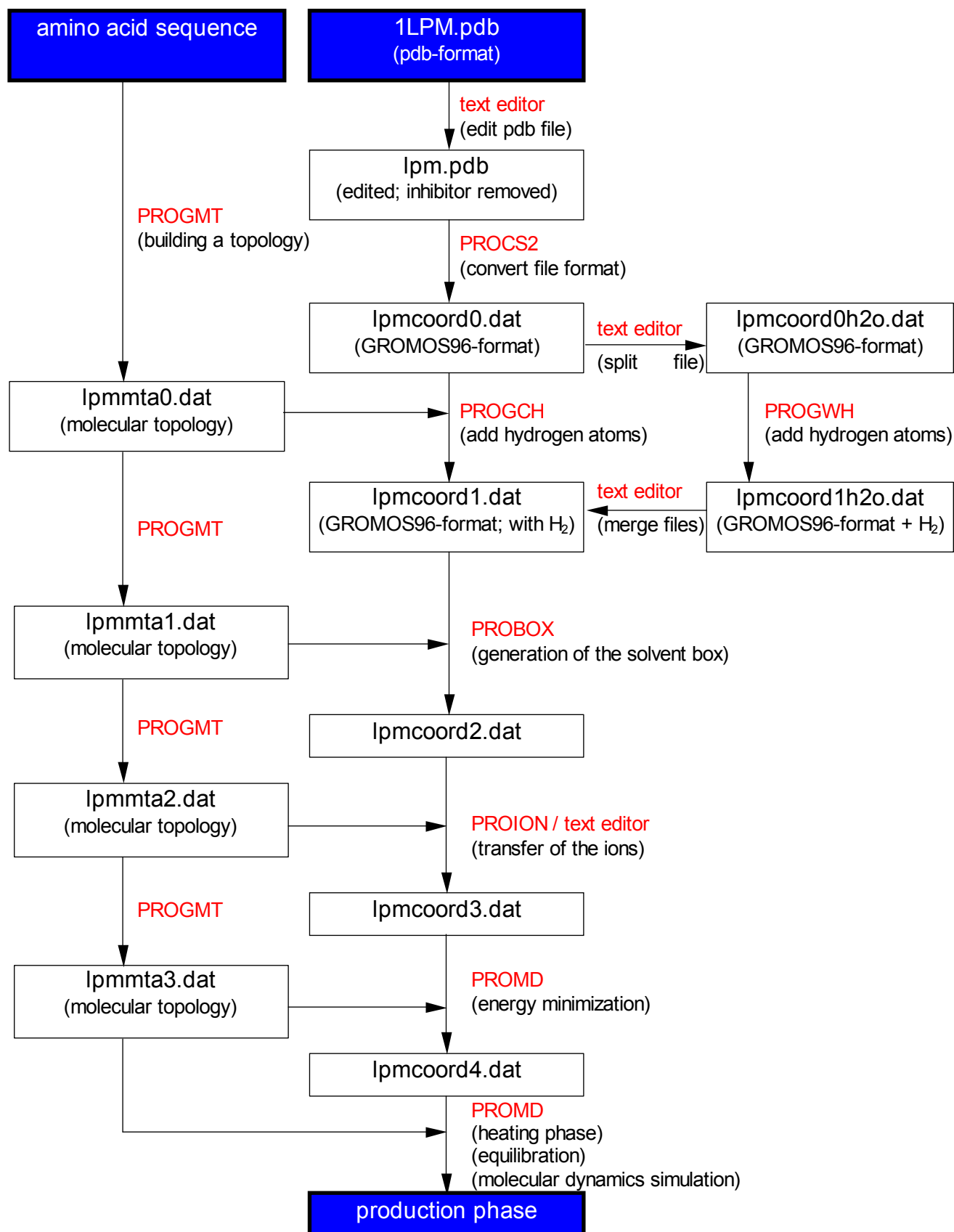


Figure 19 Setup of the simulation assembly of the open form of the *Candida rugosa* lipase for molecular dynamics simulation.

With this complex, steepest descents energy minimizations were performed 8 times for 3 steps, 7 times for 10 steps, and finally 50 steps, each with a time step of 2 fs (see Figure 20). Subsequently, the simulation assembly was heated to 1 K, 5 K, 10 K, 50 K, 100 K, and 300 K for each 25 steps using PROMD (see Figure 21). After an equilibration phase of 1 ps (500 steps), pressure coupling was set to 1 bar and the system was equilibrated for further 100 ps. Temperature coupling was set to 0.1 ps and pressure coupling was set to 0.5 ps with only the charged version of the GROMOS force field being used. Periodic boundary conditions (PBC) were applied in all simulations performed and the bond lengths were constrained applying the SHAKE algorithm. Nonbonded interactions were cut off after 8 Å and the nonbonded interaction pair list was updated every 10 simulation steps.

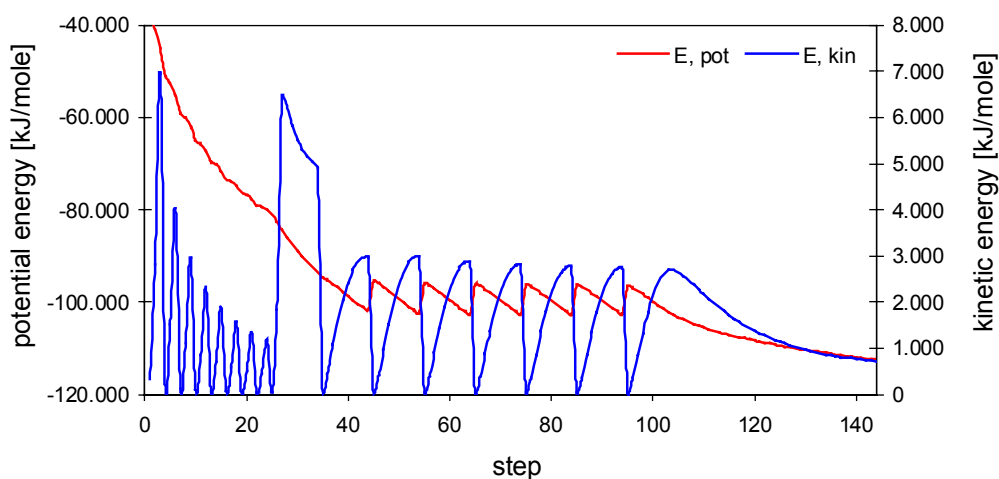


Figure 20 Trend of the potential and kinetic energy during the energy minimization.

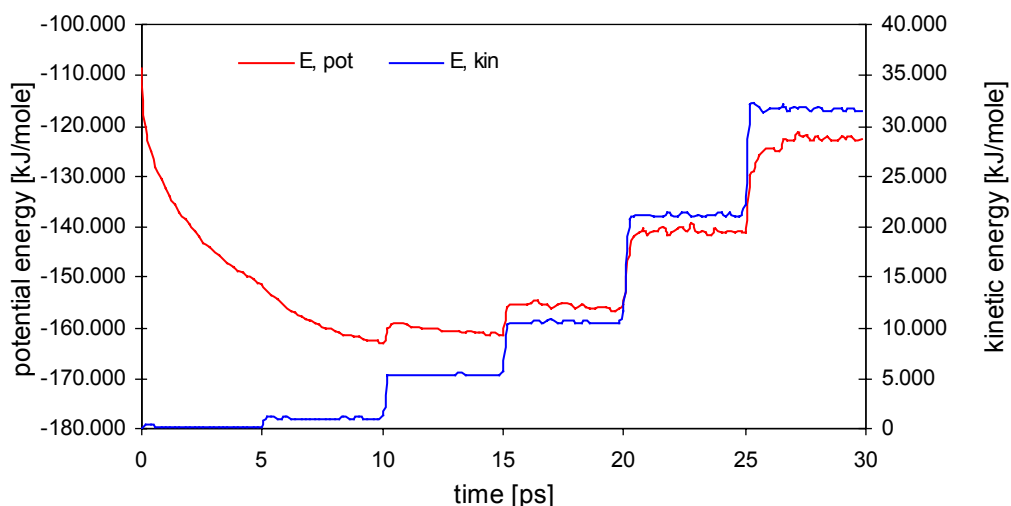


Figure 21 Trend of the potential and kinetic energy during the heating phase.



Each molecular dynamics simulation at elevated pressure was started using the configuration after 50 ps of the simulation at the previous pressure. Therefore, the overall length of the molecular dynamics simulations at different pressures is as follows: 400 ps at 1 bar, 350 ps at 10 bar, 300 ps at 50 bar, and 250 ps at 100 bar respectively. However, only structures calculated during the production phase of molecular dynamics simulations, the last 50 ps, were processed to generate an average structure of the molecule, however, without both essential water and chloroform solvent molecules. Into these averaged *Candida rugosa* lipase structures, the tetrahedral intermediate of the (+)- and (-)-menthylester was manually docked and steepest descent minimization was applied.

The molecular dynamics simulations were carried out on a DEC Alpha 433au workstation using the program package GROMOS96 (van Gunsteren and Berendsen 1987). Docking of the tetrahedral intermediate of the (+)- and (-)-menthylester into the resulting structures was performed manually applying SYBYL 6.5 (Tripos Inc., St. Louis, MO) on a SGI Indigo2 workstation.

### 3.7.6. REFORMATTING COORDINATES

#### 3.7.6.1. PROCS2

The program PROCS2 converts coordinates from pdb format to GROMOS96 format. To start the molecular dynamics simulation of the *Candida rugosa* lipase, the pdb entry 1LPM.pdb as obtained from the brookhaven database first was converted using a normal text editor to only contain the blocks ATOM, corresponding to the lipase, and HETATM, corresponding to the crystal water (marked in blue, appendix 8.1, page 119) and saved as lpm.pdb. Furthermore, the file lpm.pdb should start with a blank line, as otherwise PROCS2 would produce errors. The file lpm.pdb then was converted into GROMOS96 format (see appendix 8.2, page 127) using the program PROCS2 and saved as lpmcoord0.dat (see Figure 19).

*parameters for PROCS2*

NREA	NTF	NTS	NTX	SCALX	SCALI	NTBF	SCALB
4022	1	4	1	1.0	1.0	0	1.0

with	NREA	= 4022	number of coordinates in the edited pdb file lpm.pdb
	NTF	= 1	input in pdb format
	NTS	= 4	output in GROMOS96 format
	NTX	= 1	cartesian coordinates
	SCALX	= 1.0	no scaling of coordinates
	SCALI	= 1.0	no scaling of isotropic B factors
	NTBF	= 0	no input of B factors
	SCALB	= 1.0	no scaling of B factors

### 3.7.6.2. PROPDF

The program PROPDF was used to convert coordinates in GROMOS96 format to pdb format. As GROMOS96 is a script based molecular dynamics modeling package, it misses a graphical interface. The optional graphical front-end for GROMOS87, the program WHAT IF (Vriend and Sander 1991) unfortunately did not apply to the GROMOS96 format. Thus, visual control of the molecular dynamics simulations could only be performed by converting the simulated structures back into pdb format for visualization in any pdb viewer.

#### *parameters for PROPDF*

NPM	NTU1	MSKIP1	NTTR	ATTR	NLIS
1	2	1	0	CA	0

NRPM	NSM	NRAMS	NTU2	MSKIP2	NTXO
5145	11330	3	2	1	0

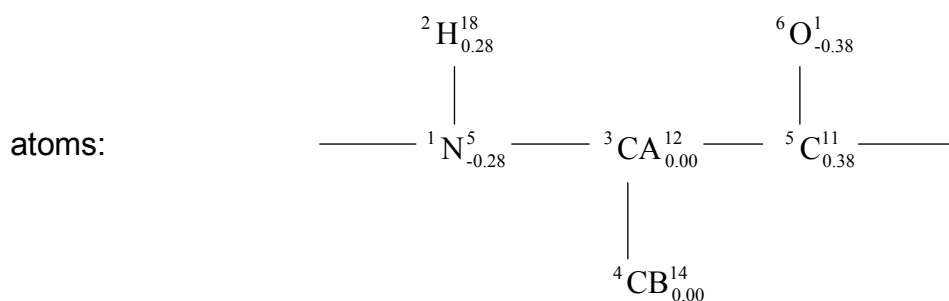
with	NPM	= 1	one solute configuration is transformed
	NTU1	= 2	nm are changed to Å
	MSKIP1	= 1	atoms with mass=1 are skipped
	NTTR	= 0	
	ATTR	= CA	no rotational least squares fit for ATTR=CA
	NLIS	= 0	no list of atoms is specified for a least squares fit
	NRPM	= 5145	number of solute atoms
	NSM	= 11330	number of solvent atoms
	NRAMS	= 3	number of atoms in a solvent molecule
	NTU2	= 2	coordinates are changed from nm to Å
	MSKIP2	= 1	atoms with mass=1 are skipped
	NTXO	= 0	output will be formatted

### 3.7.7. BUILDING A TOPOLOGY

The structure of each molecular system, which is to be simulated in GROMOS96, is completely described with two files: a coordinate file and a topology file. The topology contains information about bonds between the atoms, bond-angles or dihedral angles (see appendix 8.3, page 132). Thus, it contains the information, which and how atoms are bonded to each other.

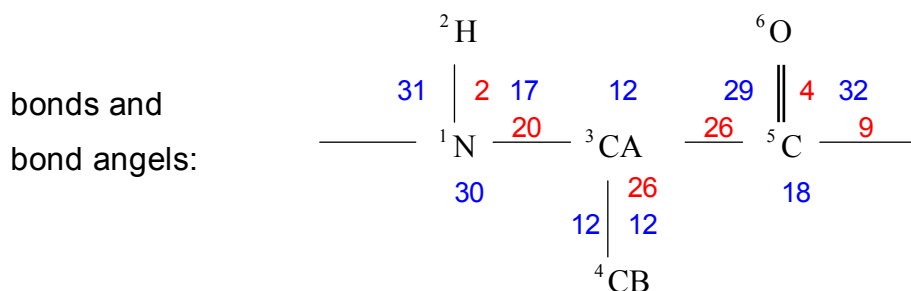
In case of the *Candida rugosa* lipase (CRL), only the coordinate file lpmcoord0.dat in GROMOS96 format was given so far. Hence, a topology for the CRL had to be generated. The program PROGMT generates molecular topologies by adding one molecular topology building block corresponding to an amino acid (aa) after another to finally yield the complete aa chain for the CRL.

Molecular topology building blocks (mtbb) in GROMOS96 are predefined groups of atoms like amino acids, heme groups, NADH, nucleotides, ions or solvent molecules. In the case of amino acids, a mtbb does not consist of the complete amino acid, but rather of the amino acid as it is found in proteins. Therefore, alanine looks like:



with:

atom number charge in vacuo	<b>atom name</b>	integer atom code charge in solution
--------------------------------	------------------	---



with:

blue:	bond type code
red:	bond-angle type code

The advantage of molecular topology building blocks being defined in such a way comes forth when a protein has to be built. Molecular topologies of proteins can be generated just by adding one mtbb to another. Only the C-termini and the N-termini have to be fixed manually. The amino acids are divided into different charged groups. These charged groups should be as small as possible, neutral or at least whole-numbered positively or negatively charged. Neutral charged groups are preferred.

For the CRL, an alanine is found in the N-terminus and thus the PROGMT generated topology contained an incomplete alanine in the N-terminus (see Figure 22).

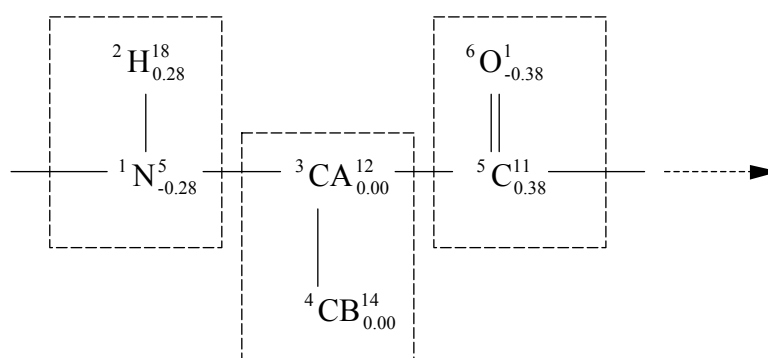


Figure 22 N-terminal end of CRL as generated in the first step by PROGMT.

In order to fix the N-terminus of the CRL, two atoms had to be added to the N-terminus ( $^1\text{H}$  and  $^2\text{H}$ ) and the properties of three further atoms ( $^4\text{H}$ ,  $^3\text{N}$ ,  $^5\text{CA}$ ) had to be edited. The charges were distributed analogous to the side chain of the protonated aa lysine. The charged group contained the  $^\alpha\text{C}$  atom (see Figure 23).

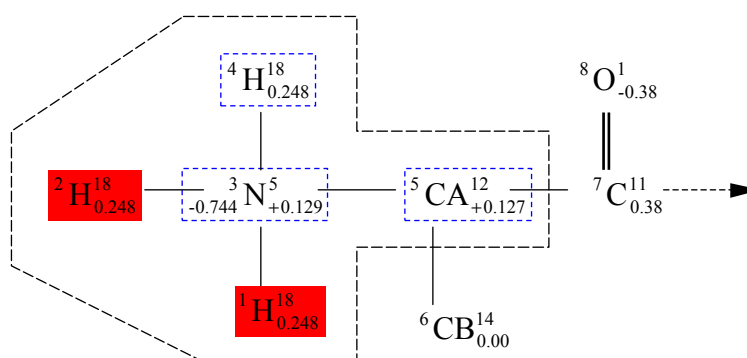


Figure 23 Manual fix of the N-terminus of the CRL. Newly added atoms are shown with a red background, atoms edited are shown with a blue border.

Likewise, the C-terminal end of the CRL consists of a valine and therefore the PROGMT generated topology contained an incomplete aa valine in the C-terminus (see Figure 24).

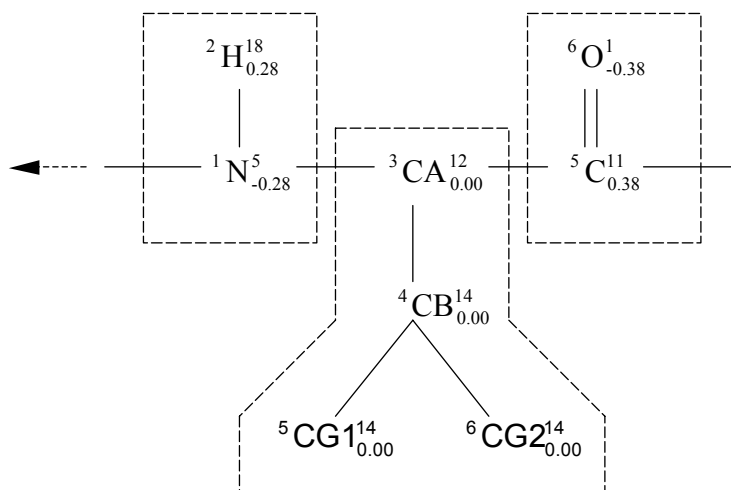


Figure 24 C-terminal end of CRL as generated in the first step by PROGMT.

In order to fix the C-terminal end of the CRL, one atom ( $^1\text{O}2$ ) had to be added to the C-terminus of the protein and the properties of two further atoms ( $^{-1}\text{C}$ ,  $^0\text{O}1$ ) had to be edited. The charges were distributed analogous to the charged side chain of aspartate or glutamate.

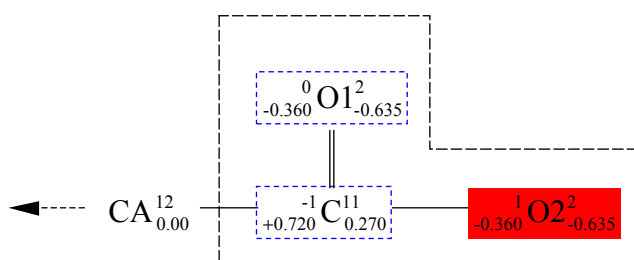


Figure 25 Manual fix of the C-terminus of the CRL. Newly added atoms are shown with a red background, atoms edited are shown with a blue border.

After the addition of atoms to the C- and N-termini, new bond types, bond-angle types and dihedral angles had to be defined manually in the generated topology file.

*parameters for PROGMT*

NRAA	NHEME	NMOL	NRAA0
534	0	0	0

AANM

ALA	PRO	THR	...			
			...	PHE	PHE	VAL

NRSS

2

NMSS

60	97
268	277

⋮

SOLV

H2O

NTPR

0

NTX

0

with	NRAA	= 534	number of mtbb, i.e. amino acids, ions, crystal water
	NHEME	= 0	number of heme groups in the molecule
	NMOL	= 0	number of further molecules
	NRAA0	= 0	molecule consists of only one covalent chain
	AANM		list of all amino acids
	NRSS	= 2	number of disulfide bonds
	NMSS		donor and acceptor of the disulfide bonds
	:		
	SOLV	= H2O	selection of the solvent
	NTPR	= 0	maximum output
	NTX	= 0	no proofreading of the topology with coordinates, in case coordinates are not completely generated

The switch NTX usually initiates proofreading of the topology to be generated with the coordinates when it is set to two. For the first molecular topology that had to be built for the CRL, only the incomplete set of coordinates in the file lpmcoord0.dat were available. As the underlying pdb file and therefore lpmcoord0.dat did not contain hydrogen atoms, whereas molecular topologies in GROMOS96 contain entries for hydrogen atoms, the proofreading has to be omitted the first time. Only thereafter coordinates of hydrogen atom could be calculated in GROMOS96 using the molecular topology together with the programs PROGCH and PROGWH. Thus, preceding the calculation of new coordinates (hydrogen atoms or ions), a molecular topology had to be generated without checking it with the coordinate file. Here, the switch NTX had to be set to zero.



### 3.7.8. GENERATING COORDINATES

In order to firstly proofread the molecular topology and secondly obtain a complete set of coordinates, the file lpmcoord0.dat was split into two files: a file lpmcoord0.dat, only containing the coordinates of the solute and a file lpmcoord0h2o.dat, containing the coordinates for the crystal water molecules (see Figure 19). The program PROGCH was used to calculate the coordinates of hydrogen atoms for the solute, the program PROGWH was used to calculate the hydrogen atoms for the crystal water molecules.

#### 3.7.8.1. PROGCH

*parameters for PROGCH*

NTH	NTXI	NTXO	NTU	NIAT
1	1	1	2	4

with	NTH	= 1	generation of hydrogen atom coordinates
	NTXI	= 1	obsolete
	NTXO	= 1	coordinate output is formatted
	NTU	= 2	scaling of coordinates
	NIAT	= 4	associated with a given geometry

#### 3.7.8.2. PROGWH

*parameters for PROGWH*

NTH	NTXI	NTXO	NTU	NRATO
1	1	1	2	261

with	NTH	= 1	generation of hydrogen atom coordinates
	NTXI	= 1	obsolete
	NTXO	= 1	coordinate output is formatted
	NTU	= 2	scaling of coordinates
	NIAT	= 4	associated with a given geometry

The coordinate files generated by PROGCH and PROGWH were copied together to finally yield one complete set of coordinates for the CRL in GROMOS96 format `lpmcoord1.dat` (see Figure 19), containing not only the coordinates for the hydrogen atoms in the solute, but also the coordinates for the crystal water molecules.

With the file `lpmcoord1.dat`, a complete set of coordinates was available to the program PROGMT in order to proofread the newly generated topology. Thus, a new molecular topology `lpmmta1.dat` was generated and proofread with the coordinate file `lpmcoord1.dat` (see Figure 19).

### 3.7.8.3. PROBOX

The program PROBOX fills a solvent box around the solute (CRL) with the coordinates of a preequilibrated standard box containing 216 molecules of a specified solvent. The choice of the solvent is accomplished by referencing the preequilibrated standard box file in the shell script file `jboxlpm.sh`.

*parameters for PROBOX*

NTXP	NPM	NSMP	NTXS	NSM	BOXS	DISM	NTXO
1	1	0	1	216	3.0637	0.5	1
NTB	BOX(1)	BOX(2)	BOX(3)	BETAA			
-1	1.2	1.2	1.2	90.0			

with	NTXP	= 1	obsolete
	NPM	= 1	only one solvent molecule is considered
	NSMP	= 0	solvent molecules are not yet present
	NTXS	= 1	obsolete
	NSM	= 216	standard solvent box contains 216 molecules
	BOXS	= 3.0637	box length of the standard box in nm
	DISM	= 0.5	minimum distance of solvent molecules to non-hydrogen atoms of the solute
	NTXO	= 1	formatted output

NTB	= -1	truncated octahedral box
BOX(1..3)	= 1.2	minimum distance of the solute to the wall of the box 1.2 nm
BETAA	= 90	angel between the axes

The parameters BOXS and DISM were estimated as follows:

For water, a box of 216 equilibrated water molecules has a length of 1.86206 nm and the parameter DISM is set to 0.23 nm. In case of chloroform, the solvent box, also containing 216 equilibrated chloroform molecules, has a length of 3.0637 nm. The parameter DISM was then estimated to 0.5 nm. As this parameter was only a rough guess, the density of the solvent box initially was not exactly correct. However, with all subsequent molecular dynamics simulations performed using pressure coupling (without constant volume), the correct density of the solvent box was to adjust itself in the course of the simulation (see Figure 29).

After the generation of the water coordinates, the program PROGMT had to be invoked again with the switch NTX set to two in order to proofread the molecular topology with the newly generated coordinates.

#### 3.7.8.4. PROION

The CRL is 17-fold negatively charged at a pH 7. In order to neutralize the molecular system, 17 sodium ions had to be added. The program PROION exchanges particular solvent molecules with specified ions. As the sodium ions were to be placed at coordinates with the highest potential, it was important to first energy minimize the molecular system (see 3.7.9). If water molecules happen to be placed too near to the protein by the program PROBOX (see 3.7.8.3), PROION would mistake these water molecules as having a high potential and therefore place ions in the wrong positions.

In case of the CRL, PROION put two of the 17 sodium ions in the core of the lipase. These two sodium ions "tunneled" through the protein in a subsequent energy minimization. In order to remedy this tunneling of ions which in the worst case could result in the abortion of the molecular dynamics simulation, 19 sodium ions were added and subsequently the two ions in the core of the lipase were then again replaced by the original water molecules.

*parameters for PROION*

NPM	NSM	NTR	NEXSM	RCUTE	IG
1	11349	1	0	0.35	214748647

NPLUS	APLUS	CGPLUS
19	NA	+1.0

with	NPM	= 1	one solute is considered
	NSM	= 11349	number of solvent molecules (CRL)
	NTR	= 1	solvent molecules with highest/lowest potential are to be replaced
	NEXSM	= 0	no solvent molecule is excluded
	RCUTE	= 0.35	ions are not to be placed at a radius of 0.35 nm around an ion, preventing the building of chains of altering ions
	IG	= 214748647	random generator seed
	NPLUS	= 19	number of ions to add
	APLUS	= NA	ion type
	CGPLUS	= +1.0	charge of the ion

In order to include the ions into the solute part of molecular topology, the switch NMOL in PROGMT had to be set to the additional 17 molecules which had to be added as NA<sup>+</sup> in the definition of the switch AANM.

For the simulation of the CRL in chloroform, two peculiarities of GROMOS96 had to be taken into account:

- GROMOS96 only offers one solvent block for the program PROGMT. But as the molecular dynamics simulation setup of the CRL in chloroform contained a mixture of chloroform as well as water molecules, only one part of the solvent could be treated as solvent in the molecular topology. The other part had to be treated as being part of the solute. Therefore, the crystal water molecules had to be added to

the solute part of the molecular topology, whereas the chloroform molecules could be treated as solvent. This is possible, as the PROGMT differentiates between solute and solvent only for historical reasons.

- The program PROION only operates on solvent molecules. Thus, it was not possible to replace the crystal water molecules, which were defined as solute atoms, by sodium ions. Therefore, the crystal water would have to be defined as solvent.

As a result, PROGMT prefers the crystal water molecules defined in the solute part, whereas PROION needs the crystal water molecules to be treated as solvent. To remedy this pitfall, the simulation of the CRL in water was used. Here, the crystal water had been defined as solvent, together with the water molecules generated by the program PROBOX. Thus, in the simulation of the CRL in water, the program PROION was able to replace 17 (19) solvent molecules by sodium ions. All replaced solvent molecules were derived from the 261 crystal water molecules. The positions of the 17 sodium ions could just be copied and pasted into the corresponding coordinate file for the simulation of the CRL in chloroform. In order to add the crystal water molecules to the solute part of the molecular topology, the switch NMOL in PROGMT had to be set to 261 additional molecules altogether, the 17 sodium ions and 244 (261-17) crystal water molecules. The additional molecules had to be added as NA<sup>+</sup> and H<sub>2</sub>O in the definition of the switch AANM, respectively.

### **3.7.9. CALCULATING MOLECULAR DYNAMICS SIMULATIONS**

The program PROMD calculates energy minimizations as well as molecular dynamics simulations. According to whether either an energy minimization or a molecular dynamics simulation is to be calculated, different parameters or input blocks are activated in the script file.

The dielectric constant of water is 80, in single point charge (SPC) water it is set to 54, in chloroform it is 4.81, in the interior of a protein it is around 4 and in vacuum it is defined to be 1. The simulation assembly contained 534 molecules of amino acids, 244 molecules of crystal water bound to the lipase and 2289 molecules of

chloroform. Thus, the dielectric constant of the solvent was estimated to be  $\epsilon_{\text{PSRF}}=4.8$ .

Energy minimization had to be applied each time, coordinates were generated with a GROMOS96 program. The generation of hydrogen coordinates (see chapter 3.7.8.1, chapter 3.7.8.2), the solvent box (see chapter 3.7.8.3) or the exchange of water molecules by ions (see chapter 3.7.8.4) were steps, where energy minimization was necessary. The lipase was restricted during the energy minimization and only the water molecules and the sodium ions were relaxed.

The shell script for molecular dynamics simulations was essentially the same as that for energy minimizations. The switch INIT in the START block was set to 1 for a minimization or a startup simulation (no velocities were read) and to 4 for a continued simulation (velocities of the preceding run were read). Differences between energy minimization and MD simulation further applied to the START, STEP, and BOX blocks, respectively.

*parameters for PROMD*

#### MINIMISE

NTEM	NCYC	DELE	DXO	DXM
1	20	0.1	0.01	0.05

#### SYSTEM

NPM	NSM
1	2289

#### START

NTX	INIT	IG	TEMPI	HEAT	NTXO	BOLTZ
1	1	210185	300.0	0.00000	1	8.31441E-3

#### STEP

NSTLIM	T	DT
300	0.0	0.002

**PRINT**

NTPR	NTPL	NTPP
1	100	1

**SHAKE**

NTC	TOL
3	0.00010

**FORCE**

bonds	angles	imp.	dihe	charge nonbonded
H	H	H	H	
0 0	1 1	1 1	1 1	1 1
NEGR	NRE(1)	NRE(2)	NRE(3)	NRE(NEGR)
4	5126	5144	5875	17320

**PLIST**

NTNB	NSNB	RCUTP	RCUTL
1	10	0.8	1.4

**LONGRANGE**

EPSRF	APPAK	RCRF
4.8	0.0	1.4

**POSREST**

NTR	CHO	NRDRX
1	2.5E4	0

with

**MINIMISE**

NTEM	= 1	steepest descents minimization
NCYC	= 20	contribution of previous search directions set to zero every 20 steps; applies only to conjugate gradient minimization (NTEM = 2)
DELE	= 0.1	minimization terminates when the change in potential energy is less than 0.1 kJmol <sup>-1</sup>

DXO = 0.01 initial step size of 0.01 nm  
DXM = 0.05 maximum step size of 0.05 nm

### SYSTEM

NPM = 1 number of solute molecules  
NSM = 2289 number of solvent molecules

### START

NTX = 1 only atomic coordinates were read  
INIT = 1(4) startup of the minimization (continuation run)  
NTXO = 1 formatted output

### STEP

NSTLIM = 300 maximum number of steps  
T = 0.0 starting point of time for the minimization (unequal zero for a continuation run)  
DT = 0.002 step size of 0.002 fs

### PRINT

NTPR = 1 output of energies every step  
NTPL = 100 only applies to MD-simulations  
NTPP = 1 dihedral angle transition monitoring

### SHAKE

NTC = 3 all bond lengths of the solute were constrained  
TOL = 0.0001 relative geometric precision by which solute and solvent bond-length and bond-angle constraints were to be maintained

### FORCE

NEGR = 4 the energies of four groups of atoms were collected  
NRE(1) = 5126 solute atoms up to atom 5126  
NRE(2) = 5143 sodium ions up to atom 5143



NRE(3) = 5875 crystal water up to atom 5875  
NRE(4) = 17320 chloroform up to atom 17320  
(MD simulation of *Candida rugosa* lipase in chloroform)

### PLIST

NTNB = 1 nonbonded interaction pair list was constructed at the first step  
NSNB = 10 update of the pair list every 10 steps  
RCUTP = 0.8 nonbonded interaction cut-off radius  
RCUTL = 1.4 long-range interaction cut-off radius

### LONGRANGE

EPSRF = 4.8 dielectric permittivity  
APPAK = 0.0 inverse Debye screening length  
RCRF = 1.4 reaction-field cut-off radius

### POSREST

NTR = 1 all atoms of the solutes were to be restricted with the same force constant  
CHO = 2.5E4 force constant in  $\text{kJmol}^{-1}\text{nm}^{-2}$   
NRDRX = 0 reference coordinates, derived from the starting positions

**3.7.10. ANALYZING MOLECULAR DYNAMICS SIMULATIONS****3.7.10.1. PROAVX**

The program PROAVX was used to generate averaged solute configurations and rmsd values from the production phase trajectory of each molecular dynamics simulation. Only averaged configuration could be subjected to further analysis, i.e. the docking of the tetrahedral intermediate of the (+)- or (-)-menthylester.

*parameters for PROAVX*

NTRR	NRFL	NRIS	NRRC	NSKP	NRR
1	1	0	1000	1	15429
NPM	NSYM	NTTR	ATTR	NRPI	
1	0	1	ALL	5143	
NTB	BOX[1]	BOX[2]	BOX[3]	BETA	
-2	0	0	0	90.0	
NRPC1	NRPC2	NPC2	NRPC3	NPC3	
5126	5126	5126	5126	5126	
NTPR	NTPLOT	ANAME	NLIS	NTWF	
1	-2	H	0	1	

with	NTRR	= 1	reading of cartesian coordinates
	NRFL	= 1	number of trajectory files used
	NRIS	= 0	number of configurations to be skipped
	NRRC	= 1000	number of configurations in the file
	NSKP	= 1	all configurations in the file were to be used
	NRR	= 15429	number of coordinates per configuration

The switches in the other blocks resemble the SYSTEM, the BOX, and the PRINT block, respectively and are therefore not further described.

**3.7.10.2. PROCOX**

The program PROCOX was used for the comparison of two solute configurations in terms of cartesian coordinates. It yields among others the radius of gyration for the two configurations compared.

*parameters for PROCOX*

NRA1	NRPI1	NPM1	NRA2	NRPI2	NPM2
5143	5143	5143	5143	5143	5143

NSYM	NTTR	ATTR
0	1	CA

NTB1	BOX[1]	BOX[2]	BOX[3]	BETA
-1	9,583323	9,583323	9,583323	90

NRPC11	NRPC21	NPC21	NRPC31	NPC31
5126	5126	5126	5126	5126

NRPC12	NRPC22	NPC22	NRPC32	NPC32
5126	5126	5126	5126	5126

RCUT	NTPR	NTPLOT	ANAME	NLIS
0,8	1	-2	CA	0

with	NRA1(2)	=5143	atoms per configuration
	NRPI1(2)	=5143	atoms per solute
	NPM1(2)	=5143	total atoms
	NSYM	=0	no crystallographic transformation performed
	NTTR	=1	translational & rotational least squares fit
	ATTR	=CA	fit was performed only for CA-atoms
	NRPCxy	=5126	restore the covalent connectivity of the solute
	RCUT	=0,8	compute the atom number density within RCUT

## 4. RESULTS

### 4.1. BIOCATALYSIS

#### 4.1.1. SCREENING FOR THE SAMPLE REACTION

A sample reaction was needed in order to determine the pressure dependence of the stereoselectivity of a lipase-catalyzed reaction. Stereoselectivity was introduced by using the secondary alcohol menthol (see 1.1.1). Altogether, 43 lipases (see Table 3) were screened either for stereoselective esterification, stereoselective transesterification or stereoselective hydrolysis. The sources of the lipases were eucaryotic as well as procaryotic organisms.

Screening was performed for 36 hours in Eppendorf tubes with 2 ml of isooctane and small amounts of crude lipase as well as substrate (menthol or menthyl ester) at room temperature. Results of the screening were assessed by thin layer chromatography.

1	<i>Candida rugosa B</i>
2	<i>Pseudomonas fluorescens</i>
3	<i>Humicola lanuginosa</i>
4	<i>Pseudomonas</i> (Nagase)
5	<i>Acid esterase</i>
6	<i>Rhizopus arrhizus</i>
7	<i>Candida lipolytica</i>
8	<i>Candida antarctica B</i>
9	<i>Pseudomonas alcaligenes</i>
10	<i>Rhizopus niveus</i>
11	<i>Lipase standard</i>
12	<i>Fusarium solani cutinase</i>
13	<i>Mucor miehei</i>
14	<i>Pseudomonas fluorescens</i>
15	<i>Rhizopus</i>
16	<i>Candida rugosa MY</i>

18	<i>Streptomyces antibioticus</i>
19	<i>Rhizopus species</i>
20	<i>Rhizopus javanicus</i>
21	<i>Candida antarctica A</i> (SP526 )
22	<i>Candida cylindracea</i>
23	<i>Pseudomonas species</i> (Showa Denko)
24	<i>Rhizopus delemar</i> (Amano D)
25	Seaprose
26	<i>Pseudomonas species</i> (Amano PS)
27	Amano M
28	<i>Pseudomonas cepacia</i> (Amano PS)
29	Ashirase
30	<i>Pseudomonas cepacia</i> (Amano AH)
31	<i>Penicillium cyclopium</i> (Amano G)
32	<i>Pseudomonas species</i> (Amano PS)
33	<i>Penicillium roquefortii</i> (Amano R)
34	<i>Rhizopus javanicus</i> (Amano F)
35	<i>Candida rugosa</i> (Amano AY)
36	<i>Rhizopus javanicus</i> (Amano F-AP15)
37	Acid esterase (Amano AC 409)
38	<i>Chromobacterium viscosum</i> (pure)
39	<i>Chromobacterium viscosum</i> (crude)
40	<i>Aspergillus niger</i> (Amano A)
41	<i>Rhizomucor miehei</i> (Novo Lipozyme IM)
42	Novozyme 435
43	Acetylcholine esterase

Table 3 Enzymes screened for stereoselective reaction

Various substrates were used for screening (see Table 4). Depending on the substrate used with the reactions investigated it was possible to shift the reaction equilibrium due to the formation of products that practically were removed from the reaction. Using acid anhydrides leads to production of a decreased amount of water during the course of reaction and, therefore, drives the reaction equilibrium towards the formation of product. During the first acylation of menthol with an anhydride,

menthyl ester and acid are formed. The acid can further react with menthol to yield another molecule of menthyl ester and water. Vinyl esters are widely used to shift the reaction equilibrium towards products. The reaction becomes irreversible as the acetaldehyde formed is volatile and, therefore, is excluded from the liquid reaction ensemble. However, one disadvantage of vinyl esters is its reaction product, the aforementioned acetaldehyde, which significantly affects lipase stability and selectivity.

- fatty acids
  - propionic acid
  - acetic acid
  - stearic acid
  - palmitic acid
- acid anhydrides
  - propionic acid anhydride
  - acetic acid anhydride
  - maleic acid anhydride
  - succinic acid anhydride
- esters
  - menthylbenzoate
  - menthylacetate
- methyl esters
  - methylisovalerate
  - methylbutyrate
  - methyl-(2-methyl)-butyrate
  - methylpropionate
  - methylcaprylate
  - methylcaprinate
  - methylcapronate
- vinyl esters
  - vinylacetate
  - vinylbenzoate

Table 4      Substrates screened with the enzymes listed in Table 3.

When enzymes are used in organic solvent, e.g. esterification or transesterification reaction immobilization can improve the stability of the biocatalyst. Therefore, various methods of immobilization for the repeated use in organic solvent were tested (see Table 5).

- celite (diatomaceous earth)
- XAD-7 (acrylic ester, weak-polar, surface area 450 m<sup>2</sup>/g)
- EP-100 (polypropylene, 200 - 400 μm)
- hyflo super cell (diatomaceous earth)

Table 5      Various immobilization methods tested for the stabilization of the enzymes screened in organic solvent.

The screening (see Table 6 to Table 11 and Figure 26) yielded several potential candidates for the sample reaction. The best candidates for the sample reaction are summarized in Table 12.

nr.	enzyme	ee <sub>menthol</sub>	ee <sub>menthyl propionate</sub>	conv	E
2	<i>Pseudomonas fluorescens</i>	11	90	11	21
4	<i>Pseudomonas</i> (Nagase)	15	48	23	3
5	<i>Acid esterase</i>	4	42	10	3
7	<i>Candida lipolytica</i>	1	0	87	1
8	<i>Candida B</i>	1	1	43	1
9	<i>Pseudomonas alcaligenes</i>	8	51	13	3
10	<i>Rhizopus niveus</i>	1	0	66	1
14	<i>Pseudomonas fluorescens</i>	10	86	10	15
16	<i>Candida rugosa MY</i>	94	87	52	50
19	<i>Rhizopus species</i>	12	66	15	6
20	<i>Rhizopus javanicus</i>	22	92	19	30
21	<i>Candida antarctica A</i> (SP526 )	20	77	21	9
22	<i>Candida cylindracea</i>	92	91	50	69
25	<i>Seaprose</i>	1	0	93	1
28	<i>Pseudomonas cepacia</i> (Amano PS)	12	87	12	16
29	<i>Ashirase</i>	1	20	5	2
30	<i>Pseudomonas cepacia</i> (Amano AH)	1	34	3	2
35	<i>Candida rugosa</i> (Amano AY)	91	59	61	11
36	<i>Rhizopus javanicus</i> (Amano F-AP15)	1	36	2	2
39	<i>Chromobacterium viscosum</i> (crude)	1	10	8	1
40	<i>Aspergillus niger</i> (Amano A)	1	9	6	1
41	<i>Rhizomucor miehei</i> (Novo Lipozym IM)	4	90	4	19

Table 6 Conversion, conv, and E-values, E, for the screening with propionic acid anhydride as acyl donor. Lipases with an E-value greater than 20 are marked red. Screening was performed for 36 hours.



nr.	enzyme	ee <sub>menthol</sub>	ee <sub>menthyl acetate</sub>	conv	E
2	<i>Pseudomonas fluorescens</i>	20	93	18	35
4	<i>Pseudomonas</i> (Nagase)	45	19	70	2
5	Acid esterase	1	17	3	1
7	<i>Candida lipolytica</i>	1	3	28	1
8	<i>Candida B</i>	0	1	25	1
9	<i>Pseudomonas alcaligenes</i>	1	30	3	2
10	<i>Rhizopus niveus</i>	1	1	35	1
14	<i>Pseudomonas fluorescens</i>	6	91	6	22
16	<i>Candida rugosa</i> MY	29	97	23	87
19	<i>Rhizopus species</i>	2	24	8	2
20	<i>Rhizopus javanicus</i>	9	72	11	7
21	<i>Candida antarctica</i> A (SP526 )	3	69	5	6
22	<i>Candida cylindracea</i>	19	97	17	85
25	Seaprose	0	13	3	1
28	<i>Pseudomonas cepacia</i> (Amano PS)	8	92	8	27
29	Ashirase	1	7	7	1
30	<i>Pseudomonas cepacia</i> (Amano AH)	1	26	4	2
35	<i>Candida rugosa</i> (Amano AY)	36	95	27	61
36	<i>Rhizopus javanicus</i> (Amano F-AP15)	1	9	8	1
39	<i>Chromobacterium viscosum</i> (crude)	1	4	16	1
40	<i>Aspergillus niger</i> (Amano A)	1	3	18	1
41	<i>Rhizomucor miehei</i> (Novo Lipozym IM)	5	93	5	30

Table 7 Conversion, conv, and E-values, E, for the screening with acetic acid anhydride as acyl donor. Lipases with an E-value greater than 20 are marked red. Screening was performed for 36 hours.

nr.	enzyme	ee <sub>menthol</sub>	ee <sub>menthyl benzoate</sub>	conv	E
5	<i>Acid esterase</i>	0	n.d.*	n.d.*	n.d.*
9	<i>Pseudomonas alcaligenes</i>	11	n.d.*	n.d.*	n.d.*
16	<i>Candida rugosa MY</i>	1	n.d.*	n.d.*	n.d.*
23	<i>Pseudomonas species</i> (Showa Denko)	14	n.d.*	n.d.*	n.d.*
35	<i>Candida rugosa</i> (Amano AY)	14	n.d.*	n.d.*	n.d.*

Table 8 Conversion, conv, and E-values, E, for the screening with benzoic acid as acyl donor. The enantiomeric excess was not yet determinable after 108 hours.

nr.	Enzyme	ee <sub>menthol</sub>	ee <sub>menthyl phenyl acetate</sub>	conv	E
9	<i>Pseudomonas alcaligenes</i>	0	n.d.*	n.d.*	n.d.*
21	<i>Candida antarctica A</i> (SP526)	17	n.d.*	n.d.*	n.d.*
23	<i>Pseudomonas species</i> (Showa Denko)	1	n.d.*	n.d.*	n.d.*

Table 9 Conversion, conv, and E-values, E, for the screening with phenyl acetate as acyl donor. The enantiomeric excess was not determinable after 108 hours.

nr.	enzyme	ee <sub>menthol</sub>	ee <sub>menthyl acetate</sub>	conv	E
0	Blind probe	-	2	-	-
4	<i>Pseudomonas</i> (Nagase)	43	4	9	3
12	<i>Cutinase</i>	57	15	21	4
13	<i>Mucor miehei</i>	100	4	4	-
14	<i>Pseudomonas fluorescens</i>	99	21	17	487
16	<i>Candida rugosa</i> MY	84	29	25	15
21	<i>Candida antarctica</i> A	51	78	60	7
22	<i>Candida cylindracea</i>	54	81	60	8
23	<i>Pseudomonas</i> species (Showa Denko)	33	87	73	5
24	<i>Rhizopus delemar</i> (Amano D)	69	29	30	7
26	<i>Pseudomonas</i> species (Amano PS)	99	39	28	404
27	Amano M	100	4	4	-
29	Ashirase	73	6	7	7
30	<i>Pseudomonas cepacia</i> (Amano AH)	90	4	4	19
31	<i>Penicillium cyclopium</i> (Amano G)	16	0	1	1
32	<i>Pseudomonas</i> species (Amano PS)	99	43	30	371
35	<i>Candida rugosa</i> (Amano AY)	67	82	55	13
36	<i>Rhizopus javanicus</i> (Amano F-AP15)	96	12	11	61
38	<i>Chromobacterium viscosum</i> (pure)	95	7	7	39
40	<i>Aspergillus niger</i> (Amano A)	14	10	41	1
43	Acetylcholine esterase	13	97	88	4

Table 10 Conversion, conv, and E-values, E, for the screening of the hydrolysis of menthyl acetate. Lipases with an E-value greater than 20 are marked red. Screening was performed for 36 hours.

<i>Candida rugosa</i> (Amano AY)	$ee_{\text{menthol}}$	$ee_{\text{menthyl propionate}}$	conv	E
AY	0,51	0,94	0,35	58
AY-celite	0,19	0,95	0,17	44
AY-EP-100	0,31	0,97	0,24	90
AY-hyflo	0,32	0,96	0,25	70
AY-XAD-7	0,04	0,67	0,06	5

Table 11 Conversion, conv, and E-values, E, for the *Candida rugosa* lipase immobilized on different carriers with propionic acid anhydride as acyl donor. Results with E-values greater than 20 are marked red. Screening was performed for 36 hours.

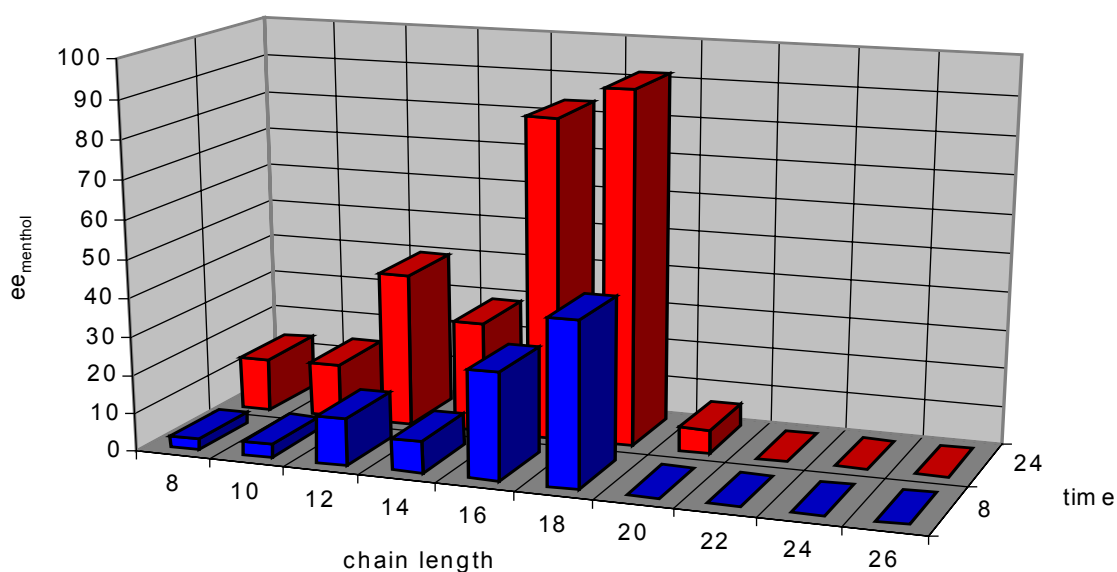


Figure 26 Esterification of menthol by *Candida rugosa* lipase. Dependency of the esterification on the chain length. The hydrophobic fatty acid used for esterification has a maximum at C18.

➤ esterification				
○ acetic acid anhydride	ee <sub>S</sub>	ee <sub>P</sub>	conv	E
▪ <i>Candida rugosa</i>	29	97	23	87
▪ <i>Pseudomonas cepacia</i>	8	97	17	85
○ propionic acid anhydride				
▪ <i>Candida rugosa</i>	94	87	52	50
▪ <i>Rhizopus javanicus</i>	22	92	19	30
➤ hydrolysis				
○ menthyl acetate				
▪ <i>Pseudomonas fluorescens</i>	21	99	17	487
▪ <i>Pseudomonas species</i>	39	99	28	404
➤ transesterification				
○ methylbutyrate				
▪ <i>Candida rugosa</i>	17	99	15	158
○ methylpropionate				
▪ <i>Candida rugosa</i>	9	98	8	100

Table 12 Screening results with the best values for enantioselectivity.

A prerequisite for the sample reaction of choice was the simplicity to set up and analyze the reaction, i.e., measuring the enantiomeric excesses. Since no difference in reaction mechanism exists between lipase-catalyzed hydrolysis and esterification, acylation of racemic menthol with propionic acid anhydride was selected as a model reaction to investigate the enantioselectivity of Amano AY *Candida rugosa* lipase in different solvents and under pressure (see Figure 11). A rationale for esterification as compared to hydrolysis was that in organic solvent the biocatalyst could easily be recycled for various reaction cycles, which was especially comfortable for the determination of the residual activity of *Candida rugosa* lipase after experiments at various pressures (see below). The lipase Amano AY was used without further processing, i.e., immobilization on different carrier materials. (±)-Menthol and the product, (±)-menthylpropionate could be well resolved by gas chromatography (see Figure 27).

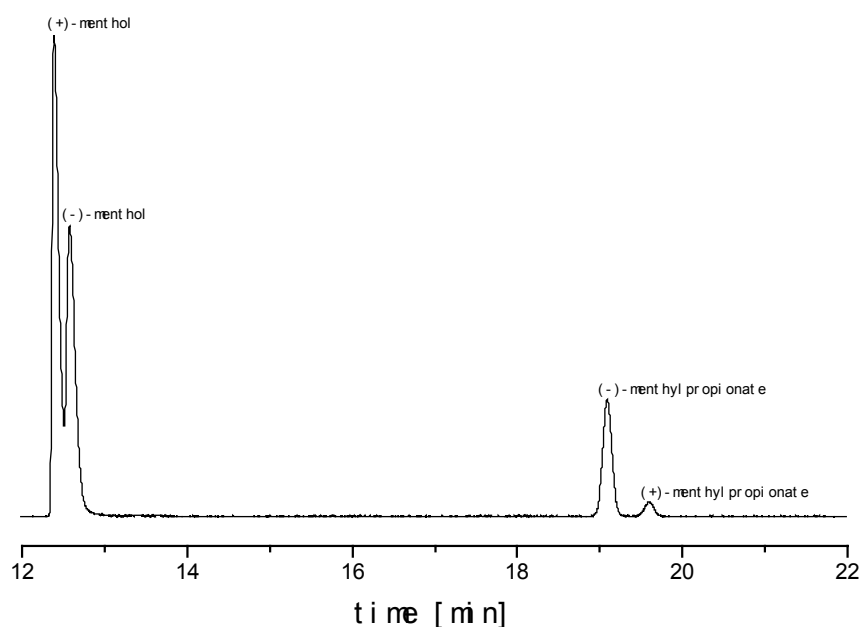


Figure 27 Chromatogram of the biotransformation sample after 48 hours at 100 bar.

The retention times were 12.4 min for (+)- menthol, 12.6 min for (-)-menthol, 19.1 min for (-)-menthylpropionate, and 19.6 min for (+)-menthylpropionate. The experimentally observed enantioselectivity of *Candida rugosa* lipase was calculated using the peak areas for (+)- and (-)-menthol and (-)- and (+)-menthylpropionate. With increasing pressure, the enantioselectivity decreased from  $E=55 \pm 1.5$  (1 bar) to  $E=47 \pm 2.1$  (10 bar),  $E=37 \pm 1.5$  (50 bar), and  $E=9 \pm 0.4$  (100 bar) (see Table 13 and Figure 28). The enantiomeric ratios of products and substrates were analyzed at a conversion  $c$  between 30 % and 15 %, which was reached at 1 bar and 10 bar after 24 hours and at 50 bar and 100 bar after 48 hours (see Table 13), equaling to a loss in activity of 50 %.

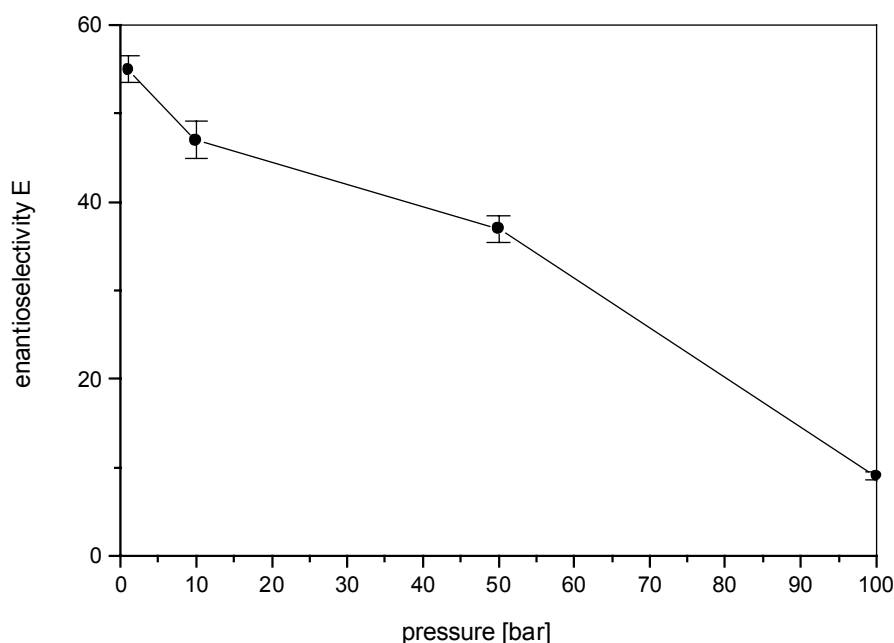


Figure 28 Experimentally determined dependence of the enantioselectivity of *Candida rugosa* lipase towards the esterification of ( $\pm$ )-menthol with propionic acid anhydride. For conversion rates  $c = 15\% - 30\%$ , the enantioselectivity significantly decreased with increasing pressure. Standard deviations were calculated for each E-value for 6 independent

measurements applying equation  $\sigma_E = \sqrt{\frac{\sum (E_i - \bar{E})^2}{n - 1}}$

with:

n: number of samples, here  $n=6$

$E_i$ : sample value of E

$\bar{E}$ : mean value of E

time[h]	pressure[bar]	conversion[%]	enantioselectivity	variation coefficient [%]
24	1	28	$55 \pm 1.5$	2.7
24	10	20	$47 \pm 2.1$	4.5
48	50	24	$37 \pm 1.5$	4.1
48	100	15	$9 \pm 0.4$	4.4

Table 13 Kinetic parameters of the transesterification reaction at different pressures. Standard deviations were calculated for each E-value with 6 independent measurements.

Increasing the pressure led to a loss of enzyme activity. The residual activity at 100 bar was 25 % of the activity at 1 bar. To account for the decrease in activity towards ( $\pm$ )-menthol at higher pressures in the experiment, the loss in residual activity of the lipase after incubation at 1 bar and 100 bar was checked using a pH-stat assay at ambient conditions. The activity of the commercially available lipase Amano AY (wild type) was 7.3 units/mg, whereas the lipase retained 6.4 units/mg (88 % of the wild type) after two days incubation in chloroform at 1 bar, and 6.8 Units/mg (93 % of the wild type) after two days incubation in chloroform at 100 bar. The residual activities of the lipase after incubation at 1 bar and 100 bar are nearly that of the wild type and no irreversible denaturation of the lipase could be observed. Thus, the loss in activity of the lipase towards ( $\pm$ )-menthol at higher pressures during the experiment is reversible and can be ascribed to the experimental conditions.

The water content of the commercially available lipase preparation, as determined by loss on drying of 1 g of lipase Amano AY (LAYX03512) at 105 °C and 4 hours [Koichi Suzuki: personal communication], was 4.11 %. Determination by Karl-Fischer titration yielded a water content of 6.3 % of the Amano AY lipase (LAYY04501025) preparation.



## 4.2. COMPUTER MODELING

### *Solvent and solute in molecular dynamics simulations*

Four molecular dynamics simulations of the *Candida rugosa* lipase were performed using chloroform as a solvent, one molecular dynamics simulation with the lipase in water. For the molecular dynamics simulation in water, the molecular weights of all parts of the simulation assembly were 200 kDa for 11,332 water molecules, 391 Da for 17 sodium ions, and 57 kDa for the solute. For the molecular dynamics simulations in chloroform, the molecular weights of all parts of the simulation assembly were 274 kDa for 2,289 chloroform molecules, 391 Da for 17 sodium ions, 57 kDa for the lipase, and 4,392 Da for 244 crystal water molecules. The 4,392 Da crystal water corresponded to 7.1 % of the overall molecular weight of the *in silico* lipase preparation. This matched well the experimentally determined 6.3 % water content of the lipase Amano AY. Pressures applied were 1 bar for the simulation in water and 1 bar, 10 bar, 50 bar, and 100 bar, respectively, for simulations in chloroform. In the course of initial energy minimization, the total energy of the molecular dynamics simulation assembly reached a minimum at about -200,000 kJ/mol (see Figure 20), however, after heating to 300 K it stabilized at about -100,000 kJ/mol (see Figure 21). The size of the simulation assembly containing chloroform as solvent decreased during minimization and stabilized at all pressures at about 740 nm<sup>3</sup> after equilibration. The size of the simulation assembly containing water as solvent stabilized at about 830 nm<sup>3</sup> after equilibration (see Figure 29).

Compared to the crystal structure 1LPM the *Candida rugosa* lipase is more compact with explicit chloroform as solvent and even more compact with explicit water as solvent. With increasing pressure in the simulation with chloroform the lipase gets slightly more compact (see Figure 30).

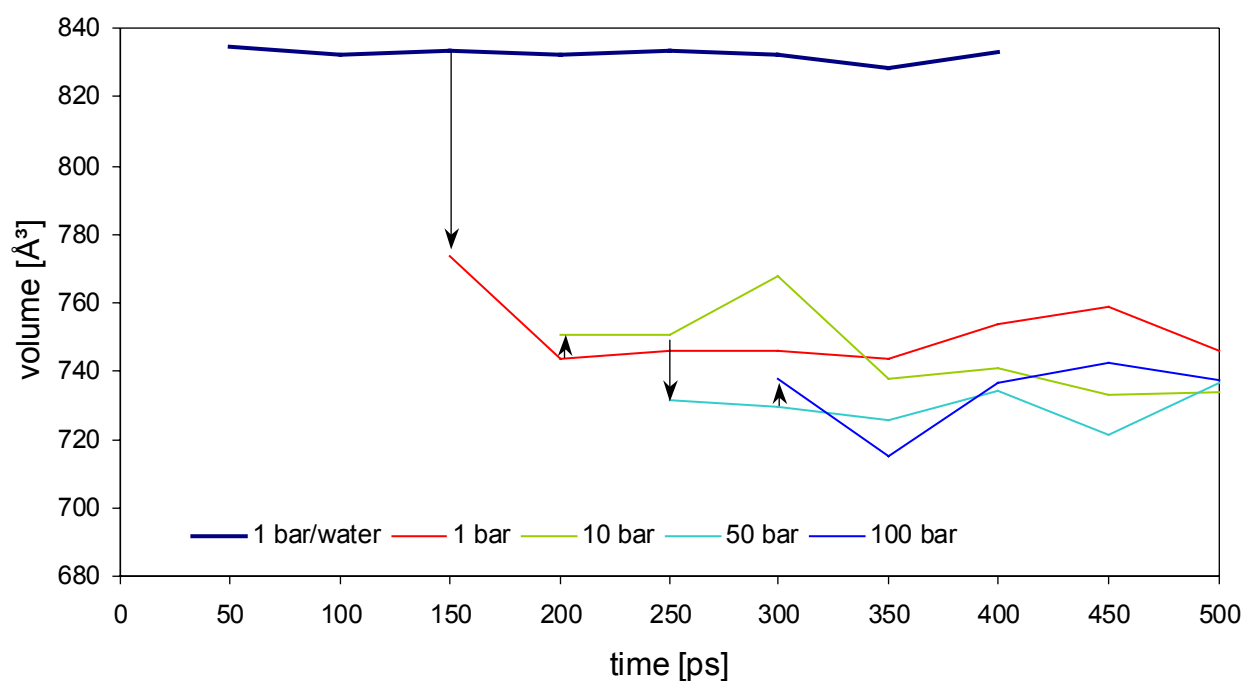


Figure 29 Volume of the simulation assembly during the molecular dynamics simulations in water and chloroform. The conformation at 100 ps in water was taken as a starting structure for the molecular dynamics simulation in chloroform at 1 bar. Starting structures for the simulation at elevated pressures were the configurations obtained after 50 ps of simulation at previous, lower, pressure (depicted by the arrows).

The number of hydrogen bonds of the amino acids in the active site increased with increasing pressure (see Figure 31). This was to expect as the volume decreased with increasing pressure (see Figure 29) and the components of the simulation cell were not changed throughout the entire process of molecular dynamics simulation. For crucial phenylalanine 415 (see below), the number of hydrogen bonds remained constant (see Figure 31).

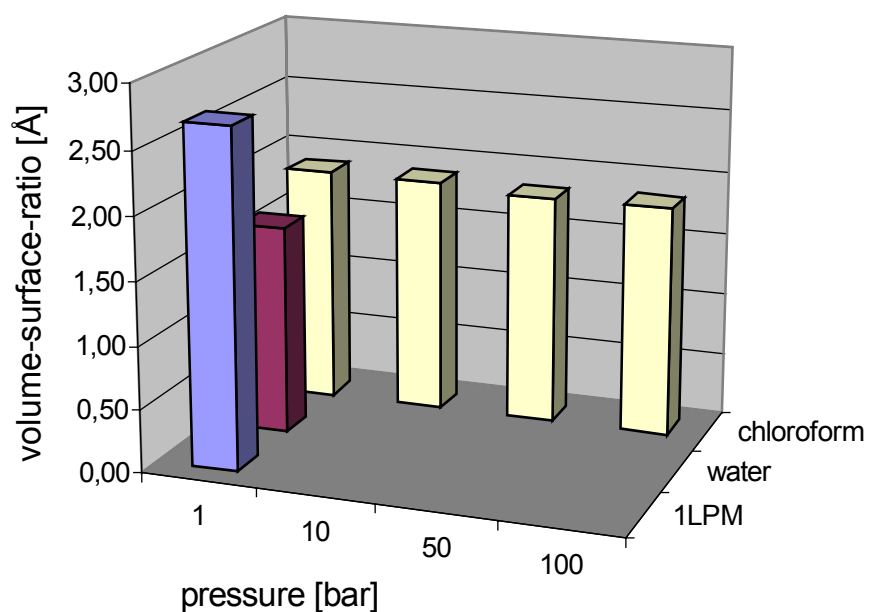


Figure 30 Volume-Surface-Ratio of the *Candida rugosa* lipase simulated in different solvents compared to the crystal structure 1LPM.

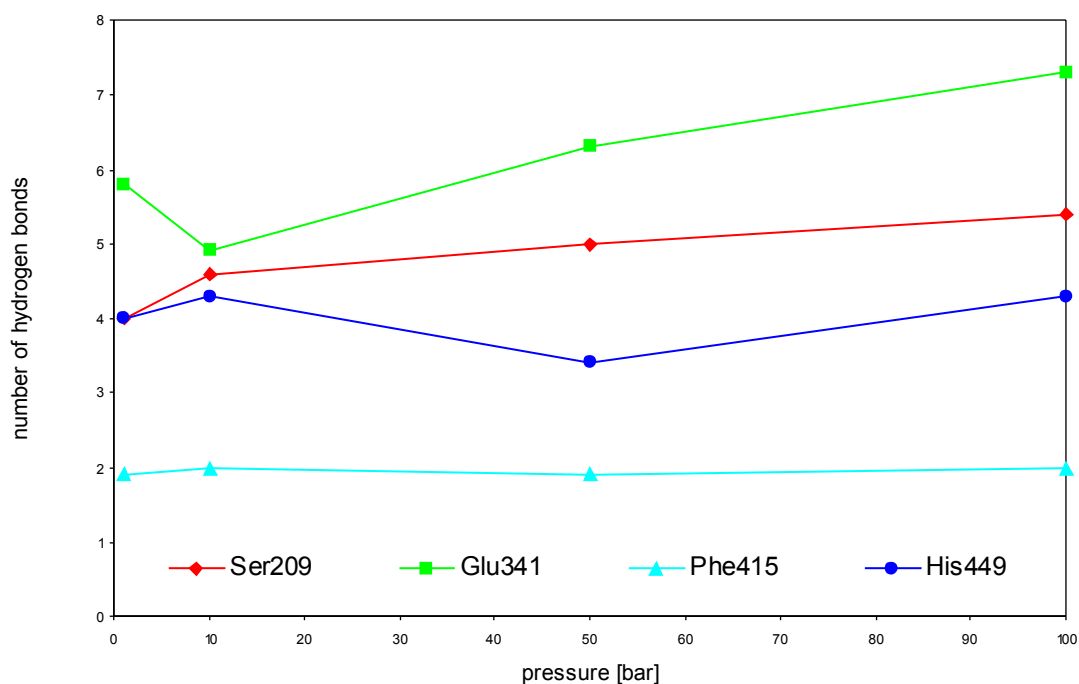


Figure 31 Averaged number of hydrogen bonds of the active site residues and F415 during each molecular dynamics simulation at different pressures.

*Averaging the protein conformations*

Simulation times for the particular molecular dynamics simulations in water as well as in chloroform were 400 ps at 1 bar, 350 ps at 10 bar, 300 ps at 50 bar, and 250 ps at 100 bar, respectively. Only the last 50 ps of each simulation were sampled in the production phase of the simulations. In case of the molecular dynamics simulation of *Candida rugosa* lipase in water, only the last 15 ps were used for averaging. Here, with 11,332 water molecules instead of 2,289 chloroform molecules plus 244 crystal water molecules, the amount of data was such that only 15 ps could be analyzed with the given infrastructure. The protein structures obtained during the production phase of the molecular dynamics simulations were averaged for further analysis. The rms-values compared to the crystal structure of all C $\alpha$ -atoms of the simulated structures averaged over the last 50 ps of each simulation (production phase) did not exceed 1.8 Å (see Table 14).

simulated pressure [bar]	rmsd [Å]
1	1.56
10	1.73
50	1.67
100	1.61
1 (water)	1.57

Table 14 rmsd values of all backbone C $\alpha$ -atoms from the crystal structure of *Candida rugosa* lipase averaged over the last 50 ps of each simulation production phase. In case of molecular dynamics simulation with explicit water as solvent, the last 15 ps were used for averaging.

The stability of the molecular dynamics simulations performed was validated by inspecting both energies (see Figure 20 and Figure 21) and volume (see Figure 29) of the simulation assembly and the radius of gyration (see Figure 32), the rms-values towards the crystal structure of all C $\alpha$ -atoms in the protein (see Figure 33) and the rms-fluctuations during the production phase of the molecular dynamics simulations (see Figure 52). In the course of the molecular dynamics simulations, strong changes in the radius of gyration and the rmsd values could be observed in the first 100 ps,

whereas only slight changes were observable after 100 ps. The radius of gyration of the conformations in the course of the molecular dynamics simulations in water as well as in chloroform decreases in the first 100 ps, thereafter only slightly drifting towards larger values (see Figure 32). Similarly, the rms-values of the conformations in the course of the molecular dynamics simulations in water as well as in chloroform increased in the first 100 ps, thereafter only slightly drifting towards larger values (see Figure 33). In case of the molecular dynamics simulation of *Candida rugosa* lipase in water, the radius of gyration started fluctuating after about 300 ps. This is due to flexible loops on the surface of the protein which began to flap in the surrounding solvent. Although the radius of gyration and the rmsd values of the molecular dynamics simulations indicated a slight drift towards larger values, the observable differences between the conformations at 1 bar, 10 bar, 50 bar, and 100 bar exceed the differences caused by the drift. Thus, it can be concluded, that the molecular dynamics simulations at different pressures can be evaluated to search for a trend caused by increased pressure, even though equilibration was not yet completely reached.

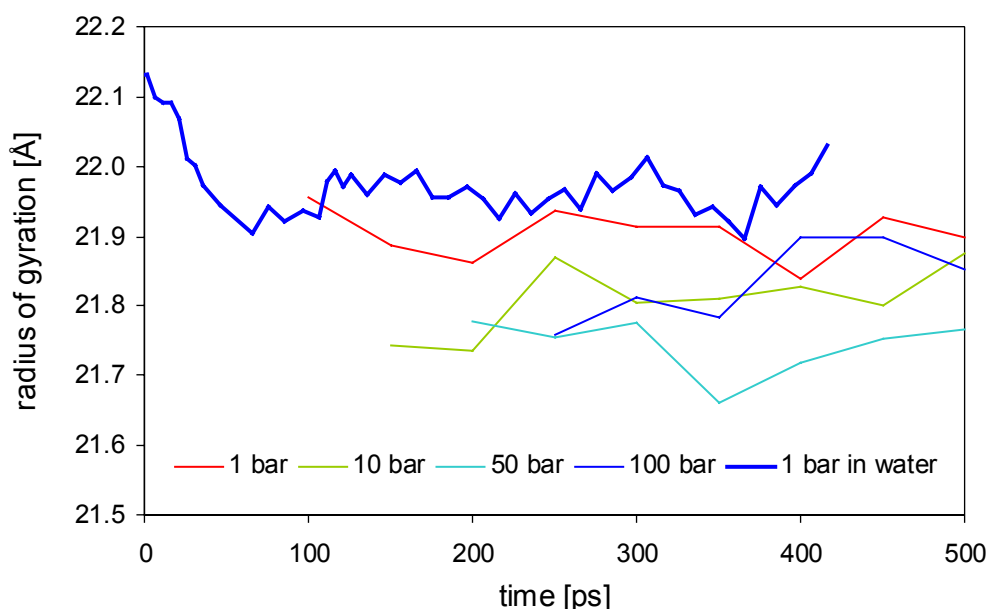


Figure 32 Radius of gyration during the molecular dynamics simulations in water at 1 bar and in chloroform at 1 bar, 10 bar, 50 bar, and 100 bar. The conformation at 100 ps in water was taken as starting structure for the molecular dynamics simulation in chloroform at 1 bar.

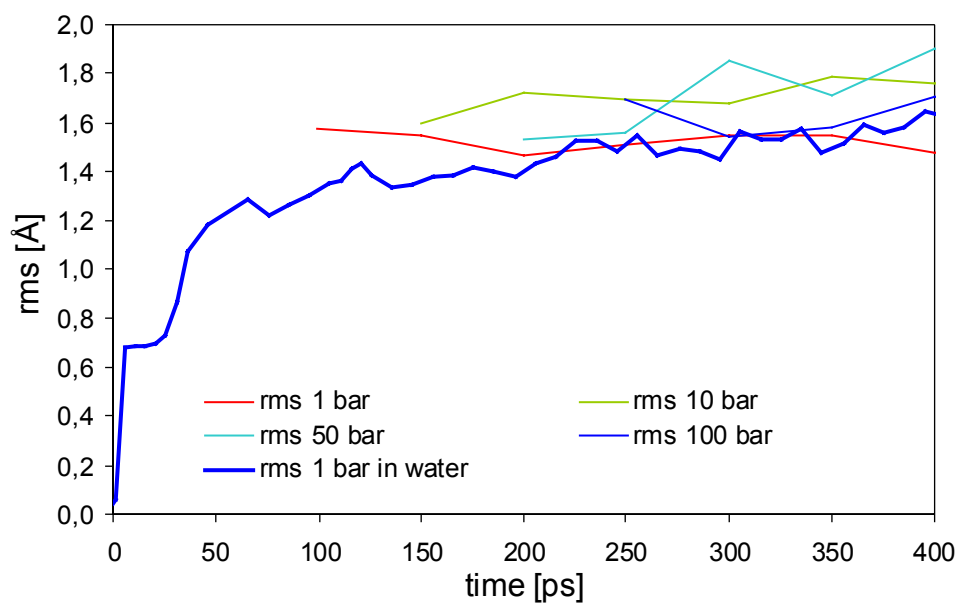


Figure 33 rms during the molecular dynamics simulations in water at 1 bar and in chloroform at 1 bar, 10 bar, 50 bar, and 100 bar. The conformation at 100 ps in water was taken as starting structure for the molecular dynamics simulation in chloroform at 1 bar.

### Analysis of the averaged structures

In the X-ray structure of CRL, 1lpm, from the overall 534 amino acid residues, 385 (86.5 %) were assigned to the most favored regions of a Ramachandran plot (Morris, MacArthur et al. 1992; Laskowski, MacArthur et al. 1993) (see Figure 34 and Figure 35), 56 (12.6 %) to the additional allowed regions (see Figure 35 and Figure 36). The amount of residues of 1lpm in disallowed regions was three or 0.7 % (see Figure 35 and Figure 40), whereas the number of amino acids in the generously allowed regions of the Ramachandran plot was one, 0.2 %, namely S301 (see Figure 35 and Figure 38). The residues occupying the disallowed regions of the Ramachandran plot were I18, S209, V444 located in a loop structure. S301 was also located in a loop region. The  $\Phi$ -values of I18, S209, and V444 were ca.  $80^\circ$ ,  $55^\circ$ , and  $60^\circ$ , their  $\Psi$ -values about  $-60^\circ$ ,  $-110^\circ$ , and  $-45^\circ$  and, therefore, could be found out of the most favored regions for a loop structure. S301 was ca.  $55^\circ$  ( $\Phi$ -value) and  $-130^\circ$  ( $\Psi$ -value) and out of the most favored area for a residue in a loop region (see Figure 35).

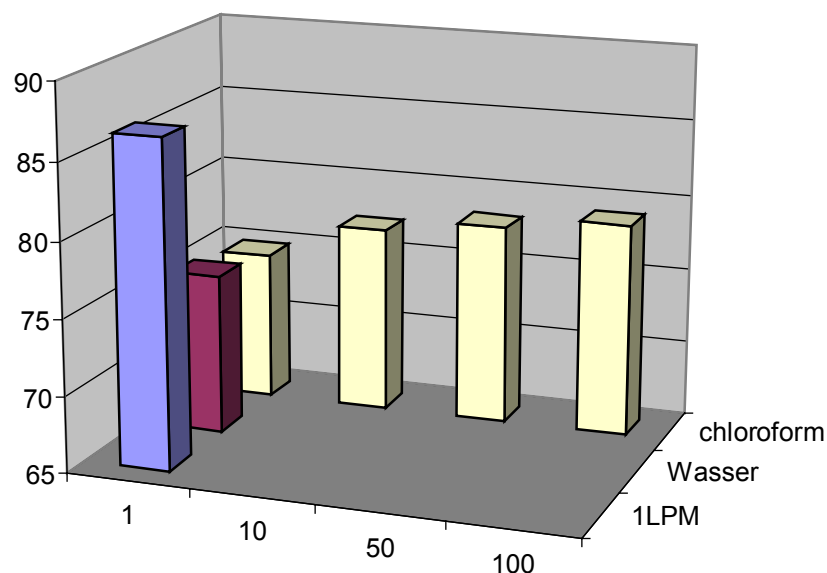
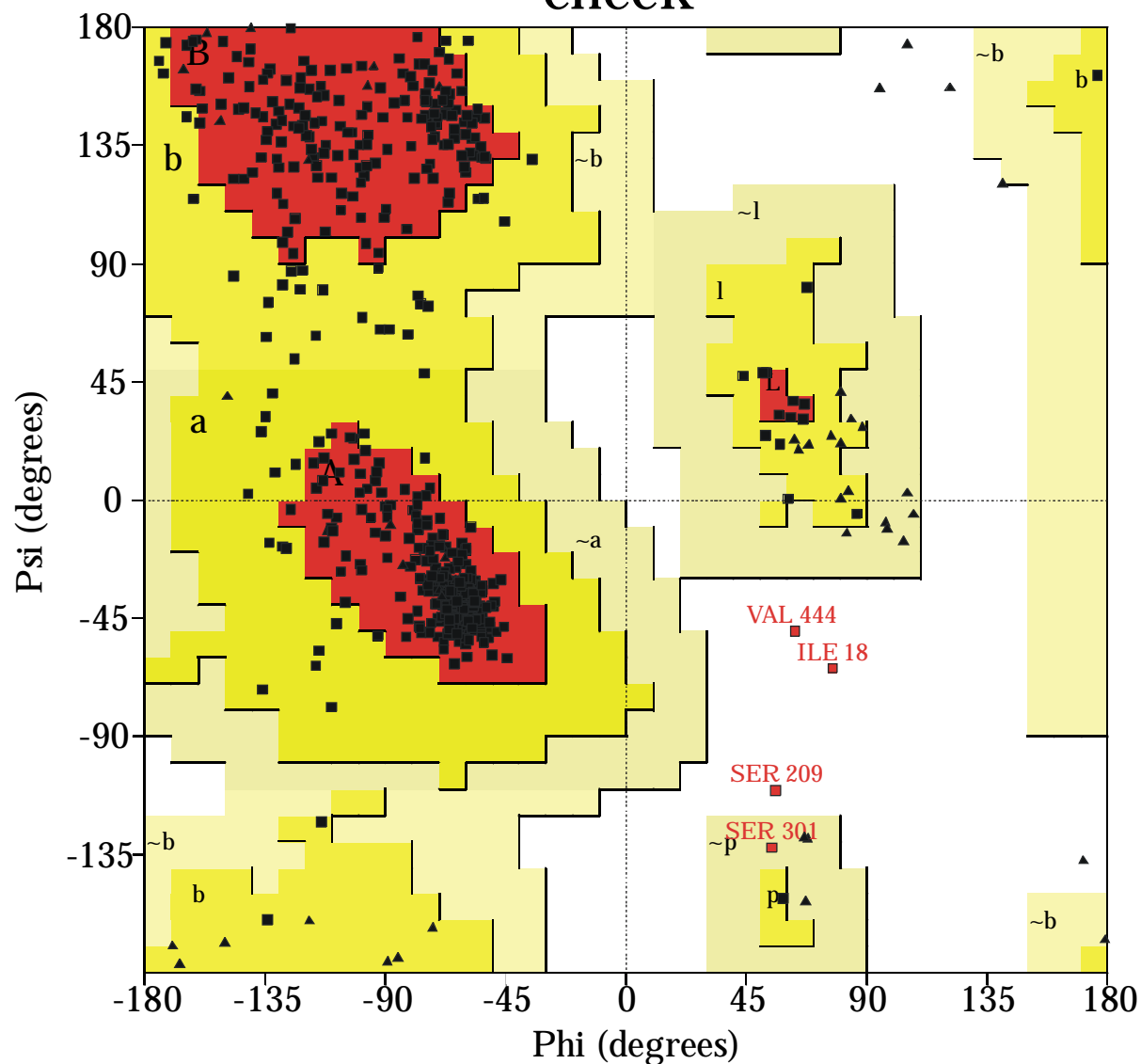


Figure 34 Percentage of amino acid residues of the *Candida rugosa* lipase in the most favored regions of the ramachandran plot simulated in different solvents compared to the crystal structure 1LPM.

# Ramachandran Plot check



## Plot statistics

Residues in most favoured regions [A,B,L]	385	86.5%
Residues in additional allowed regions [a,b,l,p]	56	12.6%
Residues in generously allowed regions [~a,~b,~l,~p]	1	0.2%
Residues in disallowed regions	3	0.7%
-----		-----
Number of non-glycine and non-proline residues	445	100.0%
Number of end-residues (excl. Gly and Pro)	2	
Number of glycine residues (shown as triangles)	56	
Number of proline residues	31	
-----		-----
Total number of residues	534	

Based on an analysis of 118 structures of resolution of at least 2.0 Angstroms and R-factor no greater than 20%, a good quality model would be expected to have over 90% in the most favoured regions.

Figure 35 Ramachandran plot for the *Candida rugosa* crystal structure 1LPM.



CRL simulated with water as a solvent yielded 336 (75.5 %) of the residues in most favored (see Figure 34 and Figure 37), 100 (22.5 %) in additional allowed (see Figure 36), and 4 or 0.9 % residues in the disallowed regions of the Ramachandran plot (see Figure 37 and Figure 40). As for 1lpm, I18 and V444 occupied disallowed loop configurations, with  $\Phi\Psi$ -angles similar to those in 1lpm. Additionally S241 (loop) and S301 were found in these regions. S301 in 1lpm was located in a so called generously allowed region of a loop region (see Figure 35 and Figure 38). The  $\Phi$ -values of I18, S241, S301, and V444 were about  $55^\circ$ ,  $65^\circ$ ,  $40^\circ$ , and  $45^\circ$ , their  $\Psi$ -values ca.  $-70^\circ$ ,  $130^\circ$ ,  $-90^\circ$ , and  $-60^\circ$  and out of the most favored regions for a loop region. Five residues, F38, S159, S209, S450, and L478 or 1.1 % of the overall residues were assigned to generously allowed regions of the Ramachandran plot being ca.  $70^\circ$ ,  $60^\circ$ ,  $15^\circ$ ,  $170^\circ$ ,  $170^\circ$  ( $\Phi$ -value) and  $-20^\circ$ ,  $-140^\circ$ ,  $-70^\circ$ ,  $-60^\circ$ ,  $-45^\circ$  ( $\Psi$ -value), also out of the most favored area for a residue in a loop /  $\alpha$ -helix (S159) region (see Figure 37 and Figure 38).

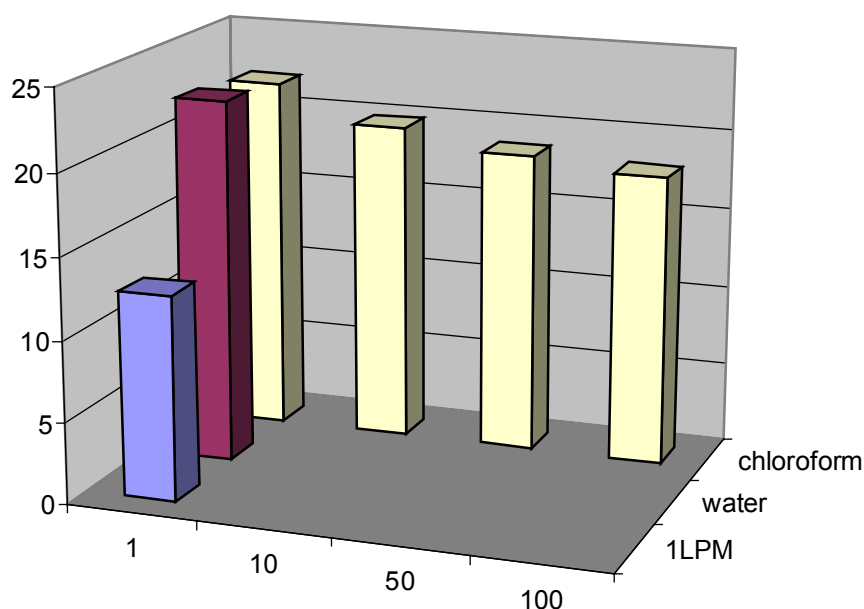
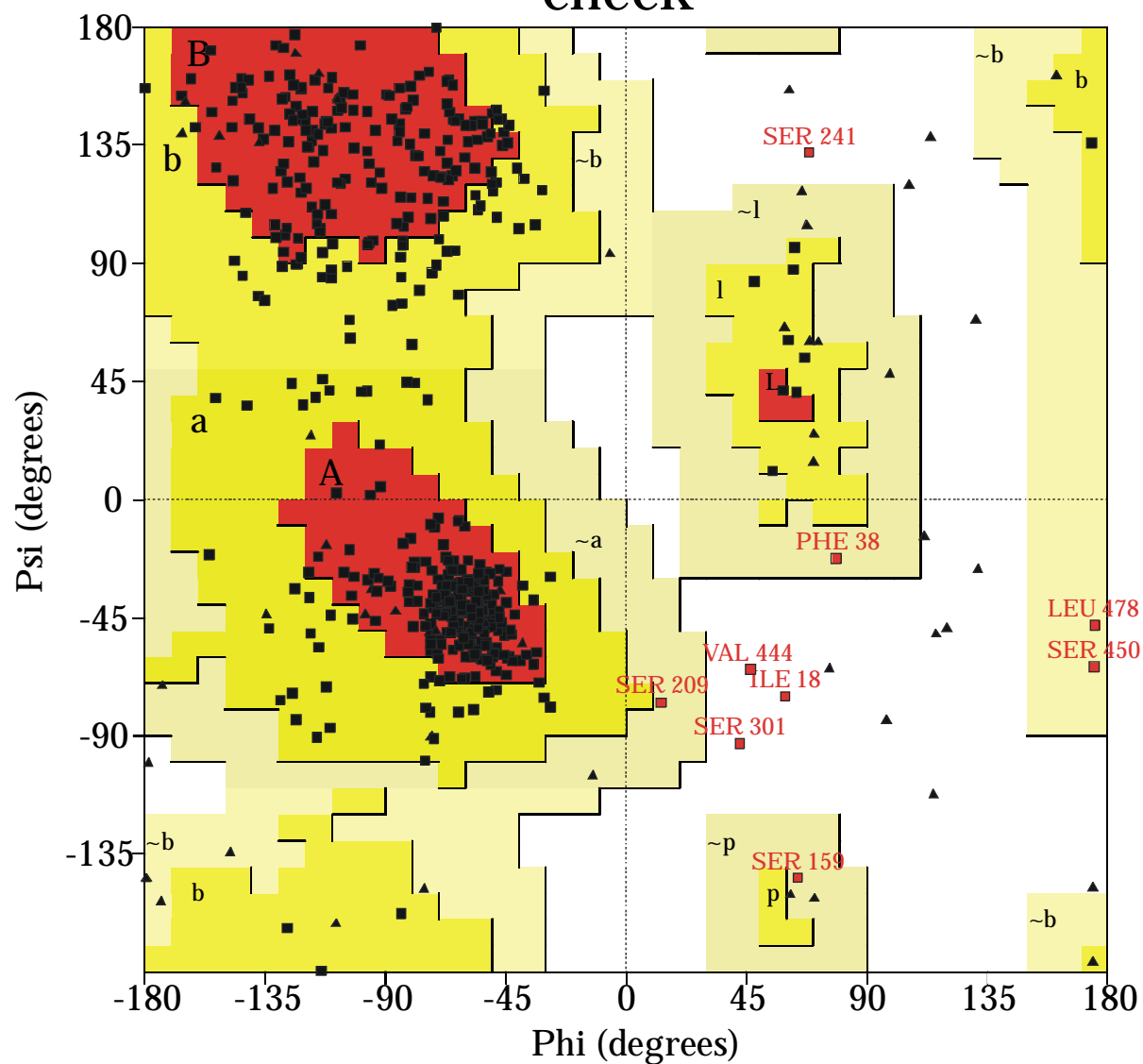


Figure 36 Percentage of amino acid residues of the *Candida rugosa* lipase in the additional allowed regions of the ramachandran plot simulated in different solvents compared to the crystal structure 1LPM.

# Ramachandran Plot check



## Plot statistics

Residues in most favoured regions [A,B,L]	336	75.5%
Residues in additional allowed regions [a,b,l,p]	100	22.5%
Residues in generously allowed regions [~a,~b,~l,~p]	5	1.1%
Residues in disallowed regions	4	0.9%
-----		
Number of non-glycine and non-proline residues	445	100.0%
Number of end-residues (excl. Gly and Pro)	2	
Number of glycine residues (shown as triangles)	56	
Number of proline residues	31	
-----		
Total number of residues	534	

Based on an analysis of 118 structures of resolution of at least 2.0 Angstroms and R-factor no greater than 20%, a good quality model would be expected to have over 90% in the most favoured regions.

Figure 37 Ramachandran plot for the *Candida rugosa* lipase simulated in water as solvent.

From the simulations of CRL in chloroform at varying pressures, the protein simulated at 1 bar had 333 (74.8 %), 98 (22.0 %), five (1.1 %), and nine residues (2.0 %) in the most favored (see Figure 34 and Figure 39), additional allowed (see Figure 36 and Figure 39), generously allowed (see Figure 38 and Figure 39), and disallowed regions, respectively (see Figure 39 and Figure 40). These values were comparable to the ones for the protein simulated in water, except for the amino acids occupying configurations in disallowed regions of the Ramachandran plot being almost double the number as compared to CRL in water (see Figure 37). I18, F38, Q51, S209, Y299, S301, L302, D318, and S450 showed  $\Phi\Psi$ -values in the disallowed regions of the Ramachandran plot. I.e., residues Y299, S301, and L302 indicated a regional rather than local distortion of the protein. I18 and S209 in all three structures analyzed so far were located in these regions, whereas, S301 also in CRL simulated in water was found in a disallowed region, however, with a shift in  $\Psi$ -torsion angle of about  $225^\circ$ . Q51 was located in a  $\beta$ -strand, I18, F38, S209, Y299, S301, L302, D318, S450 in a loop region. The  $\Phi\Psi$ -values were about  $55^\circ$ ,  $60^\circ$ ,  $75^\circ$ ,  $45^\circ$ ,  $60^\circ$ ,  $55^\circ$ ,  $75^\circ$ ,  $20^\circ$ , and  $130^\circ$  as well as ca.  $155^\circ$ ,  $-70^\circ$ ,  $-45^\circ$ ,  $-90^\circ$ ,  $-70^\circ$ ,  $155^\circ$ ,  $-45^\circ$ ,  $125^\circ$ , and  $-15^\circ$  and could be found out of the most favored regions for their respective secondary structure elements, respectively (see Figure 39).

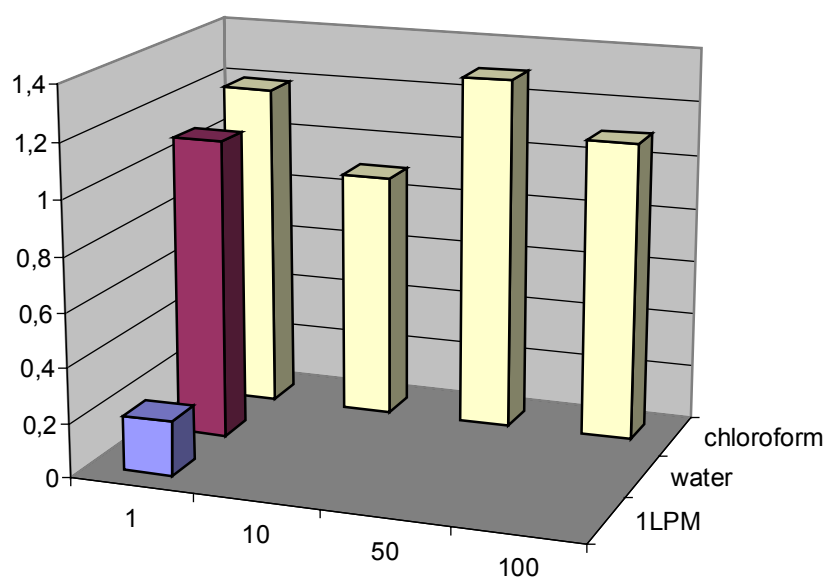
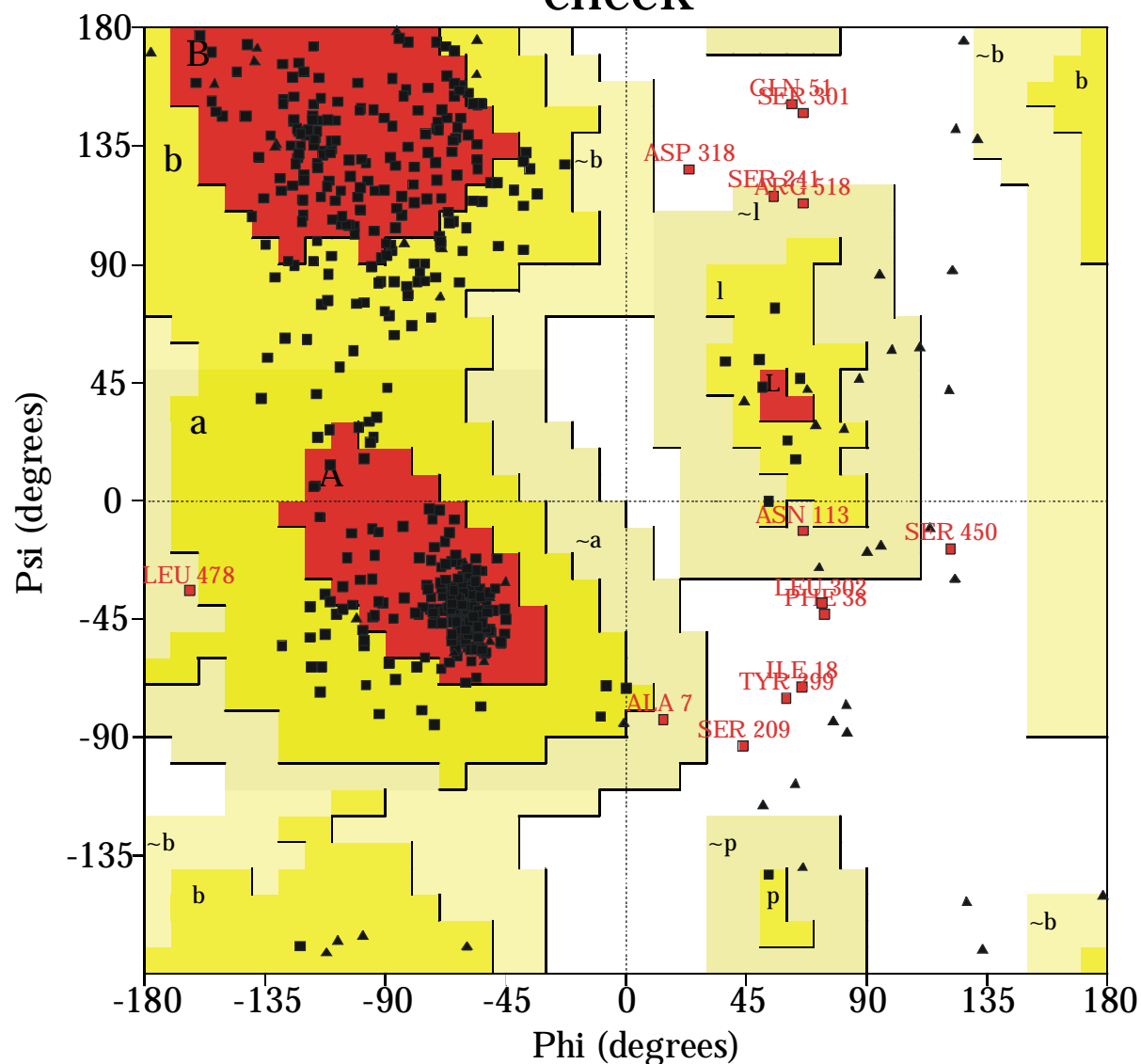


Figure 38 Percentage of amino acid residues of the *Candida rugosa* lipase in the generously allowed regions of the ramachandran plot simulated in different solvents compared to the crystal structure 1LPM.

# Ramachandran Plot check



## Plot statistics

Residues in most favoured regions [A,B,L]	333	74.8%
Residues in additional allowed regions [a,b,l,p]	98	22.0%
Residues in generously allowed regions [~a,~b,~l,~p]	5	1.1%
Residues in disallowed regions	9	2.0%
-----		
Number of non-glycine and non-proline residues	445	100.0%
Number of end-residues (excl. Gly and Pro)	2	
Number of glycine residues (shown as triangles)	56	
Number of proline residues	31	
-----		
Total number of residues	534	

Based on an analysis of 118 structures of resolution of at least 2.0 Angstroms and R-factor no greater than 20%, a good quality model would be expected to have over 90% in the most favoured regions.

Figure 39 Ramachandran plot for the *Candida rugosa* lipase simulated in chloroform as solvent at 1 bar.

From the simulation of CRL in chloroform at 10 bar, 344 (77.3 %) and 88 (19.8 %) residues were found in most favored (see Figure 34 and Figure 41) or additional allowed regions of the Ramachandran plot (see Figure 36 and Figure 41). Four amino acids, F125, D318, R518, and D592, or 0.9 % of the overall residues were located in the generously allowed regions (see Figure 38 and Figure 41). As for the simulation in chloroform at 1 bar, nine residues yielded into the disallowed regions of the Ramachandran plot (see Figure 40 and Figure 41). Of these residues, A7, I18, F38, S209, Y299, S301, V444, S450, and Q497. A7 has not yet been identified to be vulnerable in its  $\Phi\Psi$ -torsion angles. Also the backbone conformation of Q497 at 10 bar for the first time showed significant distortions. A7, I18, F38, S209, Y299, S301, V444, S450, and Q497 were placed a loop region with the  $\Phi$ -values ca.  $40^\circ$ ,  $60^\circ$ ,  $45^\circ$ ,  $55^\circ$ ,  $60^\circ$ ,  $60^\circ$ ,  $60^\circ$ ,  $125^\circ$ , and  $60^\circ$  and the  $\Psi$ -torsion angles ca.  $-90^\circ$ ,  $-80^\circ$ ,  $-90^\circ$ ,  $-95^\circ$ ,  $-95^\circ$ ,  $-50^\circ$ ,  $-45^\circ$ ,  $-20^\circ$ , and  $145^\circ$  and out of the most favored regions of their secondary structure elements, respectively (see Figure 41).

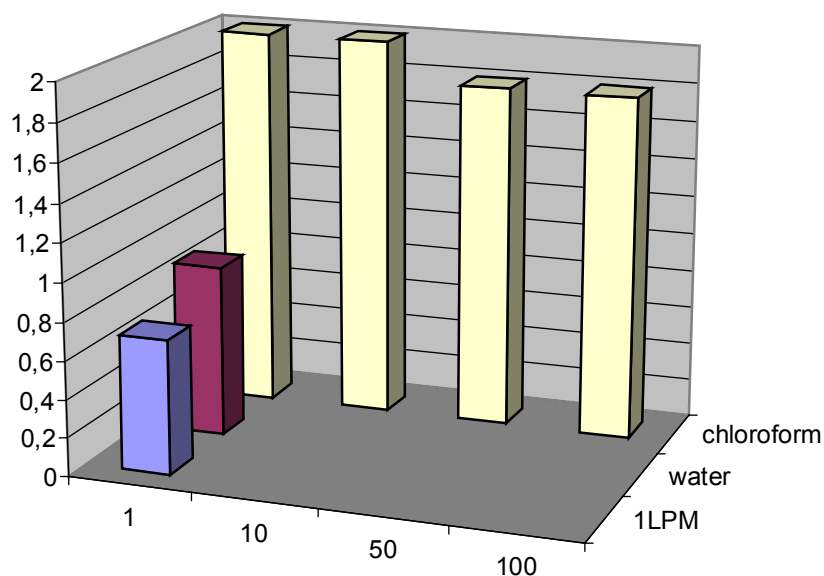
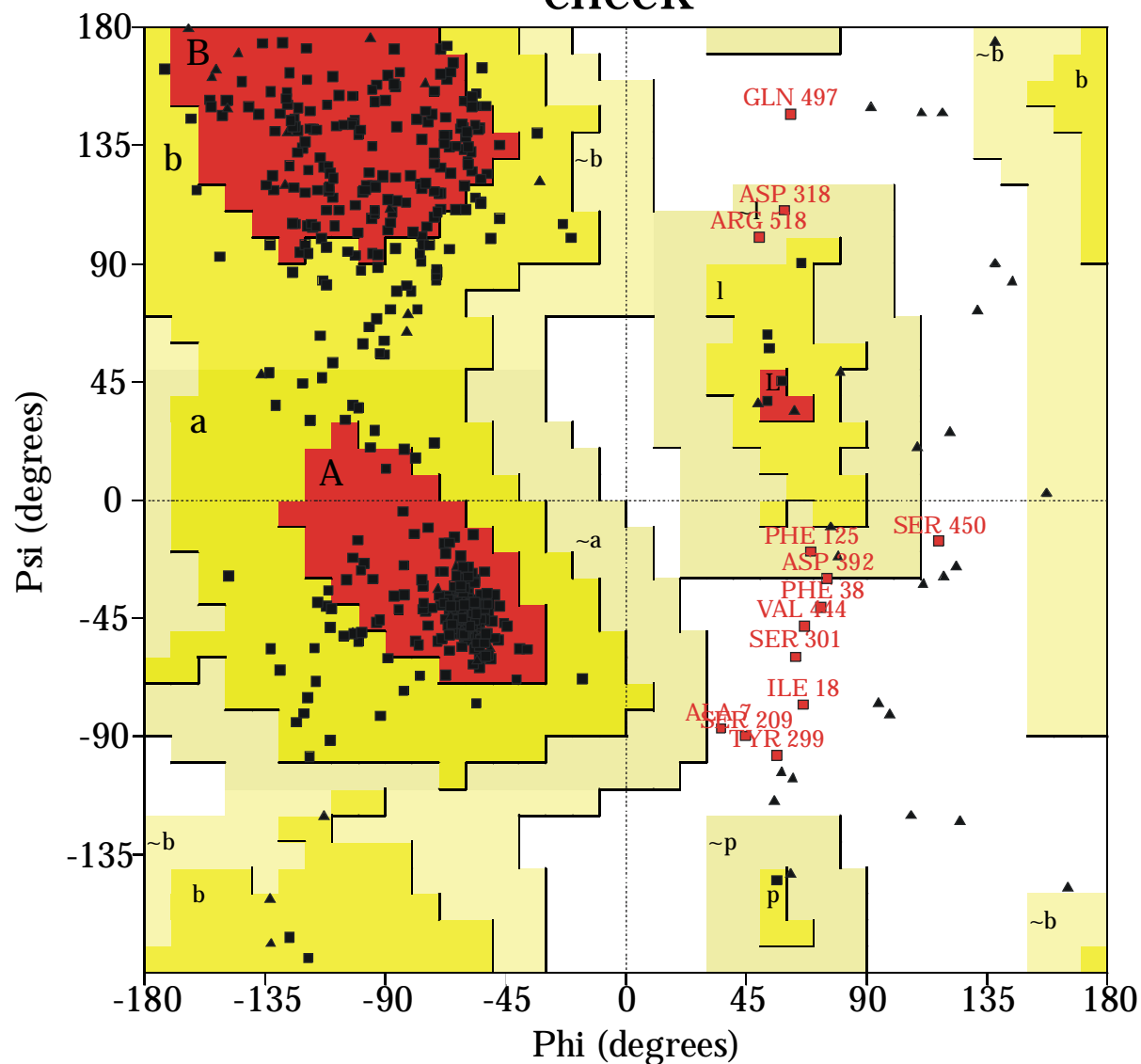


Figure 40 Percentage of amino acid residues of the *Candida rugosa* lipase in the disallowed regions of the ramachandran plot simulated in different solvents compared to the crystal structure 1LPM.

# Ramachandran Plot check



## Plot statistics

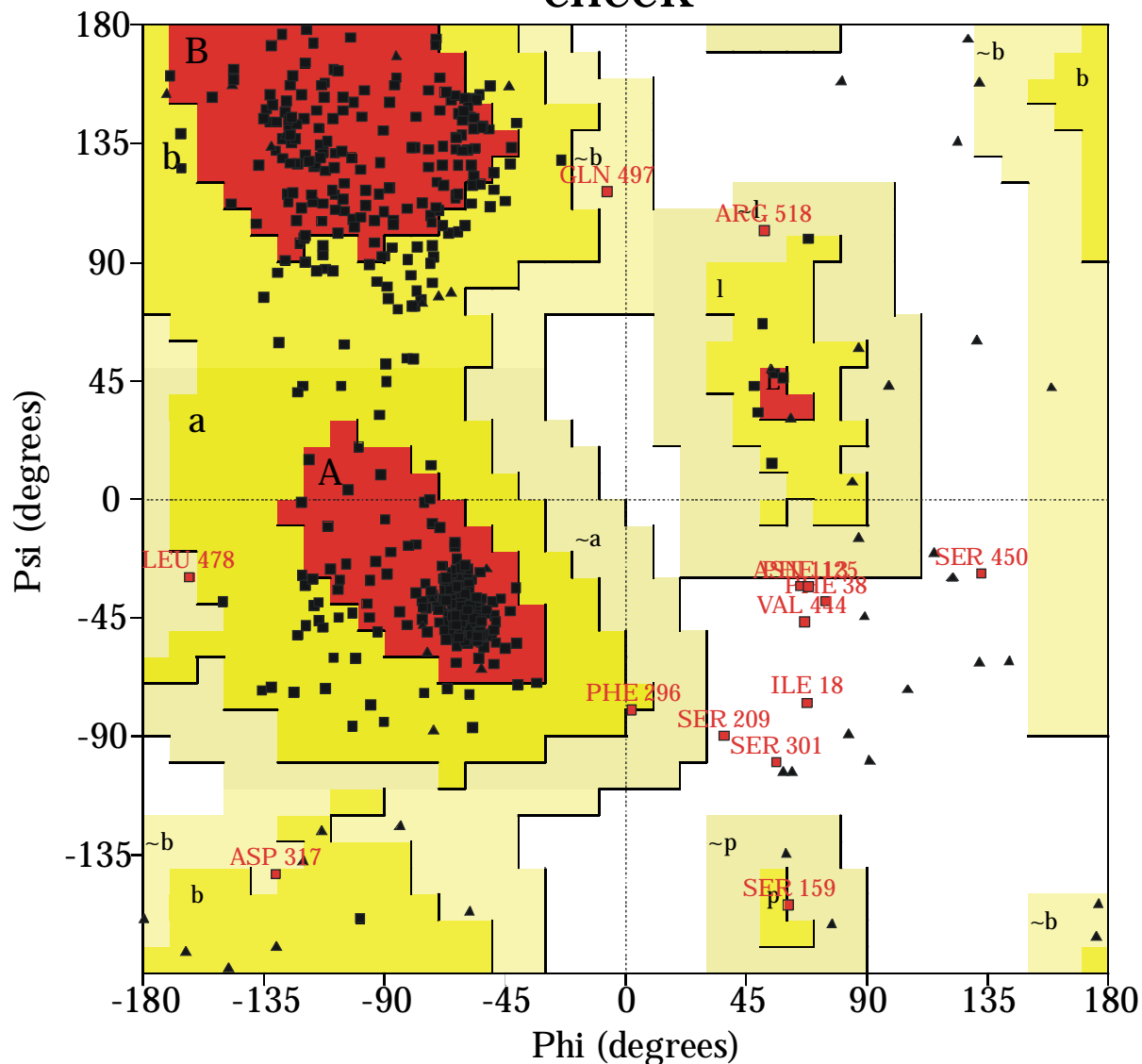
Residues in most favoured regions [A,B,L]	344	77.3%
Residues in additional allowed regions [a,b,l,p]	88	19.8%
Residues in generously allowed regions [~a,~b,~l,~p]	4	0.9%
Residues in disallowed regions	9	2.0%
-----		
Number of non-glycine and non-proline residues	445	100.0%
Number of end-residues (excl. Gly and Pro)	2	
Number of glycine residues (shown as triangles)	56	
Number of proline residues	31	
-----		
Total number of residues	534	

Based on an analysis of 118 structures of resolution of at least 2.0 Angstroms and R-factor no greater than 20%, a good quality model would be expected to have over 90% in the most favoured regions.

Figure 41 Ramachandran plot for the *Candida rugosa* lipase simulated in chloroform as solvent at 10 bar.

From the simulation of CRL in chloroform at 50 bar, 348 residues or 78.2 % were in most favored (see Figure 34 and Figure 42), 83 or 18.7 % in additional allowed (see Figure 36 and Figure 42), six or 1.3 % in generously allowed (see Figure 38 and Figure 42), and eight or 1.8 % in disallowed regions (see Figure 40 and Figure 42). S159, F296, D317, L478, Q497, and R518 occupied the generously allowed regions, whereas I18, F38, N113, F125, S209, S301, V444, and S450 were in the disallowed regions of the Ramachandran plot (see Figure 42). N113 and F125 showed distortions in their backbone conformation while A7 and Q497 were more relaxed as compared to the simulation at 10 bar. The following residues were found to be located in a loop region: I18, F38, N113, F125, S209, S301, V444, and S450. The  $\Phi\Psi$ -backbone torsion angles of residues I18, F38, N113, F125, S209, S301, V444, and S450 were identified to be about 60°, 60°, 60°, 60°, 40°, 55°, 60°, and 135° and -70°, -30°, -25°, -25°, -90°, -95°, -45°, and -20°, respectively, and out of the range for most favored regions for the respective secondary structure (see Figure 42).

# Ramachandran Plot check



## Plot statistics

Residues in most favoured regions [A,B,L]	348	78.2%
Residues in additional allowed regions [a,b,l,p]	83	18.7%
Residues in generously allowed regions [~a,~b,~l,~p]	6	1.3%
Residues in disallowed regions	8	1.8%
-----		
Number of non-glycine and non-proline residues	445	100.0%
Number of end-residues (excl. Gly and Pro)	2	
Number of glycine residues (shown as triangles)	56	
Number of proline residues	31	
-----		
Total number of residues	534	

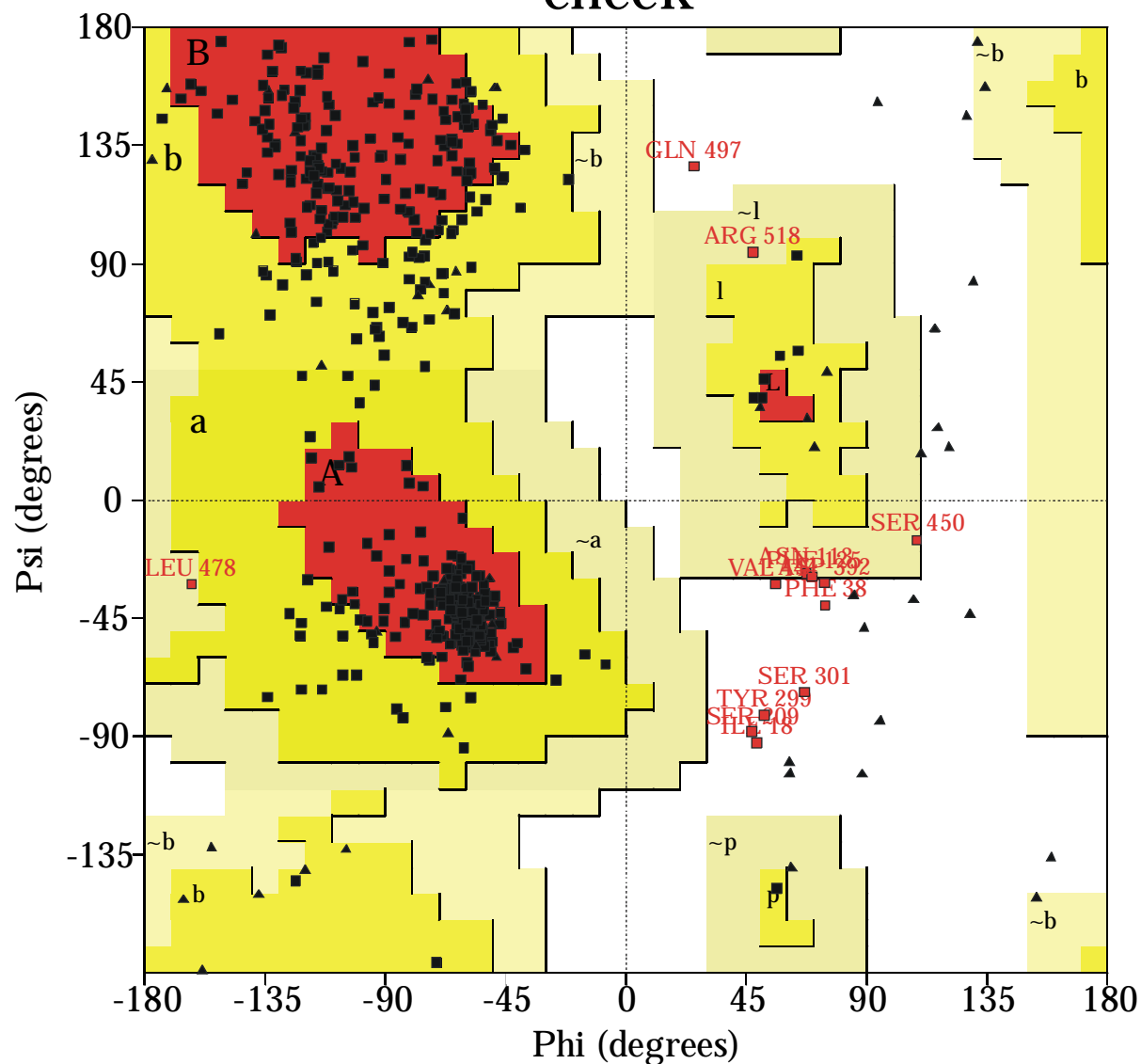
Based on an analysis of 118 structures of resolution of at least 2.0 Angstroms and R-factor no greater than 20%, a good quality model would be expected to have over 90% in the most favoured regions.

Figure 42 Ramachandran plot for the *Candida rugosa* lipase simulated in chloroform as solvent at 50 bar.



From the simulation of CRL in chloroform at 100 bar, the backbone of 352 (79.1 %) residues could be assigned to most favored regions of the Ramachandran plot (see Figure 34 and Figure 43). The  $\Phi\Psi$ -backbone torsion angles of 80 (18.0 %) residues were in the additional allowed (see Figure 36 and Figure 43), of five amino acids (1.1 %), N113, F125, S450, L478, and R518, in the generously allowed regions (see Figure 38 and Figure 43). I18, F38, S209, S299, S301, D392, V444, and Q497 were found in the disallowed regions occupying loop substructures (see Figure 40 and Figure 43). Their  $\Phi$ - and  $\Psi$ -torsion angles were about 45°, 50°, 45°, 50°, 65°, 70°, 70°, and 20° and -90°, -40°, -90°, -85°, -70°, -35°, -30°, and 130°, respectively, and out of the range for most favored regions for the respective secondary structure (see Figure 43).

# Ramachandran Plot check



## Plot statistics

Residues in most favoured regions [A,B,L]	352	79.1%
Residues in additional allowed regions [a,b,l,p]	80	18.0%
Residues in generously allowed regions [~a,~b,~l,~p]	5	1.1%
Residues in disallowed regions	8	1.8%
-----		
Number of non-glycine and non-proline residues	445	100.0%
Number of end-residues (excl. Gly and Pro)	2	
Number of glycine residues (shown as triangles)	56	
Number of proline residues	31	
-----		
Total number of residues	534	

Based on an analysis of 118 structures of resolution of at least 2.0 Angstroms and R-factor no greater than 20%, a good quality model would be expected to have over 90% in the most favoured regions.

Figure 43 Ramachandran plot for the *Candida rugosa* lipase simulated in chloroform as solvent at 100 bar.

*Docking of ( $\pm$ )-menthylester into the simulated structures*

The tetrahedral intermediate of (+)- and (-)-menthylester was docked into the averaged structures obtained from the molecular dynamics simulations at different pressures. Subsequently, an energy minimization was carried out to release the greatest stress of the structure after manual docking. For (+)-menthol, the non-preferred enantiomer, the atom-atom distance from H449-N $\epsilon$  to (+)-menthyl-alcohol-O significantly decreased with pressure (Table 3), whereas for (-)-menthol, the preferred enantiomer, the atom-atom distance from H449-N $\epsilon$  to (-)-menthyl-alcohol-O ( $d_{\text{NE-O}}^-$ ) was only slightly affected (see Table 15). This difference in behavior of the atom-atom-distances ( $\Delta d_{\text{NE-O}} = d_{\text{NE-O}}^+ - d_{\text{NE-O}}^-$ ) in the *in silico* experiment could be correlated to the *in vitro* experiment. Correlation could be observed between the E-value on one hand and geometrical properties of the simulated *Candida rugosa* lipase on the other. The experimentally observed E-values correlated well to the difference in distance between H449-N $\epsilon$  and (+)-menthyl-alcohol-O (slow reacting enantiomer), and (-)-menthyl-alcohol-O (fast reacting enantiomer) ( $\Delta d_{\text{NE-O}} = d_{\text{NE-O}}^+ - d_{\text{NE-O}}^-$ ), respectively: Large differences  $\Delta d_{\text{NE-O}}$  at low pressures corresponded to high enantioselectivity, small differences  $\Delta d_{\text{NE-O}}$  at high pressures to low E-values (see Figure 45, filled squares). A second factor contributed to the decreased enantioselectivity at high pressures: the lone electron pair of the alcohol oxygen in (+)-menthol, the non-preferred enantiomer, with increasing pressure oriented towards H449 (see Figure 57 to Figure 60), thus facilitating the hydrogen transfer. The differences in the angle (N-O) $^+$  (Figure 39) with increasing pressure in the *in silico* experiment could be correlated to the *in vitro* experiment: large angles (N-O) $^+$  at low pressures correspond to high enantioselectivity, small angles (N-O) $^+$  at high pressures to low E-values (see Table 15). Unlike the difference in the atom-atom distances,  $\Delta d_{\text{NE-O}}$ , no gradual decrease of the angle (N-O) $^+$  was observed. The angle abruptly switched from high values at 1 bar and 10 bar to low values at 50 bar and 100 bar (Table 15).

simulated press. [bar]	distance [Å] between His449-N $\epsilon$ and (-)-menthyl- alcohol-O	(+)-menthyl- alcohol-O	Phe415-C $\delta$	angle [°] (N-O) <sup>+</sup>
1	3.0	4.6	4.4	81.0
10	2.9	4.5	4.6	76.3
50	2.9	3.9	4.8	12.0
100	2.6	3.3	6.7	20.6

Table 15 Geometrical analysis of the averaged and energy minimized structures of *Candida rugosa* lipase containing the manually docked tetrahedral intermediate of the (-)-and (+)-menthylester at increasing pressure. The angle (N-O)<sup>+</sup> was calculated using the scalar product of the vector from the H449-N $\epsilon$  to its hydrogen atom and the sum of the vectors of the neighboring carbon atoms towards the (+)-menthyl ester oxygen atom. For the visualization of the calculation see also Figure 44. The distances listed in column 4 were taken from the averaged structure without docking of the transition state analogue.

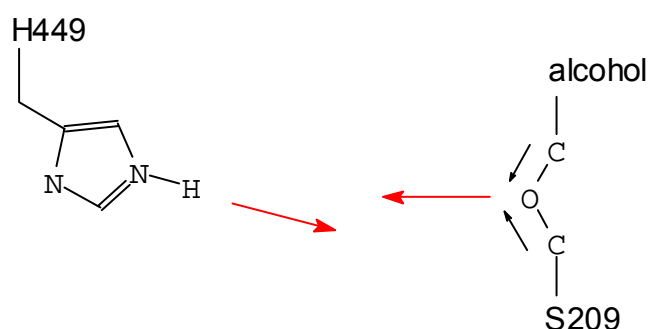


Figure 44 Calculation of the angle (N-O)<sup>+</sup>. The tetrahedral intermediate of the (+)-menthylester was docked into the energy minimized structures of the *Candida rugosa* lipase simulated at different pressures.

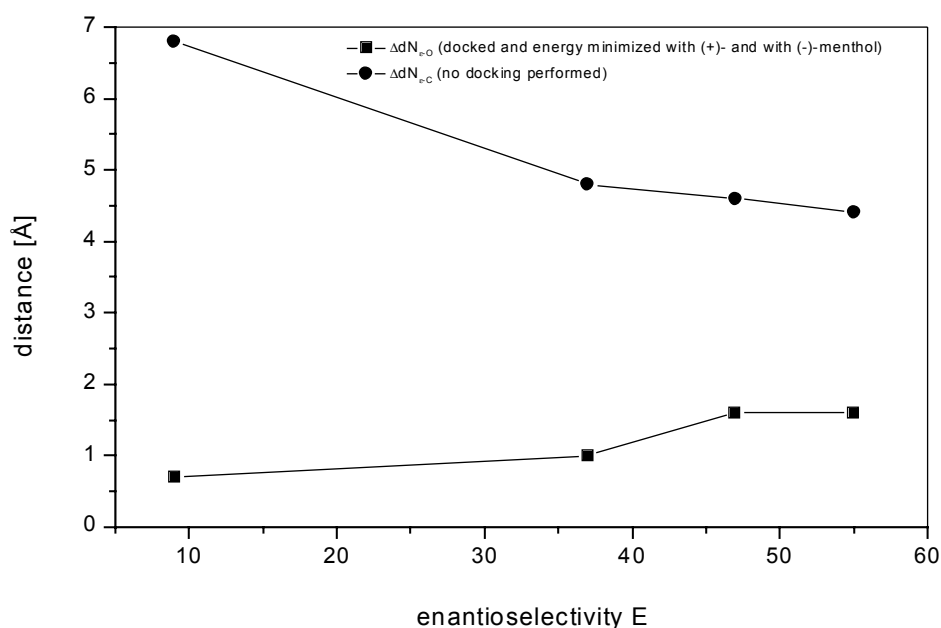


Figure 45 Correlation between biotransformation (experimentally determined E-value) and molecular dynamics simulation. The correlation for the distance of H449-N $\epsilon$  to F415-C $\phi$  and the E-values was 97.5 %. For the differences in distance of H449-N $\epsilon$  to ( $\pm$ )-menthyl-O and the E-values, the correlation was 91.5 %. The correlation was calculated by the following equation:

$$\rho_{XY} = \frac{Cov(X,Y)}{\sigma_X \cdot \sigma_Y}$$

with  $-1 \leq \rho_{XY} \leq 1$  and  $Cov(X,Y) = \frac{1}{n} \sum_{i=1}^n (x_i - \mu_x)(y_i - \mu_y)$  and  $\mu_x, \mu_y$  : averages of x (E-values) and y ( $\Delta d_{N\epsilon-O}$ ) and  $\sigma_x, \sigma_y$  standard deviations.

$$\Delta d_{N\epsilon-O} = d_{N\epsilon-O}^+ - d_{N\epsilon-O}^-$$

with  $d_{N\epsilon-O}^+$  : distance between H449-N $\epsilon$  and (+)-menthyl-alcohol-O

$d_{N\epsilon-O}^-$  : distance between H449-N $\epsilon$  and (-)-menthyl-alcohol-O

The distances were measured according to Figure 56.

#### Analysis of the averaged structures

Analyzing the crystal structure 1LPM revealed a cavity beginning at the surface of the lipase distinct from the substrate binding site, extending through the interior of the protein and ending near the catalytic histidine. The cavity is formed by side chains of E208, Q240, S241, G242, G336, D337, Q338, N339, D340, E341, G342, F345, Q387, G388, S389, F391, D392, K404, S407, A408, G411, D412, T416, L417, R419,

R420, F434, L435, S436, K437, L502, M504, Y511, G513, K514, D515, N516, F517, and R518. It is filled with 6 water molecules (see Figure 48). In the molecular dynamics simulation with explicit water as solvent and at pressure 1 bar, it was filled with 10 water molecules (see Figure 49). The number of water molecules in this cavity gradually increased with increasing pressure in the molecular dynamics simulations with crystal water and chloroform as solvent: 6 molecules in the molecular dynamics simulation at 1 bar (see Figure 50), 10 molecules at 10 bar, 12 molecules at 50 bar, and 13 molecules at 100 bar (see Figure 51 and Table 16). The side chain of H449 was gradually displaced from its initial position in the crystal structure as measured by the distance between Phe415-C $\alpha$  and H449-N $\epsilon$  (see Table 15).

simulated pressure [bar]	volume [Å <sup>3</sup> ]	number of water molecules in the cavity
1	1864	6
10	2529	10
50	2526	12
100	2617	13

Table 16 Properties of the proposed water channel as analyzed in the averaged structures without docking. The volume of the cavity was estimated with the C $\alpha$ -atoms of three amino acid pairs, R518/N339, L435/F391, and F517/G341, respectively. Only the water molecules were counted in the last configuration of each molecular dynamics simulation. The volume was determined by measuring the distances between Arg518/Asn339, Leu435/Phe391 and Phe517/Glu341.

The number of buried atoms in the proposed cavity varies with the solvent as well as the pressure applied (see Figure 46). In the crystal structure, 386 atoms of the cavity were buried, whereas only 372 atoms were buried in the molecular dynamics simulation with explicit water as solvent. In the molecular dynamics simulation with explicit chloroform as solvent at 1 bar pressure, 376 atoms of the cavity were buried. With increasing pressure subsequently more atoms of the cavity became solvent accessible (see Figure 46). The number of solvent accessible atoms in the proposed cavity varied with solvent as well as pressure. In the crystal structure, 230 atoms of

the cavity were buried, 232 atoms in the molecular dynamics simulation with explicit water as solvent. In the molecular dynamics simulation with explicit chloroform as solvent at 1 bar pressure, 226 atoms of the cavity were buried. With increasing pressure more and more atoms of the cavity became solvent accessible (see Figure 46) indicating opening of the proposed water channel with increasing pressure.

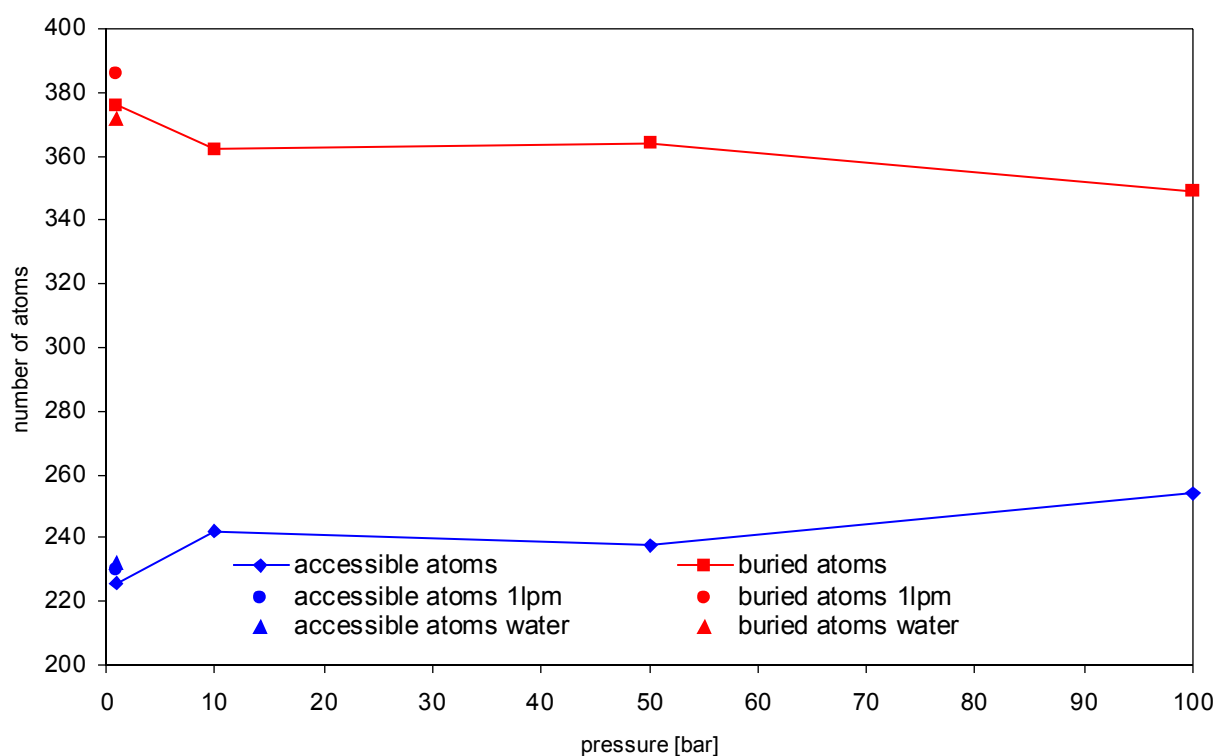


Figure 46 Number of buried and accessible residues in the proposed water channel in the molecular dynamics simulations at varying pressures.

In the simulation at 100 bar, a water molecule was observed to place itself between H449 and F415, thus, turning aside the H449 side chain (see Figure 45, filled circles; Figure 47; Figure 56). The cavity opened towards the active site and formed a continuous water channel (see Figure 51). The distance between H449-N $\epsilon$  and the (+)-menthyl-O atom displayed a similar distance between H449-N $\epsilon$  and the (-)-menthyl-O atom leading to converging reaction rates for (+)-menthol and (-)-menthol and, therefore, decreased enantioselectivity (see Figure 45 and Table 15). Each stereo view is in parallel eye mode.

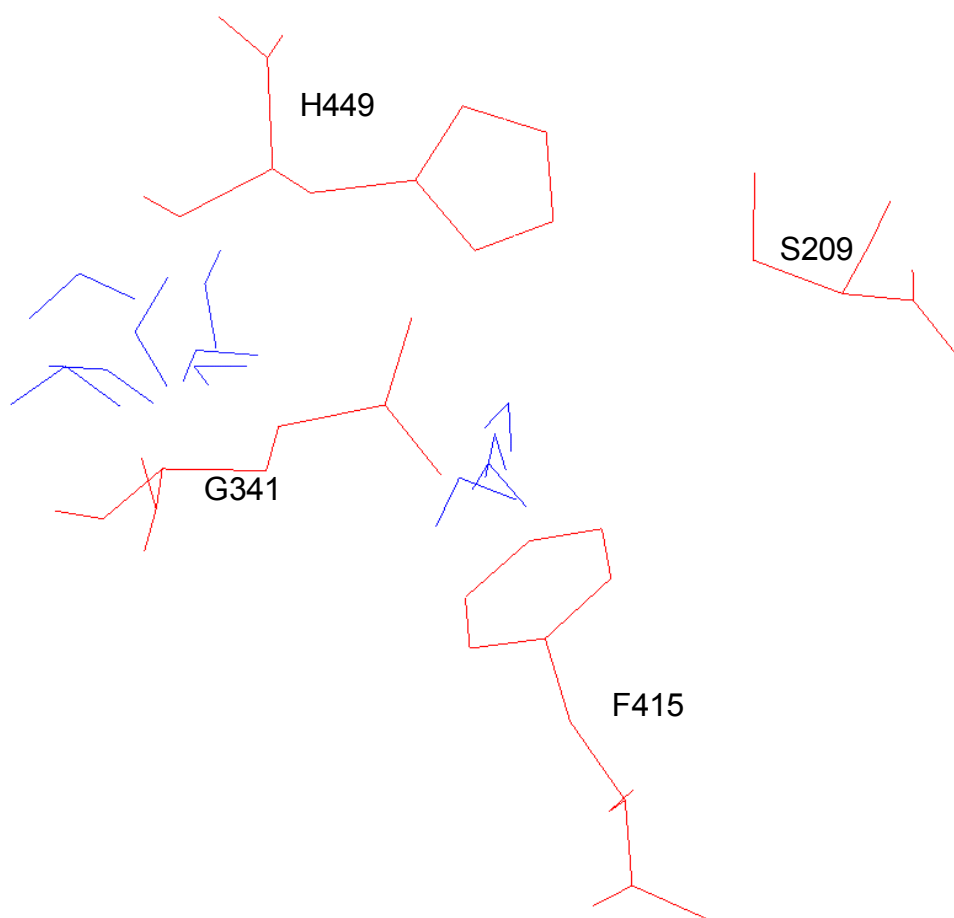


Figure 47 Location of the water molecule 631 throughout the molecular dynamics simulations at various pressures. The positions of water molecule 631, shown in blue, were taken from every 50 ps of the molecular dynamics simulations at various pressures, whereas the active site residues and F415, shown in red, were from the configuration after 250 ps at 100 bar. Left sample of positions of water molecule 631: occupied at pressures 1 bar, 10 bar, 50 bar, and for the first 50 ps of the simulation at 100 bar. Right sample of positions of water molecule 631: occupied after 50 ps of the simulation at 100 bar.



At pressures up to 50 bar and the first 50 ps of the molecular dynamics simulation at 100 bar, the water molecule 631 was located outside the active site between H449 and G341 (Figure 42, left sample of water 631 positions). After 50 ps at 100 bar, water molecule 631 shifted towards the core of the protein into the active site and displaced the two amino acids H449 and F415 from their original position in the crystal structure (Figure 42, right sample of water 631 positions).

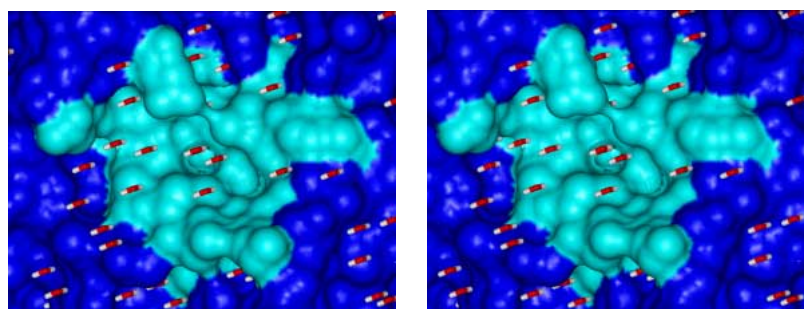


Figure 48 Stereo view of the water channel in the crystal structure of *Candida rugosa* lipase, 1LPM. The channel is closed. The hydrogen atoms of the water molecules were calculated.

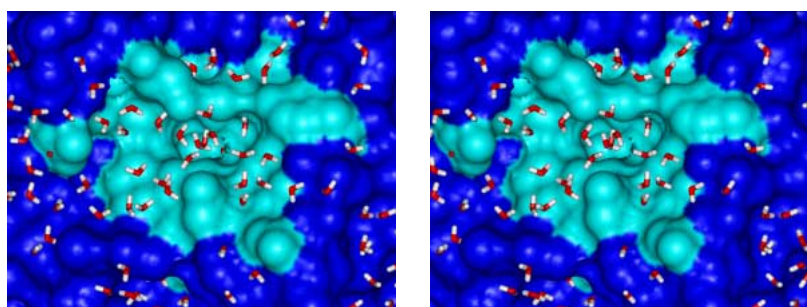


Figure 49 Stereo view of the water channel in the simulated structure of *Candida rugosa* lipase with explicit water as solvent at 1 bar. The conformation shown is a snapshot at 400 ps. The channel is closed.

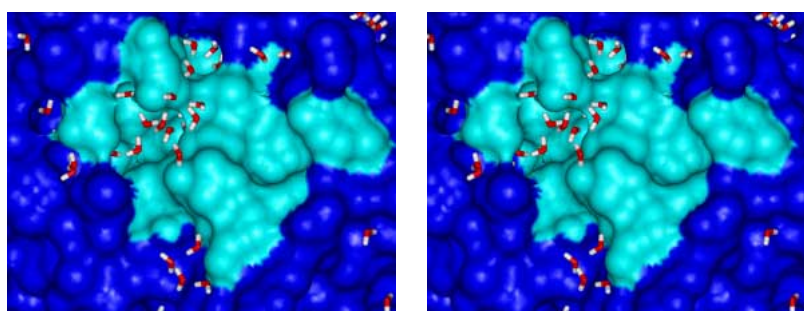


Figure 50 Stereo view of the water channel in the simulated structure of the *Candida rugosa* lipase with explicit chloroform as solvent and 244 essential water molecules at 1 bar. The conformation shown is a snapshot at 400 ps. The channel is closed.

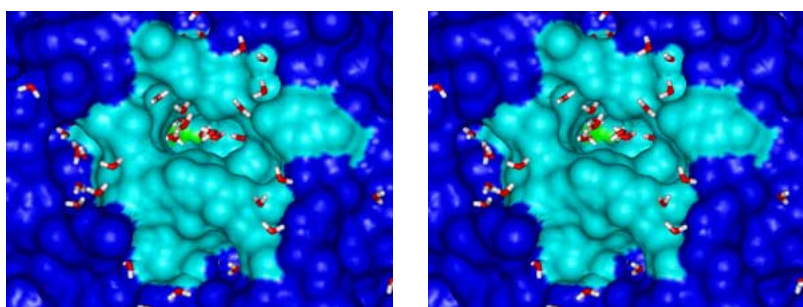


Figure 51 Stereo view of the water channel in the simulated structure of the *Candida rugosa* lipase with explicit chloroform as solvent 244 essential water molecules at 100 bar. The conformation shown is a snapshot at 250 ps. The channel is open.

## 5. DISCUSSION

### 5.1. BIOCATALYSIS

#### *Rational for the reaction, reaction conditions, and biocatalyst investigated*

The lipase-catalyzed racemic resolution of ( $\pm$ )-menthol is one of the most thoroughly studied reactions (Baratti, Buono et al. 1988; Salleh, Basri et al. 1993; Tseng, Kazlauskas et al. 1994; Kamiya and Goto 1997; Furukawa and Kawakami 1998) allowing for a well documented test case to place this work in, since the pressure dependence of enantioselectivity and protein stability has not yet been studied in this extend for lipases. A prerequisite, high quality of analysis of the experiments performed favored esterification over hydrolysis, which was reasonable, since both reactions follow the same reaction mechanism and pathway (Carter and Wells 1988). Of all lipases investigated for stereoselective reaction with menthol (see 1.1.1), only the lipases from *Candida rugosa* and *Pseudomonas species* performed sufficiently well in the screens (see Table 12) and were also commercially available in adequate amounts. In terms of synthesis planning, only the esterification of racemic ( $\pm$ )-menthol with acetic or propionic acid anhydride catalyzed by *Candida rugosa* lipase and reaction of ( $\pm$ )-menthol with menthyl acetate in presence of *Pseudomonas species* lipase yielded conversion rates above 20 % (see Table 12). However, from this already reduced set of possible test reactions, only the *Candida rugosa* lipase-catalyzed reaction of racemic ( $\pm$ )-menthol with propionic acid anhydride yielded 50 % conversion and an E-value of 50 and, thus, the highest ratio between enzyme turnover and enantioselectivity of all reactions and biocatalysts screened (see Table 12). Screens for the most suitable solvent system for the esterification of racemic ( $\pm$ )-menthol with propionic acid anhydride in presence of *Candida rugosa* lipase showed that no significant in- or decrease in the kinetic reaction parameters occurred between different solvent systems. Since the solvent was used in both molecular dynamics simulations and experiment, chloroform was the solvent of choice. Also, no additional immobilization was applied to the commercially available lipase Amano AY because no significant increase in the lipase stability could be observed. In contrast, immobilizing the lipase decreased the maximum conversion rate possible (see Table 5).

### *Analyzing biochemical studies of esterification*

The peaks for (+)- and (-)- menthol were not completely separated down to the baseline but still able to be evaluated, whereas the corresponding peaks for (-)- and (+)- menthylpropionate were well separated. The standard deviation of the E-value was calculated using 6 samples. Variation coefficients of the standard deviation were smaller than 5 %, indicative for a well reproducible amount of data.

The enantioselectivity E cannot reliably be calculated at very low or very high conversions c (Chen, Fujimoto et al. 1982). In the beginning of the enzymatic reaction, at very low conversions, an unproportional large amount of the fast-reacting enantiomer would be converted yielding E values much too high compared to the real enantioselectivity. On the other hand, at conversions near 50 %, the calculated enantioselectivity E would be too low compared to the real enantioselectivity, as now an unproportional large amount of the slow-reacting enantiomer would be found in the bulk. The enantioselectivity in this work was calculated at conversions between 15 and 30 % to ensure it to be independent of the conversion.

With the experimentally determined water content of 6.3 % for the lipase preparation in the *in vitro* and the water content of 7.1 % in the *in silico* experiment, an appropriate model of the *in vitro* experiment was set up and results made comparable. In addition, the water content in the experiment further increased by the ongoing reaction as water was produced as a by-product in any esterification reaction.

## **5.2. MODELING**

### **5.2.1. MOLECULAR DYNAMICS SIMULATIONS OF BIOLOGICAL SYSTEMS**

The first molecular dynamics simulation performed during the course of this work was the simulation of *Candida rugosa* lipase with explicit water as solvent. The simulation time was 400 ps at 300 K and 1 bar pressure showing no change of the volume of the simulation cell. The other molecular dynamics simulations were carried out with explicit chloroform as solvent, retaining the essential water molecules contained in the crystal structure of the *Candida rugosa* lipase, 1LPM.

All molecular dynamics simulations in this work were carried out with the inhibitor removed. There are several pdb-entries of the open form of *Candida rugosa* lipase with different inhibitors co-crystallized in the active site: 1LPM with (1R)-menthylhexylphosphonate, 1LPN and 1LPO with dodecanesulfonate, 1LPP with hexadecanesulfonate and 1LPS with (1S)-menthylhexylphosphonate. Although containing different inhibitors, the backbone of the protein structure in the substrate binding site is not altered in these complexes, with *Candida rugosa* lipase displaying a rather rigid active site structure. Given this rigidity of the backbone of *Candida rugosa* lipase, Scheib et al. performed molecular dynamics simulations with the protein backbone fixed developing a model for the stereoselectivity of microbial lipases (Scheib, Pleiss et al. 1999; Pleiss, Scheib et al. 2000). Thus, simulating a lipase structure without co-crystallized inhibitor is a valid approach and should not interfere with the objective to model the reality as close as possible.

Molecular dynamics simulations shorter than a nanosecond have been considered too short to be completely equilibrate (Daggett 2000), but only few long time scale simulations of large proteins have been reported yet (Aqvist 1999; Daura, van Gunsteren et al. 1999; Alonso and Daggett 2000; Radkiewicz and Brooks 2000). In this work, after significant changes during the first 100 ps, the rms value of the simulated model structure as compared to the crystal structure, in all simulations reached a value of 1.5 Å - 1.8 Å after 400 ps of simulation. The differences in several atom-atom distances (see Table 15) and the volume of the cavity (see Table 16) in the averaged structures of the molecular dynamics simulations were larger than the differences caused by the small drift in both rms values and radius of gyration (see Figure 32 and Figure 33) justifying further investigations of pressure induced structural variations. Additionally, Alonso and Daggett stated that the radius of gyration can be misleading as a reaction coordinate for unfolding/folding as of the dimension of the denatured state of any given protein is sequence-dependant and does not correlate to structure (Alonso and Daggett 2000).

For the studies presented here, for the pressure range from 1 bar to 100 bar, no significant change in volume was found (see Figure 30). These results are in line with Kitchen et al. who found a compressibility of proteins of  $\beta = 1.8 \times 10^{-2} \text{ kbar}^{-1}$  (Kitchen, Reed et al. 1992). This would correspond to a change in volume of 0.18 %.

### 5.2.2. ANALYSIS OF THE MOLECULAR DYNAMICS SIMULATIONS – EFFECTS ON CRL-STRUCTURE

For the enantioselectivity of *Candida rugosa* lipase-catalyzed esterification of ( $\pm$ )-menthol with propionic acid anhydride, a significant correlation could be observed between specific geometrical values of the averaged conformations obtained by molecular dynamics simulations and the experimentally determined E-values. The lipase undergoing molecular dynamics simulations with chloroform as a solvent became more rigid with increasing pressure indicated by a decrease of the radius of gyration compared to the molecular dynamics simulation in water as a solvent (see Figure 32) and decreased fluctuations over the last 50 ps of each molecular dynamics simulation in chloroform (see Figure 52). Kitchen and coworkers (Kitchen, Reed et al. 1992) found a bisection of the average mean square fluctuations in molecular dynamics simulations at 1 bar and 10 kbar, respectively. With the more rigid structure of the lipase, the activity towards ( $\pm$ )-menthol also decreased with increasing pressure (see Table 13).

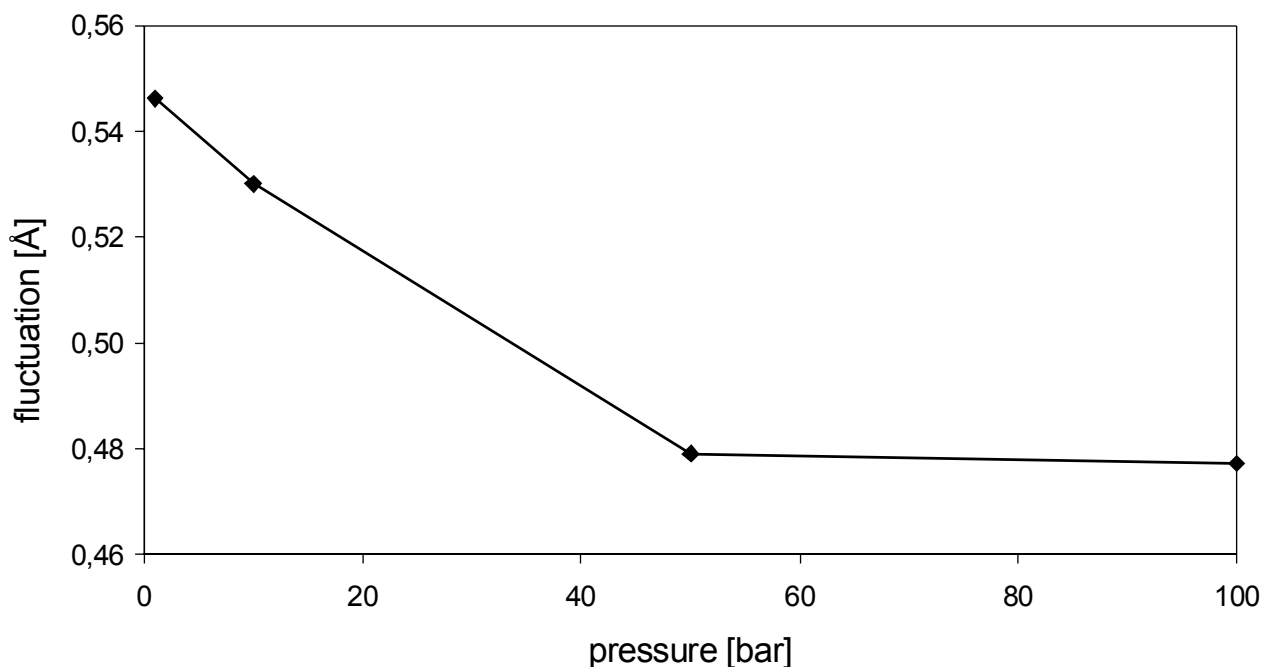


Figure 52 Fluctuations averaged over all  $C\alpha$ -atoms in the last 50 ps of each molecular dynamics simulation at 1 bar, 10 bar, 50 bar, and 100 bar, respectively.

In this work, a water channel in the structure of *Candida rugosa* lipase was observed which, with increasing pressure, was subsequently populated with water molecules.

The water channel was limited by residues F415 and the active site H449 in the core of the protein. Opening towards the surface of the lipase, its depth was limited by the active site H449 which plays a key role in the reported pressure dependent denaturation of *Candida rugosa* lipase. The catalytic triad H449 in *Candida rugosa* lipase has been known for long to be involved in the function of the lipase (Cygler, Grochulski et al. 1994). With no pressure applied, (+)-(1S)-menthol induces a tilt of the imidazole ring of active site histidine 449 of 60° (see Figure 8 or Figure 53). This prevents the formation of a hydrogen bond at the active site and as a result, the mechanism of the catalytic triad is assumed to be disturbed (see Figure 6 or Figure 54).

Earlier studies on the enantioselectivity of lipases towards different classes of triacylglycerols and analogs as well as esters of primary and secondary alcohols carried out by Scheib et al., Gentner et al., and Schulz and coworkers yielded substrate class specific parameters to distinguish between preferred and non-preferred enantiomers. For triacylglycerols and their in *sn*-2 substituted analogs, a torsion angle within the substrate allowed discrimination (Scheib, Pleiss et al. 1998; Scheib, Pleiss et al. 1999). Moreover, for primary alcohols as well as for carbonic acids, a torsion angle within the substrate allowed discrimination (Gentner et al., submitted). Schulz et al. (Schulz, Pleiss et al. 2000) discussed for *Pseudomonas cepacia* lipase the atom-atom distance between H449-N and substrate ester-O to correlate to stereoselectivity for the hydrolysis of secondary alcohol derivatives. While Schulz et al. correlated only the non-preferred enantiomer to stereoselectivity, the model derived from this work correlates the difference between the preferred and the non-preferred enantiomer to the enantioselectivity of the lipase and can thus be seen as a semi-quantitative measure of lipase-catalyzed resolution of racemic ( $\pm$ )-menthol under elevated pressures.





*The value of this work in the context of protein folding and unfolding*

The so called protein folding problem remains one of the most intriguing mysteries in modern biology. Based on the findings of Anfinsen (Anfinsen 1973) that the protein sequence determines its 3-dimensional structure the molecular principles of how a protein folds should be encoded only in the order of its building blocks, the polypeptide sequence of amino acids. Although the principles of protein folding in general seem to be clear, the folding problem itself remains mostly unsolved which is due to several facts (for a review (Dill 1999; Tsai, Kumar et al. 1999; Radford 2000; Grantcharova, Alm et al. 2001)):

- a) Even for small proteins with only a very limited number of amino acids, a vast and because of its size unsearchable amount of theoretically possible conformations exist with only one of these conformations representing the active protein, the so called native state
- b) Even for large proteins the energy differences between the native state and all other conformations is in the range of 5 to 15 kcal. The native state is, therefore, extremely difficult to identify in a vast sample of possible structures
- c) The underlying principles are not yet fully understood. Physico-chemical representations and interaction equations are based on assumptions and simplifications introducing an increasing systematic error to a protein system. As a consequence, the small energy differences between inactive and active states are indistinctive from the systematic error originating from protein structure modeling.

However, progress has been made over the years in understanding the general principles of protein folding. Initially, the driving forces for a protein sequence to collapse into a 3D-structure were assigned to the generation of an H-bond network. Pioneered by the work of Kauzmann, today the formation of a hydrophobic core is assumed to play a major role in protein folding (Kauzmann 1959; Kauzmann 1987). Here, hydrophobic residues in polar environment, such as water, reduce their contact volume with the solvent and collapse to form a hydrophobic interior of the protein. Polar side chains are, hence, more likely to be located at the protein surface.

A long and still ongoing debate has been centered around whether proteins fold following a distinct folding pathway (Kim and Baldwin 1982; Houry, Sauder et al. 1998; Wedemeyer, Welker et al. 2000; Welker, Narayan et al. 2001) or if they more “randomly” find their native state. The latter and more modern hypothesis assumes that the ensemble of possible protein structures is represented by an n-dimensional

folding funnel with the native state being the lowest energy conformation and, thus, the bottom of the funnel (see Figure 55). As in the “old” view of protein folding, proteins fold following thermodynamic and kinetic pathways, however, a myriad of possible pathways is available for any protein sequence to be transformed into the native state rather than a distinct route (Lazaridis and Karplus 1997). Hence, the folding pathways seem to be degenerate and varying among proteins.

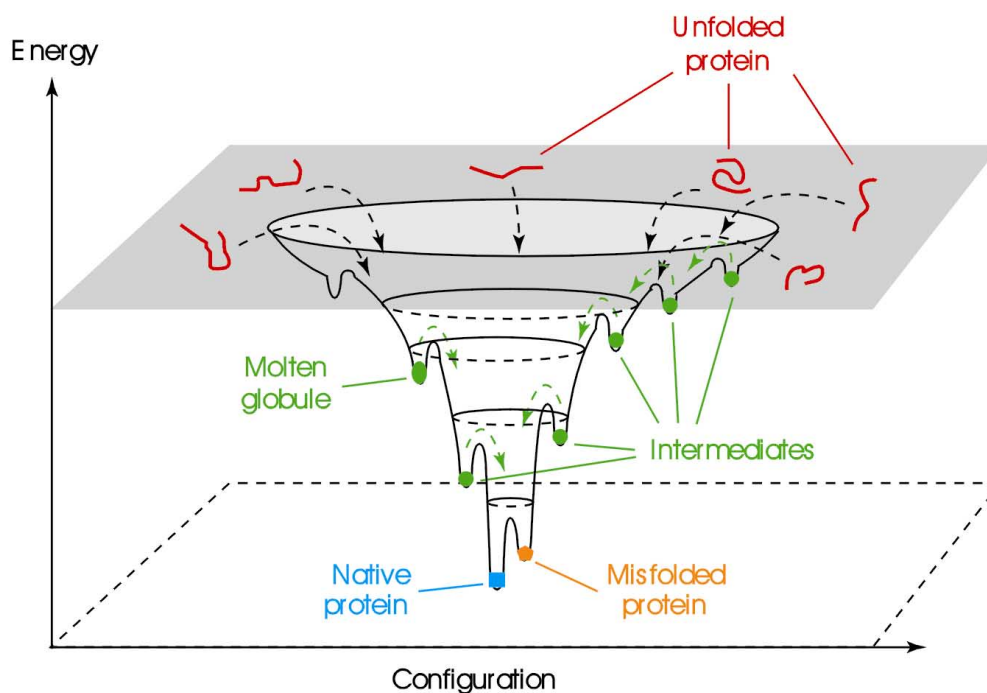


Figure 55 Schematic diagram of a folding energy landscape. Denatured molecules at the top of the funnel might fold to the native state by a myriad of different routes, some of which involve transient intermediates (local energy minima) whereas others involve significant kinetic traps (misfolded states). For proteins that fold without populating intermediates, the surface of the funnel would be smooth. Reproduced from (Schultz 2000).

Various modeling approaches have been developed to approach the protein folding problem (<http://PredictionCenter.Ilnl.gov/>). Force field based methods, such as molecular dynamics simulations can be used to mimic the folding process (Duan and Kollman 1998) and have successfully applied to e.g. crambin (LeGrand and Merz 1993). Baker and coworkers (ROSETTA approach), however, assemble proteins

from six to nine residue long protein structure fragments stored in a database (Bystroff and Baker 1997; Bystroff and Baker 1998; Simons, Bonneau et al. 1999; Simons, Ruczinski et al. 1999). In an effort to simulate *ab initio* folding of a simple protein, IBM launched the Blue Gene initiative to simulate protein folding on a 1,000,000 CPU supercomputer (Allen, Almasi et al. 2001).

As protein folding is still a very tedious task and to date virtually impossible to extensively simulate and, therefore, understand, the inverse process gained attraction of researchers – the unfolding of protein structures (Dinner and Karplus 1999). A protein is subject to denaturation if it is exposed to chemicals, high temperature, and/or pressure. An example for chemically induced denaturation of a protein is the classical Anfinsen experiment, where the disulfide bonds of ribonuclease were reduced by urea to cysteine sulfhydryl groups associated with a breakdown of the entire protein structure (Anfinsen, Haber et al. 1961; Anfinsen 1973).

In contrast to heat denaturation when a non-polar molecule is transferred from the non-polar protein core towards its polar surface and, therefore, polar solvent, pressure denaturation can be understood as the transfer of water molecules into the protein (Hummer, Garde et al. 1998). Cavities in the protein structure are then filled with water molecules, destabilizing the protein and, eventually, unfolding it. This is accompanied by an initial increase in volume, followed by a decrease at pressures above 1 - 2 kbar. This work clearly showed the transfer of water molecules into the core of the protein, thus, giving evidence for pressure induced denaturation of *Candida rugosa* lipase which has not yet been reported. A pre-built cavity in the *Candida rugosa* lipase was enlarged altering the enantioselectivity of the lipase by displacing the catalytically active histidine 449 by water (see Figure 56).

Furthermore, it was observed that the geometry of the ester bond in the first tetrahedral intermediate in the two enantiomers became similar with increasing pressure (see Figure 54, Figure 57, Figure 58, Figure 59, Figure 60). This might be due to the displacement of the H449 side chain in a similar way induced by pressure as found for the opposite enantiomers in the respective X-ray structures (see Figure 53) (Ahmed, Kazlauskas et al. 1994).

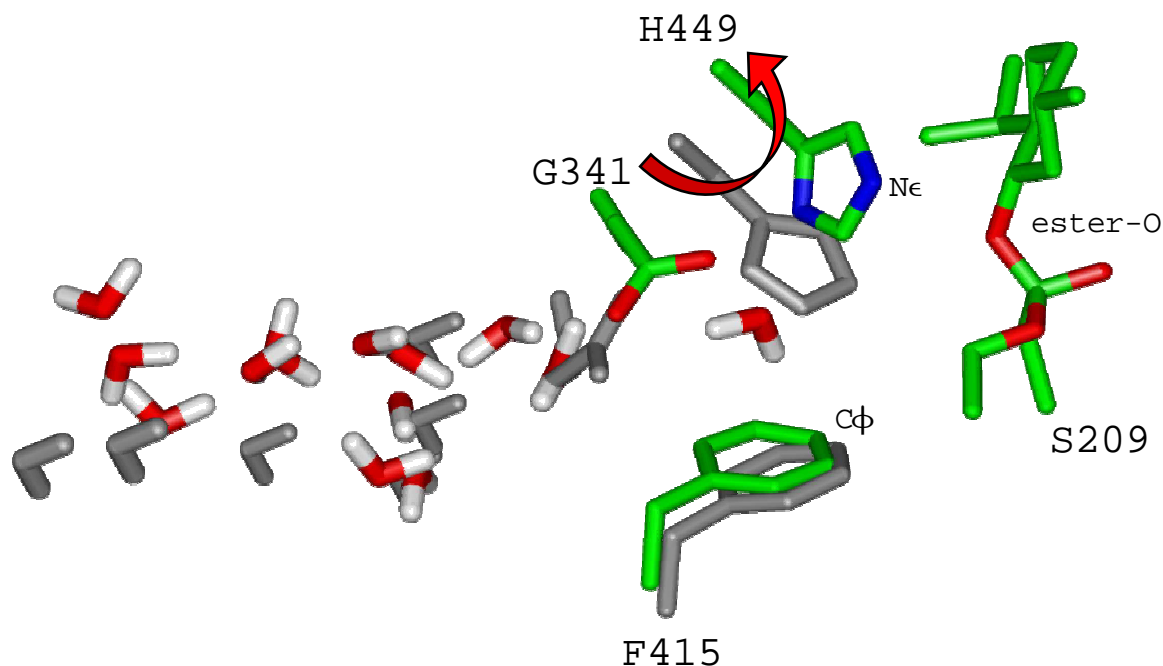


Figure 56 Pressure induced displacement of the H449 side chain in the active site of *Candida rugosa* lipase. The lipase structure was averaged over the last 50 ps of the 100 bar simulation with the coordinates of the 13 water molecules in the water channel taken from the snapshot at 250 ps (colored by atom: green (C), red (O), blue (N), white (H)). The (+)-menthylester was docked as tetrahedral intermediate to the averaged structure and energy minimized. For comparison, the crystal structure (1LPM) is shown in gray; it contains only 6 water molecules in the water channel.

Both thermally and pressure induced unfolding were studied applying either molecular dynamics simulations at elevated temperatures or targeted molecular dynamics simulations to the problem. Simulating a system at high temperature allows each atom to overcome higher energy barriers in the n-dimensional energy surface as compared to lower energy. Therefore, a larger conformational space becomes accessible for the protein. This approach is followed in the Simulated Annealing method of molecular dynamics (Homans and M. 1992; Breed and Sansom 1994; Kerr, Sankararamakrishnan et al. 1994; Laughton 1994). Examples for unfolding simulations at elevated temperatures are, e.g., BPTI (basic pancreatic trypsin inhibitor) (Daggett and Levitt 1992), lysozyme (Mark and van Gunsteren 1992; Kazmirski and Daggett 1998), chymotrypsin inhibitor (Daggett, Li et al. 1996; Li and Daggett 1996; Lazaridis and Karplus 1997), ubiquitin (Alonso and Daggett 1995), and the classical example barnase (Caflisch and Karplus 1994; Caflisch and Karplus 1995). In targeted molecular dynamics, however, a harmonic constraint is imposed

on the structure in order to increase the distance from the native state when simulating the unfolding process of a protein (Ferrara, Apostolakis et al. 2000; Ferrara, Apostolakis et al. 2000; Ferrara, Apostolakis et al. 2000; Ferrara and Caflisch 2000).

Where multiple folding and unfolding events can be observed at the melting point,  $T_m$ , of a protein (Ferrara, Apostolakis et al. 2000), the question remains whether a similar “melting” point,  $P_m$ , exists for pressure induced unfolding. In contrast to temperature induced unfolding, pressure induced unfolding is not reversible at its transition point. Whereas at high temperature energy barriers can be reversibly overcome with greater ease, at high pressure the accessible portion of the configurational space is significantly reduced that even the native state vanishes and the protein eventually denatures.

Although limitations of the experimental gear restricted the investigations of this work to 100 bar excluding effects on protein structure under extreme pressure (up to 1,000 bar range), the molecular dynamics simulations obviously reflected the early stages of pressure induced protein denaturation. The channel in *Candida rugosa* lipase ranging from its surface to the center of the lipase is described for the first time hosting polar water molecules which may in parts challenge the general hypothesis that protein cores are hydrophobic. However, the six polar water molecules as found in the initial X-ray structure are mainly restricted to the protein surface. Since several experimental structures of *Candida rugosa* lipase have been resolved under different experimental conditions (Grochulski, Li et al. 1993; Schrag and Cygler 1993; Cygler, Grochulski et al. 1994; Grochulski, Bouthillier et al. 1994; Grochulski, Li et al. 1994), it is unlikely that the observed water channel is due to a crystallization artifact.

However, with increasing pressure, additional water molecules are forced into the center of the protein widening the channel and exposing more atoms of the channel residues facing to the solvent. Interestingly, pressure induced denaturation of *Candida rugosa* lipase seems to be initiated apart from the active site subsequently challenging the hydrophobic core of the lipase and eventually affecting the immediate structure of the active site residues. Moreover, from analyzing the H-bond pattern of the active site residues in *Candida rugosa* lipase over increasing pressure, there is evidence that increasing pressure does not necessarily lead to a direct breakdown of the catalytic machinery. Hence, focusing on the active site residues only misses out the phenomenon of pressure induced denaturation. It is, therefore, conceivable that

---

biochemical properties of proteins, i.e., their enantioselectivity, are altered before protein denaturation is completed coinciding with the findings in this work.

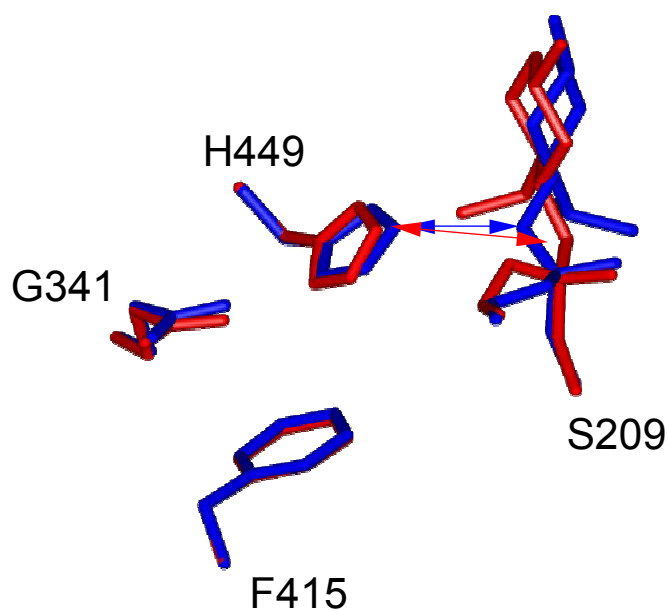


Figure 57 The tetrahedral intermediate of (-)-menthylester (blue: isopropyl moiety oriented to the right side) and (+)-menthylester (red: isopropyl moiety oriented to the left side) docked to the averaged structure of the molecular dynamics simulation at 1 bar. The distance between H449-N $\epsilon$  and the alcohol oxygen is marked by arrows (blue: (-), red: (+)).

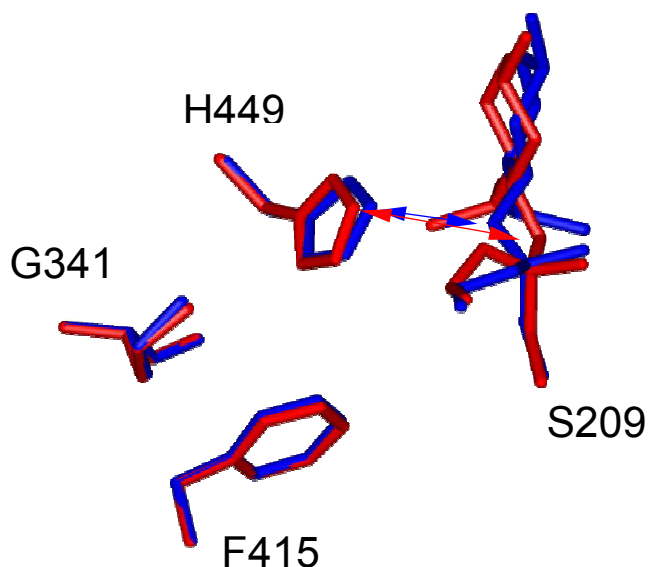


Figure 58 The tetrahedral intermediate of (-)-menthylester (blue: isopropyl moiety oriented to the right side) and (+)-menthylester (red: isopropyl moiety oriented to the left side) docked to the averaged structure of the molecular dynamics simulation at 10 bar. The distance between H449-N $\epsilon$  and the alcohol oxygen is marked by arrows (blue: (-), red: (+)).

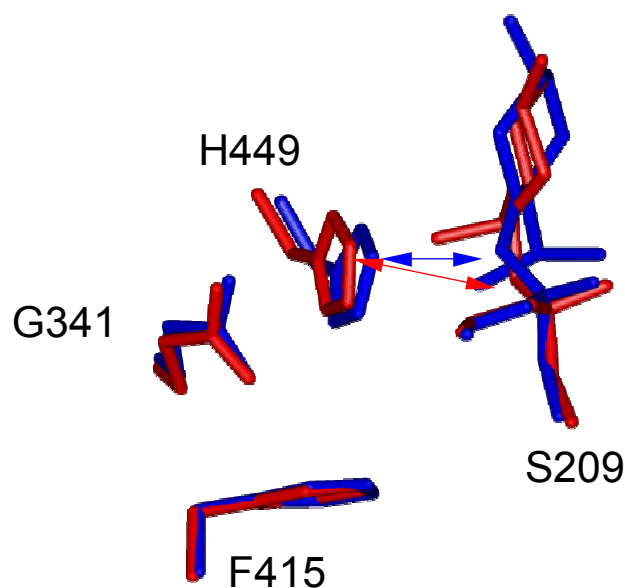


Figure 59 The tetrahedral intermediate of (-)-menthylester (blue: isopropyl moiety oriented to the right side) and (+)-menthylester (red: isopropyl moiety oriented to the left side) docked to the averaged structure of the molecular dynamics simulation at 50 bar. The distance between H449-N $\epsilon$  and the alcohol oxygen is marked by arrows (blue: (-), red: (+)).

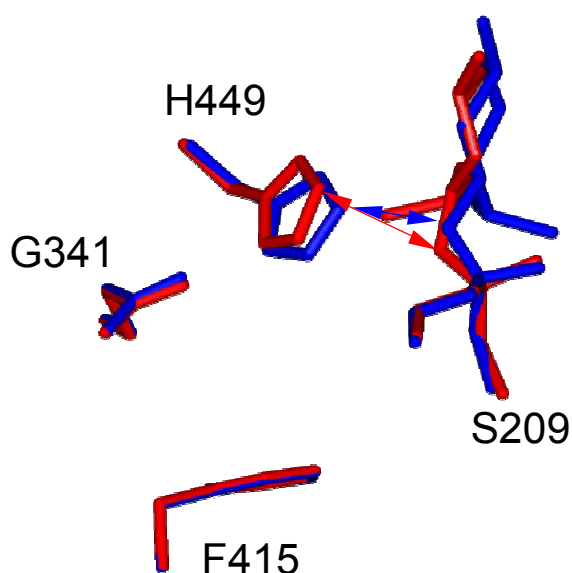


Figure 60 The tetrahedral intermediate of (-)-menthylester (blue: isopropyl moiety oriented to the right side) and (+)-menthylester (red: isopropyl moiety oriented to the left side) docked to the averaged structure of the molecular dynamics simulation at 100 bar. The distance between H449-N $\epsilon$  and the alcohol oxygen is marked by arrows (blue: (-), red: (+)).



## 6. OUTLOOK

A model for the pressure dependence of the enantioselectivity of the *Candida rugosa* lipase was developed in this work. The comparison of only one quite simple geometric property, the distance between the substrate ester oxygen atom and the His449-N $\delta$  atom, for two given enantiomers is indicative for the enantioselectivity.

A molecular dynamics simulation at 1 bar of the configuration with the water channel open obtained at 100 bar could show whether the observed pressure dependence is reversible or not.

Further validation of this model has to be done by extending the model reaction, the esterification of rac-menthol with propionic acid anhydride, to various other model reactions.

Extension of this model towards other lipases or related enzymes only seems possible provided that they show a pressure dependence of enantioselectivity. As the pressure dependence of an enzyme can be verified in quite a short time of approximately one week, it seems promising to first screen various enzymes for pressure dependence of enantioselectivity. Given an assortment of proteins coming into question, a preliminary geometric analysis of the active site of the enzymes should show in early stages, if MD simulation of a pressure dependence could be reasonable or not.

Extension of this model to pressures below 1 bar, i.e. vacuum, is not readily accomplished, because the experimental setup used in this work only operates on pressures higher than 1 bar. In contrast, extension of the pressure range significantly above 100 bar should increase the understanding of pressure effects in proteins.

## 7. REFERENCES

- Ahmed, S. N., R. J. Kazlauskas, et al. (1994). "Enantioselectivity of *Candida rugosa* lipase toward carboxylic acids: A predictive rule from substrate mapping and x-ray crystallography." Biocatalysis **9**(1-4): 209-25.
- Akasaka, K., H. Li, et al. (1999). "Pressure response of protein backbone structure. Pressure-induced amid 15n chemical shifts in BPTI." Protein Science **8**: 1946-1953.
- Alberghina, L., R. D. Schmid, et al., Eds. (1991). Lipases: Structure, Mechanism and Genetic Engineering. GBF Monographs. Weinheim, VCH.
- Allen, F., G. Almasi, et al. (2001). "Blue Gene: A Vision for Protein Science Using a Petaflop Supercomputer." IBM Systems Journal **40**(2): 310-327.
- Alonso, D. O. V. and V. Daggett (2000). "Staphylococcal protein A: Unfolding pathways, unfolded states, and differences between the B and E domains." PNAS **97**(1): 133-138.
- Alonso, D. O. W. and V. Daggett (1995). "Molecular dynamics simulations of protein unfolding and limited refolding: characterization of partially unfolded states of ubiquitin in 60 % methanol and water." J. Mol. Biol. **247**: 501-520.
- Anfinsen, C. B. (1973). "Principles that govern the folding of protein chains." Science **181**: 223-230.
- Anfinsen, D., E. Haber, et al. (1961). "The kinetics of formation of native ribonuclease during oxidation of the reduced polypeptide chain." Proc. Natl. Acad. Sci. U.S.A. **47**: 1309-1314.
- Aqvist, J. (1999). "Long-range electrostatic effects on peptide folding." FEBS Letters **457**: 414-418.
- Baratti, J., G. Buono, et al. (1988). "Enzymatic separation and resolution of nucleophiles: a predictive kinetic model." Biocatalysis **1**: 231-248.
- Barrett, A. J. (1995). "Nomenclature Committee of the International Union of Biochemistry and Molecular Biology (NC-IUBMB). Enzyme nomenclature. Recommendations 1992. Supplement 2: corrections and additions (1994)." Eur J Biochem **232**(1): 1-6.

- Barrett, A. J. (1996). "Nomenclature Committee of the International Union of Biochemistry and Molecular Biology (NC-IUBMB). Enzyme nomenclature. Recommendations 1992. Supplement 3: corrections and additions (1995)." Eur J Biochem **237**(1): 1-5.
- Beckman, E. J., A. J. Russell, et al. (1995). "Enzyme Activity in Supercritical Fluids." Crit. Rev. Biotech. **15**(1): 41-71.
- Bernstein, F. C., T. F. Koetzle, et al. (1977). "The Protein Data Bank: a computer-based archival file for macromolecular structures." J. Mol. Biol. **112**: 525-542.
- Bianchi, D., E. Battistel, et al. (1993). "Effects of chemical modification on stereoselectivity of *Pseudomonas cepacia* lipase." Tetrahedron: Asymmetry **4**(5): 777-782.
- Borgstrom, B. and H. L. Brockman (1984). Lipases. New York, Elsevier Science Publishing Co.
- Bornscheuer, U., A. Herar, et al. (1995). "Lipase-catalyzed kinetic resolution of 3-hydroxy esters: Optimization, batch, and continuous reactions." Ann. N. Y. Acad. Sci. **750**(Enzyme Engineering XII): 215-221.
- Bornscheuer, U., A. Herar, et al. (1993). "Factors affecting the lipase catalyzed transesterification reactions of 3-hydroxy esters in organic solvents." Tetrahedron: Asymmetry **4**(5): 1007-1016.
- Bornscheuer, U. T. and R. J. Kazlauskas (1999). Hydrolases in Organic Synthesis - Regio- and Stereoselective Biotransformations. Weinheim, Wiley-VCH.
- Botta, M., E. Cernia, et al. (1997). "Probing the substrate specificity for lipases. II. Kinetic and modeling studies on the molecular recognition of 2-arylpropionic esters by *Candida rugosa* and *Rhizomucor miehei* lipases." Biochimica et Biophysica Acta **1337**: 302-310.
- Breed, J. and M. S. Sansom (1994). "Alamethicin channels modelled by simulated annealing and molecular dynamics." Biochem Soc Trans **22**(2): 157S.
- Bystroff, C. and D. Baker (1997). "Blind predictions of local protein structure in CASP2 targets using the I-sites library." Proteins Suppl **1**: 167-171.
- Bystroff, C. and D. Baker (1998). "Prediction of local structure in proteins using a library of sequence-structure motifs." J. Mol. Biol. **281**: 565-577.
- Cafilisch, A. and M. Karplus (1994). "Molecular dynamics simulations of protein denaturation: Solvation of the hydrophobic cores and secondary structure of barnase." Proc. Natl. Acad. Sci. USA **91**: 672-708.

- Cafilisch, A. and M. Karplus (1995). "Acid and thermal denaturation of barnase investigated by molecular dynamics simulations." J. Mol. Biol. **252**: 672-708.
- Carter, P. and J. Wells (1988). "Dissecting the catalytic triad of a serine protease." Nature **322**(6164): 564-568.
- Chen, C. S., Y. Fujimoto, et al. (1982). "Quantitative analyses of biochemical kinetic resolutions of enantiomers." J. Am. Chem. Soc. **104**: 7294-7299.
- Chen, C. S., S. H. Wu, et al. (1987). "Quantitative analyses of biochemical kinetic resolution of enantiomers. 2. Enzyme-catalyzed esterifications in water-organic solvent biphasic systems." J. Am. Chem. Soc. **109**: 2812-2817.
- Cygler, M., P. Grochulski, et al. (1994). "A Structural Basis for the Chiral Preferences of Lipases." J. Am. Chem. Soc. **116**(8): 3180-3186.
- Cygler, M., P. Grochulski, et al. (1995). "Structural determinants defining common stereoselectivity of lipases toward secondary alcohols." Can. J. Microbiol. **41**(Suppl. 1): 289-96.
- Cygler, M., J. D. Schrag, et al. (1993). "Relationship between sequence conservation and three-dimensional structure in a large family of esterases, lipases, and related proteins." Protein Sci. **2**(3): 366-382.
- Daggett, V. (2000). "Long timescale simulations." Current Opinion in Structural Biology **10**: 160-164.
- Daggett, V. and M. Levitt (1992). "A model of the molten globule state from molecular dynamics simulations." Proc. Natl. Acad. Sci. USA **89**: 5142-5146.
- Daggett, V., A. Li, et al. (1996). "Structure of the transition state for folding of a protein derived from experiment and simulation." J. Mol. Biol. **257**: 430-440.
- Daura, X., W. F. van Gunsteren, et al. (1999). "Folding-Unfolding Thermodynamics of a b-Heptapeptide From Equilibrium Simulations." Proteins **34**: 269-280.
- Dill, K. A. (1999). "Polymer principles and protein folding." Protein Science **8**: 1166-1180.
- Dinner, A. R. and M. Karplus (1999). "Is Protein Unfolding the Reverse of Protein Folding? A Lattice Simulation Analysis." J. Mol. Biol. **292**: 403-419.
- Duan, Y. and P. Kollman (1998). "Pathways to a protein folding intermediate observed in a 1-microsecond simulation in aqueous solution." Science **282**: 740-744.

- Ferrara, P., J. Apostolakis, et al. (2000). "Computer Simulations of Protein Folding by Targeted Molecular Dynamics." Proteins: Structure, Function and Genetics **39**: 252-260.
- Ferrara, P., J. Apostolakis, et al. (2000). "Targeted Molecular Dynamics Simulations of Protein Unfolding." J. Phys. Chem. B **104**: 4511-4518.
- Ferrara, P., J. Apostolakis, et al. (2000). "Thermodynamics and Kinetics of Folding of Two Model Peptides Investigated by Molecular Dynamics Simulations." J. Phys. Chem. B **104**: 5000-5010.
- Ferrara, P. and A. Caflisch (2000). "Folding simulations of a three-stranded antiparallel b-sheet peptide." PNAS **97**(20): 10780-10785.
- Floriano, W. B., M. A. C. Nascimento, et al. (1998). "Effects of pressure on the structure of metmyoglobin: Molecular dynamics predictions for pressure unfolding through a molten globule intermediate." Protein Science **7**(11): 2301-2313.
- Furukawa, S. and K. Kawakami (1998). "Characterization of *Candida rugosa* lipase entrapped into organically modified silicates in esterification of menthol with butyric acid." J. Ferment. Bioeng. **85**(2): 240-242.
- Grantcharova, V., E. J. Alm, et al. (2001). "Mechanism of protein folding." Current Opinion in Structural Biology **11**: 70-82.
- Grochulski, P., F. Bouthillier, et al. (1994). "Analogues of Reaction Intermediates Identify a Unique Substrate Binding Site in *Candida rugosa* Lipase." Biochemistry **33**(12): 3494-500.
- Grochulski, P., Y. Li, et al. (1993). "Insights into interfacial activation from an open structure of *Candida rugosa* lipase." J. Biol. Chem. **268**(17): 12843-12847.
- Grochulski, P., Y. Li, et al. (1994). "Two conformational states of *Candida rugosa* lipase." Protein Sci. **3**(1): 82-91.
- Haeffner, F., T. Norin, et al. (1998). "Molecular modeling of the enantioselectivity in lipase-catalyzed transesterification reactions." Biophysical Journal **74**: 1251-1262.
- Holmquist, M., F. Haeffner, et al. (1996). "A structural basis for enantioselective inhibition of *Candida rugosa* lipase by long-chain aliphatic alcohols." Protein Science **5**(1): 83-88.

- Homans, S. W. and F. M. (1992). "Application of restrained minimization, simulated annealing and molecular dynamics simulations for the conformational analysis of oligosaccharides." Glycobiology **2**(2): 143-151.
- Hopp, R. (1993). "Menthol: its origins, chemistry, physiology and toxicological properties." Rec. Ad. Tobacco Science **19**: 3-46.
- Houry, W. A., J. M. Sauder, et al. (1998). "Definition of amide protection factors for early kinetic intermediates in protein folding." Proc. Natl. Acad. Sci. USA **95**: 4299-4302.
- Hummer, G., S. Garde, et al. (1998). "The pressure dependence of hydrophobic interactions is consistent with the observed pressure denaturation of proteins." Proc. Natl. Acad. Sci. USA **95**(Biophysics): 1552-1555.
- Ikushima, Y. (1997). "Supercritical fluids: an interesting medium for chemical and biochemical processes." Advances in colloid and interface science **71**(72): 259-280.
- Inoue, K., H. Yamada, et al. (2000). "Pressure-induced local unfolding of the Ras binding domain of RaIGDS." Nature Structural Biology **7**(7): 547-550.
- Ivanov, A. E. and M. P. Schneider (1997). "Methods for the immobilization of lipases and their use for ester synthesis." J. Mol. Catal. B: Enzymatic **3**: 303-309.
- Kalbitzer, H. R., A. Görler, et al. (2000). "<sup>15</sup>N and <sup>1</sup>H NMR study of histidine containing protein (HPr) from *Staphylococcus carnosus* at high pressure." Protein Science **9**: 693-703.
- Kamiya, N. and M. Goto (1997). "How is enzymatic selectivity of menthol esterification catalyzed by surfactant-coated lipase determined in organic media?" Biotechnol. Prog. **13**: 488-492.
- Kamiya, N., M. Goto, et al. (1995). "Surfactant-Coated Lipase Suitable for the Enzymic Resolution of Menthol as a Biocatalyst in Organic Media." Biotechnol. Prog. **11**(3): 270-275.
- Kauzmann, W. (1959). "Some factors in the interpretation of protein denaturation." Adv. Prot. Chem. **14**: 1-63.
- Kauzmann, W. (1987). "Thermodynamics of unfolding." Nature **325**: 763-764.
- Kazlauskas, R. J. (1994). "Elucidating structure-mechanism relationships in lipases: prospects for predicting and engineering catalytic properties." TIBTECH **12**: 464-472.

- Kazlauskas, R. J. (2000). "Molecular modeling and biocatalysis: explanations, predictions, limitations, and opportunities." Curr Opin Chem Biol **4**(1): 81-88.
- Kazlauskas, R. J. and U. T. Bornscheuer (1998). Biotransformations with Lipases. Biotransformations, VCH. **8**: 37-191.
- Kazlauskas, R. J., A. N. E. Weissfloch, et al. (1991). "A rule to predict which enantiomer of a secondary alcohol reacts faster in reactions catalyzed by cholesterol esterase, lipase from *Pseudomonas cepacia*, and lipase from *Candida rugosa*." J. Org. Chem. **56**(8): 2656-2665.
- Kazmirski, S. L. and V. Daggett (1998). "Non-native interactions in protein folding intermediates: molecular dynamics simulations of hen lysozyme." J. Mol. Biol. **284**: 793-806.
- Kerr, I. D., R. Sankararamkrishnan, et al. (1994). "Parallel helix bundles and ion channels: molecular modeling via simulated annealing and restrained molecular dynamics." Biophysical Journal **67**(4): 1501-1515.
- Kharakoz, D. P. (2000). "Protein Compressibility, Dynamics, and Pressure." Biophysical Journal **79**: 511-525.
- Kim, P. S. and R. L. Baldwin (1982). "Specific intermediates in the folding reactions of small proteins and themechanism of folding." Annu. Rev. Biochem. **51**: 459-489.
- Kitchen, D. B., L. H. Reed, et al. (1992). "Molecular dynamics simulation of solvated protein at high pressure." Biochemistry **31**: 10083-10093.
- Koteshwar, K. and N. W. Fadnavis (1997). "Remote control of stereoselectivity: lipase catalyzed enantioselective esterification of racemic  $\alpha$ -lipoic acid." Tetrahedron:Asymmetry **8**(2): 337-339.
- Laskowski, R. A., M. W. MacArthur, et al. (1993). "PROCHECK: a program to check the stereochemical quality of protein structures." J. Appl. Cryst. **26**: 283-291.
- Laughton, C. A. (1994). "A study of simulated annealing protocols for use with molecular dynamics in protein structure prediction." Protein Engineering **7**(2): 235-241.
- Lazaridis, T. and M. Karplus (1997). "'New view" of protein folding reconciled with the old through multiple unfolding simulations." Science **287**: 1928-1931.
- Leach, A. R. (1996). Molecular modelling - principles and applications. Harlow, Addison Wesley Longman Limited.

- Leffingwell, J. C. and R. E. Shakelford (1974). "Laevo-Menthol - Synthesis and organoleptic properties." Cosmetics and Perfumery **89**(6): 69-89.
- LeGrand, S. M. and K. M. Merz (1993). "The application of the genetic algorithm to the minimization of potential energy functions." J. Global Optim. **3**: 49-66.
- Li, A. and V. Daggett (1996). "Identification and characterization of the unfolding transition state of chymotrypsin inhibitor 2 by molecular dynamics simulations." J. Mol. Biol. **257**: 412-429.
- Li, H., H. Yamada, et al. (1999). "Effect of pressure on the tertiary structure and dynamics of folded basic pancreatic trypsin inhibitor." Biophysical Journal **77**: 2801-2812.
- Manetti, F., D. Mileto, et al. (2000). "Design and realization of a tailor-made enzyme to modify the molecular recognition of 2-arylpropionic esters by candida rugosa lipase." Biochim Biophys Acta **1543**(1): 146-158.
- Mark, A. E. and W. F. van Gunsteren (1992). "Simulation of the thermal denaturation of hen egg white lysozyme: trapping the molten globule state." Biochemistry **31**: 7745-7748.
- Marty, A., W. Chulalaksananukul, et al. (1992). "Kinetics of lipase-catalyzed esterification in supercritical carbon dioxide." Biotechnol. Bioeng. **39**: 273-280.
- Morris, A. L., M. W. MacArthur, et al. (1992). "Stereochemical quality of protein structure coordinates." Proteins **12**: 345-364.
- Narang, J. S., S. A. Barker, et al. (1990). "Immobilization of lipase from *Candida cylindracea* and its use in the synthesis of menthol esters by transesterification." Enzyme Microb. Technol. **12**: 800-807.
- Norin, M., F. Haeffner, et al. (1994). "Molecular dynamics simulations of an enzyme surrounded by vacuum, water, or a hydrophobic solvent." Biophys. J. **67**(2): 548-59.
- Ollis, D. L., E. Cheah, et al. (1992). "The a/b hydrolase fold." Protein Engineering **5**(3): 197-211.
- Otero, C., A. Ballesteros, et al. (1988). "Immobilization/stabilization of lipase from *Candida rugosa*." Appl. Biochem. Biotechnol. **19**: 163-175.
- Otero, C., L. Robledo, et al. (1995). "Study of the stabilization of pure lipases: comparison of two different lipase-microgel derivatives." J. Mol. Catal. B: Enzym. **1**(1): 23-28.



- Paci, E. and M. Marchi (1996). "Intrinsic compressibility and volume compression in solvated proteins by molecular dynamics simulation at high pressure." Proc. Natl. Acad. Sci. USA **93**: 11609-11614.
- Peters, G. H., D. M. van Aalten, et al. (1996). "Dynamics of proteins in different solvent systems: analysis of essential motion in lipases." Biophysical Journal **71**(5): 2245-2255.
- Pleiss, J., H. Scheib, et al. (2000). "The His gap motif in microbial lipases: a determinant of stereoselectivity toward triacylglycerols and analogs." Biochimie **82**(11): 1043-1052.
- Radford, S. E. (2000). "Protein folding: progress made and promises ahead." TIBS **25**: 611-618.
- Radkiewicz, J. L. and C. L. Brooks (2000). "Protein Dynamics in Enzymatic Catalysis: Exploration of Dihydrofolate Reductase." J. Am. Chem. Soc. **122**: 225-231.
- Ransac, S., E. Rogalska, et al. (1991). "Stereoselectivity of lipases. Hydrolysis of enantiomeric glyceride analogs by gastric and pancreatic lipases, a kinetic study using the monomolecular film technique." GBF Monogr. **16**: 117-122.
- Rogalska, E., C. Cudrey, et al. (1993). "Stereoselective hydrolysis of triglycerides by animal and microbial lipases." Chirality **5**(1): 24-30.
- Rogalska, E., S. Ransac, et al. (1990). "Stereoselectivity of lipases. II. Stereoselective hydrolysis of triglycerides by gastric and pancreatic lipases." J. Biol. Chem.: 20170-6.
- Rogalska, E., S. Ransac, et al. (1991). "Stereoselectivity of lipases. Stereoselective hydrolysis of triglycerides by gastric and pancreatic lipases." GBF Monogr. (Lipases) **16**: 135-9.
- Rogalska, E., S. Ransac, et al. (1993). "Controlling lipase stereoselectivity via the surface pressure." J Biol Chem **15**(268(2)): 792-794.
- Salleh, A. B., M. Basri, et al. (1993). "Synthesis of oleic esters by lipase from *Candida rugosa*." Proc. Malays. Biochem. Soc. Conf. **Volume Date 1992, 17th**: 21-24.
- Scheib, H., J. Pleiss, et al. (1999). "Stereoselectivity of Mucorales lipases - a simple solution to a complex problem." Prot. Sci. **8**(1): 215-221.
- Scheib, H., J. Pleiss, et al. (1998). "Rational design of *Rhizopus oryzae* lipase with modified stereoselectivity toward triacylglycerols." Protein Eng. **11**(8): 675-682.

- Schmid, R. D. and R. Verger (1998). "Lipases - interfacial enzymes with attractive applications." Angew. Chem. Int. Ed. Engl. **37**: 1608-1633.
- Schrag, J. D. and M. Cygler (1993). "1.8 Å Refined structure of the lipase from *Geotrichum candidum*." J. Mol. Biol. **230**(2): 575-91.
- Schultz, C. P. (2000). "Illuminating folding intermediates." Nat. Struct. Biol. **7**: 58-61.
- Schulz, T., J. Pleiss, et al. (2000). "Stereoselectivity of *Pseudomonas cepacia* lipase toward secondary alcohols: A quantitative model." Protein Science **9**: 1053-1062.
- Simons, K. T., R. Bonneau, et al. (1999). "Ab initio protein structure prediction of CASP III targets using ROSETTA." Proteins Suppl. **3**: 171-176.
- Simons, K. T., I. Ruczinski, et al. (1999). "Improved recognition of native-like protein structures using a combination of sequence-dependent and sequence-independent features of proteins." Proteins **34**(1): 82-95.
- Stadler, P., A. Kovac, et al. (1995). "Stereoselectivity of microbial lipases . The substitution at position sn-2 of triacylglycerol analogs influences the stereoselectivity of different microbial lipases." Eur. J. Biochem. **227**(1/2): 335-343.
- Tafi, A., A. van Almsick, et al. (2000). "Computer simulations of enantioselective ester hydrolyses catalyzed by *Pseudomonas cepacia* lipase." J Org Chem **65**(12): 3659-3665.
- Tipton, K. F. (1994). "Nomenclature Committee of the International Union of Biochemistry and Molecular Biology (NC-IUBMB). Enzyme nomenclature. Recommendations 1992. Supplement: corrections and additions." Eur J Biochem **223**(1): 1-5.
- Tsai, C.-J., S. Kumar, et al. (1999). "Folding funnels, binding funnels, and protein function." Protein Science **8**: 1181-1190.
- Tseng, G. W. M., R. J. Kazlauskas, et al. (1994). "Kinetic resolutions concentrate the minor enantiomer and aid measurement of high enantiomeric purity." Tetrahedron: Asymmetry **5**(1): 83-92.
- Uppenberg, J., N. Ohrner, et al. (1995). "Crystallographic and molecular-modeling studies of lipase B from *Candida antarctica* reveal a stereospecificity pocket for secondary alcohols." Biochemistry **34**: 16838-16851.

- van Gunsteren, W. F. and H. J. C. Berendsen (1987). Groningen molecular simulation (GROMOS) Library Manual. Groningen, biosmos.
- van Gunsteren, W. F., S. R. Billeter, et al. (1996). Biomolecular Simulation: The GROMOS96 Manual and User Guide. Zürich / Groningen, vdf Hochschulverlag AG / BIOMOS b. v.
- van Gunsteren, W. F. and R. M. Brunne (1993). "Dynamical properties of bovine pancreatic trypsin inhibitor from a molecular dynamics simulation at 5000 atm." FEBS **323**(3): 215-217.
- Vriend, G. and C. Sander (1991). "Detection of common three-dimensional substructures in proteins." Proteins **11**(1): 52-8.
- Wedemeyer, W. J., E. Welker, et al. (2000). "Disulfide Bonds and Protein Folding." Biochemistry **39**(15): 4207-4216.
- Weiner, S. J., P. A. Kollman, et al. (1984). "A new force field for molecular mechanical simulation of nucleic acids and proteins." J. Am. Chem. Soc. **106**: 765-784.
- Welker, E., M. Narayan, et al. (2001). "Structural determinants of oxidative folding in proteins." PNAS **98**(5): 2312-2316.
- Yagnik, A. T., J. A. Littlechild, et al. (1997). "Molecular modelling studies of substrate binding to the lipase from *Rhizomucor miehei*." J Comput Aided Mol Des **11**(3): 256-264.
- Yang, H., S. Cao, et al. (1996). "Enhancing the stereoselectivity and activity of *Candida* species lipase in organic solvent by noncovalent enzyme modification." Ann. N. Y. Acad. Sci. **799**(Enzyme Engineering XIII): 358-363.
- Zhang, J., X. Peng, et al. (1995). Biochemistry **34**: 8631-8641.
- Zipp, A. and W. Kauzmann (1973). "Pressure denaturation of metmyoglobin." Biochemistry **12**: 4217-4227.

## 8. APPENDIX

### 8.1. PDB ENTRY 1LPM.PDB

Marked in blue are the entries that were used to set up the molecular dynamics simulations of the *Candida rugosa* lipase in water and chloroform as solvent.

Marked in red are the inhibitor (1R)-menthyl hexyl phosphonate as well as the detergent N-acetyl-D-glucosamine.

```

HEADER      HYDROLASE                               06-JAN-95  1LPM    1LPM    2
COMPND      LIPASE (E.C.3.1.1.3) (TRIACYLGLYCEROL LIPASE) COMPLEXED WITH  1LPM    3
COMPND      2 (1R)-MENTHYL HEXYL PHOSPHONATE                                1LPM    4
SOURCE      YEAST (CANDIDA RUGOSA) (FORMERLY CANDIDA CYLINDRACEA)         1LPM    5
AUTHOR      P.G.GROCHULSKI,M.C.CYGLER                                    1LPM    6
REVDAT      1 20-APR-95 1LPM 0                                           1LPM    7
JRNL        AUTH  M.CYGLER,P.GROCHULSKI,R.J.KAZLAUSKAS,J.D.SCHRAG,       1LPM    8
JRNL        AUTH 2 F.BOUTHILLIER,B.RUBIN,A.N.SERREGI,A.K.GUPTA           1LPM    9
JRNL        TITL  A STRUCTURAL BASIS FOR THE CHIRAL PREFERENCES OF       1LPM   10
JRNL        TITL 2 LIPASES                                                1LPM   11
JRNL        REF   J.AM.CHEM.SOC.                V. 116  3180 1994         1LPM   12
JRNL        REFN ASTM JACSAT  US ISSN 0002-7863                0004 1LPM   13
REMARK      1                                           1LPM   14
REMARK      1 REFERENCE 1                                           1LPM   15
REMARK      1 AUTH  P.GROCHULSKI,Y.LI,J.D.SCHRAG,M.CYGLER               1LPM   16
REMARK      1 TITL  TWO CONFORMATIONAL STATES OF CANDIDA RUGOSA LIPASE    1LPM   17
REMARK      1 REF   PROTEIN SCI.                V. 3    82 1994           1LPM   18
REMARK      1 REFN ASTM PRClEI  US ISSN 0961-8368                0795 1LPM   19
REMARK      1 REFERENCE 2                                           1LPM   20
REMARK      1 AUTH  P.GROCHULSKI,F.BOUTHILLIER,R.J.KAZLAUSKAS,          1LPM   21
REMARK      1 AUTH 2 A.N.SERREGI,J.D.SCHRAG,E.ZIOMEK,M.CYGLER           1LPM   22
REMARK      1 TITL  ANALOGS OF REACTION INTERMEDIATES IDENTIFY A        1LPM   23
REMARK      1 TITL 2 UNIQUE SUBSTRATE BINDING SITE IN CANDIDA RUGOSA     1LPM   24
REMARK      1 TITL 3 LIPASE                                              1LPM   25
REMARK      1 REF   BIOCHEMISTRY                V. 33  3494 1994         1LPM   26
REMARK      1 REFN ASTM BICHAW  US ISSN 0006-2960                0033 1LPM   27
REMARK      1 REFERENCE 3                                           1LPM   28
REMARK      1 AUTH  P.GROCHULSKI,Y.LI,J.D.SCHRAG,F.BOUTHILLIER,P.SMITH,  1LPM   29
REMARK      1 AUTH 2 D.HARRISON,B.RUBIN,M.CYGLER                       1LPM   30
REMARK      1 TITL  INSIGHTS INTO INTERFACIAL ACTIVATION FROM AN OPEN    1LPM   31
REMARK      1 TITL 2 STRUCTURE OF CANDIDA RUGOSA LIPASE                 1LPM   32
REMARK      1 REF   J.BIOL.CHEM.                V. 268 12843 1993       1LPM   33
REMARK      1 REFN ASTM JBCHA3  US ISSN 0021-9258                0071 1LPM   34
REMARK      2                                           1LPM   35
REMARK      2 RESOLUTION. 2.2  ANGSTROMS.                               1LPM   36
REMARK      3                                           1LPM   37
REMARK      3 REFINEMENT.                                             1LPM   38
REMARK      3 PROGRAM                X-PLOR                               1LPM   39
REMARK      3 AUTHORS                BRUNGER                             1LPM   40
REMARK      3 R VALUE                0.139                               1LPM   41
REMARK      3 MEAN B VALUE            21.1  ANGSTROMS**2               1LPM   42
REMARK      3 NUMBER OF REFLECTIONS   19378                             1LPM   43
REMARK      3 RESOLUTION RANGE        8. - 2.18  ANGSTROMS            1LPM   44
REMARK      3 DATA CUTOFF            4.  SIGMA(F)                     1LPM   45
REMARK      3 RMSD BOND DISTANCES     0.011  ANGSTROMS                 1LPM   46
REMARK      3 RMSD BOND ANGLES        1.82  DEGREES                     1LPM   47
REMARK      3                                           1LPM   48
REMARK      3 DATA COLLECTION.                                           1LPM   49
REMARK      3 NUMBER OF UNIQUE REFLECTIONS 25316                       1LPM   50

```

```

REMARK 3 COMPLETENESS OF DATA 84.8 % 1LPM 51
REMARK 3 REJECTION CRITERIA 1. SIGMA(I) 1LPM 52
REMARK 3 1LPM 53
REMARK 3 SOLVENT CONTENT (VS) 48. % 1LPM 54
REMARK 3 1LPM 55
REMARK 3 NUMBER OF ATOMS USED IN REFINEMENT. 1LPM 56
REMARK 3 NUMBER OF PROTEIN ATOMS 4022 1LPM 57
REMARK 3 NUMBER OF NUCLEIC ACID ATOMS 0 1LPM 58
REMARK 3 NUMBER OF HETEROGEN ATOMS 63 1LPM 59
REMARK 3 NUMBER OF SOLVENT ATOMS 261 1LPM 60
REMARK 4 1LPM 61
REMARK 4 EXPERIMENTAL DETAILS 1LPM 62
REMARK 4 SINGLE CRYSTAL X-RAY DIFFRACTION 1LPM 63
REMARK 4 MONOCHROMATIC RADIATION 1LPM 64
REMARK 4 DATE OF DATA-COLLECTION (DD-MON-YY) : 29-04-93 1LPM 65
REMARK 4 WAVELENGTH OR WAVELENGTH RANGE : CUKA 1LPM 66
REMARK 4 DETECTOR TYPE/MANUFACTURER : RAXIS II 1LPM 67
REMARK 4 INTENSITY-INTEGRATION SOFTWARE : RAXIS SOFTWARE 1LPM 68
REMARK 4 DATA REDUNDANCY : 2.7 1LPM 69
REMARK 5 1LPM 70
REMARK 5 KEYWDS: CARBOXYLIC ESTERASE, CRL 1LPM 71
REMARK 6 1LPM 72
REMARK 6 SOURCE 1LPM 73
REMARK 6 MOLECULE_NAME: O-(1R,2S,5R)-MENTHYL 1LPM 74
REMARK 6 HEXYLPHOSPHONCHLORIDATE. AFTER REACTION WITH CRL LIPASE 1LPM 75
REMARK 6 THE MOLECULE FOUND IN THE CRYSTAL IS, (1R)-MENTHYL HEXYL 1LPM 76
REMARK 6 PHOSPHONATE COMPLEX. 1LPM 77
REMARK 7 1LPM 78
REMARK 7 CA 590 AND WATER HOH 834 ARE IN SPECIAL POSITIONS. 1LPM 79
REMARK 36 1LPM 80
REMARK 36 TOPIC: STEREOCHEMISTRY 1LPM 81
REMARK 36 1LPM 82
REMARK 36 SUBTOPIC: BOND LENGTHS (36.1) 1LPM 83
REMARK 36 1LPM 84
REMARK 36 STANDARD TEXT: 1LPM 85
REMARK 36 1LPM 86
REMARK 36 THE STEREOCHEMICAL PARAMETERS OF THE FOLLOWING RESIDUES 1LPM 87
REMARK 36 HAVE VALUES WHICH DEVIATE FROM EXPECTED VALUES BY MORE 1LPM 88
REMARK 36 THAN 4*RMSD (M=MODEL NUMBER; RES=RESIDUE NAME; C=CHAIN 1LPM 89
REMARK 36 IDENTIFIER; SSEQ=SEQUENCE NUMBER; I=INSERTION CODE). 1LPM 90
REMARK 36 1LPM 91
REMARK 36 STANDARD TABLE: 1LPM 92
REMARK 36 FORMAT: (10X,I3,1X,A3,1X,A1,I4,A1,A4,3X,A4,16X,F5.1) 1LPM 93
REMARK 36 1LPM 94
REMARK 36 EXPECTED VALUES: ENGH AND HUBER, 1991 1LPM 95
REMARK 36 1LPM 96
REMARK 36 M RES CSSEQI ATM1 ATM2 DEVIATION_IN_ANGSTROMS 1LPM 97
REMARK 36 1LPM 98
REMARK 36 0 THR 11 CB - CA 0.042 1LPM 99
REMARK 36 0 MET 61 SD - CE 0.044 1LPM 100
REMARK 36 0 MET 82 SD - CE 0.053 1LPM 101
REMARK 36 0 ILE 100 CB - CA 0.043 1LPM 102
REMARK 36 0 LYS 141 CD - CE 0.050 1LPM 103
REMARK 36 0 MET 145 SD - CE 0.048 1LPM 104
REMARK 36 0 ILE 149 CB - CA 0.048 1LPM 105
REMARK 36 0 MET 319 SD - CE 0.059 1LPM 106
REMARK 36 0 VAL 333 CB - CA 0.057 1LPM 107
REMARK 36 0 GLU 341 CG - CD 0.043 1LPM 108
REMARK 36 0 MET 503 SD - CE 0.053 1LPM 109
REMARK 36 1LPM 110
REMARK 36 TOPIC: STEREOCHEMISTRY 1LPM 111
REMARK 36 1LPM 112
REMARK 36 SUBTOPIC: COVALENT BOND ANGLES (36.2) 1LPM 113
REMARK 36 1LPM 114
REMARK 36 STANDARD TEXT: 1LPM 115
REMARK 36 1LPM 116
REMARK 36 THE STEREOCHEMICAL PARAMETERS OF THE FOLLOWING RESIDUES 1LPM 117
REMARK 36 HAVE VALUES WHICH DEVIATE FROM EXPECTED VALUES BY MORE 1LPM 118
REMARK 36 THAN 4*RMSD (M=MODEL NUMBER; RES=RESIDUE NAME; C=CHAIN 1LPM 119
REMARK 36 IDENTIFIER; SSEQ=SEQUENCE NUMBER; I=INSERTION CODE). 1LPM 120

```

```
REMARK 36 1LPM 121
REMARK 36 STANDARD TABLE: 1LPM 122
REMARK 36 FORMAT: (10X,I3,1X,A3,1X,A1,I4,A1,3(2X,A4,17X,F5.1) 1LPM 123
REMARK 36 1LPM 124
REMARK 36 EXPECTED VALUES: ENGH AND HUBER, 1991 1LPM 125
REMARK 36 1LPM 126
REMARK 36 M RES CSSEQI ATM1 ATM2 ATM3 1LPM 127
REMARK 36 1LPM 128
REMARK 36 0 ASN 16 N - CA - C ANGL. DEV. = 6.9 DEGREES 1LPM 129
REMARK 36 0 PHE 23 N - CA - C ANGL. DEV. = 8.3 DEGREES 1LPM 130
REMARK 36 0 GLY 25 N - CA - C ANGL. DEV. = 7.8 DEGREES 1LPM 131
REMARK 36 0 SER 59 N - CA - C ANGL. DEV. = 6.9 DEGREES 1LPM 132
REMARK 36 0 GLU 71 N - CA - C ANGL. DEV. = 6.5 DEGREES 1LPM 133
REMARK 36 0 LEU 80 CA - CB - CG ANGL. DEV. = 13.5 DEGREES 1LPM 134
REMARK 36 0 ASP 96 N - CA - C ANGL. DEV. = 11.1 DEGREES 1LPM 135
REMARK 36 0 LEU 118 CA - CB - CG ANGL. DEV. = 7.0 DEGREES 1LPM 136
REMARK 36 0 ASN 155 N - CA - C ANGL. DEV. = 6.4 DEGREES 1LPM 137
REMARK 36 0 GLY 162 N - CA - C ANGL. DEV. = 6.8 DEGREES 1LPM 138
REMARK 36 0 ASP 181 N - CA - C ANGL. DEV. = 7.1 DEGREES 1LPM 139
REMARK 36 0 ASN 192 N - CA - C ANGL. DEV. = 10.3 DEGREES 1LPM 140
REMARK 36 0 TYR 228 N - CA - C ANGL. DEV. = 8.1 DEGREES 1LPM 141
REMARK 36 0 VAL 245 N - CA - C ANGL. DEV. = 6.7 DEGREES 1LPM 142
REMARK 36 0 LEU 278 CA - CB - CG ANGL. DEV. = 7.2 DEGREES 1LPM 143
REMARK 36 0 THR 293 N - CA - C ANGL. DEV. = 11.1 DEGREES 1LPM 144
REMARK 36 0 PRO 294 N - CA - C ANGL. DEV. = 7.4 DEGREES 1LPM 145
REMARK 36 0 PHE 296 N - CA - C ANGL. DEV. = 7.1 DEGREES 1LPM 146
REMARK 36 0 ARG 303 N - CA - C ANGL. DEV. = 6.4 DEGREES 1LPM 147
REMARK 36 0 LEU 304 CA - CB - CG ANGL. DEV. = 6.5 DEGREES 1LPM 148
REMARK 36 0 LEU 307 CA - CB - CG ANGL. DEV. = 6.6 DEGREES 1LPM 149
REMARK 36 0 ILE 315 N - CA - C ANGL. DEV. = 15.9 DEGREES 1LPM 150
REMARK 36 0 THR 316 N - CA - C ANGL. DEV. = 9.4 DEGREES 1LPM 151
REMARK 36 0 PRO 332 N - CA - C ANGL. DEV. = 6.9 DEGREES 1LPM 152
REMARK 36 0 ILE 334 N - CA - C ANGL. DEV. = 11.4 DEGREES 1LPM 153
REMARK 36 0 GLN 338 N - CA - C ANGL. DEV. = 9.4 DEGREES 1LPM 154
REMARK 36 0 GLY 342 N - CA - C ANGL. DEV. = 9.9 DEGREES 1LPM 155
REMARK 36 0 VAL 352 N - CA - C ANGL. DEV. = 8.1 DEGREES 1LPM 156
REMARK 36 0 THR 379 N - CA - C ANGL. DEV. = 6.5 DEGREES 1LPM 157
REMARK 36 0 TYR 381 N - CA - C ANGL. DEV. = 6.7 DEGREES 1LPM 158
REMARK 36 0 PRO 390 C-1 - N - CA ANGL. DEV. = 10.6 DEGREES 1LPM 159
REMARK 36 0 LEU 399 CA - CB - CG ANGL. DEV. = 7.7 DEGREES 1LPM 160
REMARK 36 0 THR 400 N - CA - C ANGL. DEV. = 7.4 DEGREES 1LPM 161
REMARK 36 0 PHE 415 N - CA - C ANGL. DEV. = 6.9 DEGREES 1LPM 162
REMARK 36 0 THR 416 N - CA - C ANGL. DEV. = 11.5 DEGREES 1LPM 163
REMARK 36 0 LYS 437 N - CA - C ANGL. DEV. = 7.0 DEGREES 1LPM 164
REMARK 36 0 VAL 444 N - CA - C ANGL. DEV. = 6.4 DEGREES 1LPM 165
REMARK 36 0 LEU 445 N - CA - C ANGL. DEV. = 6.5 DEGREES 1LPM 166
REMARK 36 0 THR 447 N - CA - C ANGL. DEV. = 7.4 DEGREES 1LPM 167
REMARK 36 0 PHE 448 N - CA - C ANGL. DEV. = 9.5 DEGREES 1LPM 168
REMARK 36 0 SER 450 N - CA - C ANGL. DEV. = 7.5 DEGREES 1LPM 169
REMARK 36 0 TYR 458 N - CA - C ANGL. DEV. = 8.4 DEGREES 1LPM 170
REMARK 36 0 LEU 460 CA - CB - CG ANGL. DEV. = 8.8 DEGREES 1LPM 171
REMARK 36 0 GLY 461 N - CA - C ANGL. DEV. = 6.5 DEGREES 1LPM 172
REMARK 36 0 ASN 469 N - CA - C ANGL. DEV. = 6.6 DEGREES 1LPM 173
REMARK 36 0 ASP 477 N - CA - C ANGL. DEV. = 8.2 DEGREES 1LPM 174
REMARK 36 0 ASP 479 N - CA - C ANGL. DEV. = 6.5 DEGREES 1LPM 175
REMARK 36 0 SER 498 N - CA - C ANGL. DEV. = 6.7 DEGREES 1LPM 176
REMARK 36 0 LEU 502 CA - CB - CG ANGL. DEV. = 10.1 DEGREES 1LPM 177
REMARK 36 0 MET 503 N - CA - C ANGL. DEV. = 10.2 DEGREES 1LPM 178
REMARK 36 0 LEU 525 CA - CB - CG ANGL. DEV. = 11.5 DEGREES 1LPM 179
REMARK 36 0 PHE 526 N - CA - C ANGL. DEV. = 9.8 DEGREES 1LPM 180
REMARK 36 0 ASN 528 N - CA - C ANGL. DEV. = 8.1 DEGREES 1LPM 181
REMARK 36 1LPM 182
REMARK 36 TOPIC: STEREOCHEMISTRY 1LPM 183
REMARK 36 1LPM 184
REMARK 36 SUBTOPIC: TORSION ANGLES (36.4) 1LPM 185
REMARK 36 1LPM 186
REMARK 36 STANDARD TEXT: 1LPM 187
REMARK 36 1LPM 188
REMARK 36 TORSION ANGLES OUTSIDE THE EXPECTED RAMACHANDRAN REGIONS: 1LPM 189
REMARK 36 (M=MODEL NUMBER; RES=RESIDUE NAME; C=CHAIN IDENTIFIER; 1LPM 190
```

```

REMARK 36 SSEQ=SEQUENCE NUMBER; I=INSERTION CODE). 1LPM 191
REMARK 36 1LPM 192
REMARK 36 STANDARD TABLE: 1LPM 193
REMARK 36 FORMAT: (10X,I3,1X,A3,1X,A1,I4,A1,4X,F7.2,3X,F7.2) 1LPM 194
REMARK 36 1LPM 195
REMARK 36 M RES CSSEQI PSI PHI 1LPM 196
REMARK 36 1LPM 197
REMARK 36 0 ILE 18 77.14 -64.09 1LPM 198
REMARK 36 0 THR 68 176.21 161.57 1LPM 199
REMARK 36 0 SER 159 58.49 -151.59 1LPM 200
REMARK 36 0 SER 209 55.99 -110.72 1LPM 201
REMARK 36 0 ALA 243 -113.98 -122.49 1LPM 202
REMARK 36 0 SER 301 54.36 -132.48 1LPM 203
REMARK 36 0 VAL 444 63.07 -49.91 1LPM 204
REMARK 36 0 SER 450 86.17 -5.14 1LPM 205
REMARK 999 1LPM 206
REMARK 999 CROSS REFERENCE TO SEQUENCE DATABASE 1LPM 207
REMARK 999 SWISS-PROT ENTRY NAME PDB ENTRY CHAIN NAME 1LPM 208
REMARK 999 LIPI1_CANRU 1LPM 209
SEQRES 1 549 MET GLU LEU ALA LEU ALA LEU SER LEU ILE ALA SER VAL 1LPM 210
SEQRES 2 549 ALA ALA ALA PRO THR ALA THR LEU ALA ASN GLY ASP THR 1LPM 211
SEQRES 3 549 ILE THR GLY LEU ASN ALA ILE ILE ASN GLU ALA PHE LEU 1LPM 212
SEQRES 4 549 GLY ILE PRO PHE ALA GLU PRO VAL GLY ASN LEU ARG 1LPM 213
SEQRES 5 549 PHE LYS ASP PRO VAL PRO TYR SER GLY SER LEU ASP GLY 1LPM 214
SEQRES 6 549 GLN LYS PHE THR SER TYR GLY PRO SER CYS MET GLN GLN 1LPM 215
SEQRES 7 549 ASN PRO GLU GLY THR TYR GLU GLU ASN LEU PRO LYS ALA 1LPM 216
SEQRES 8 549 ALA LEU ASP LEU VAL MET GLN SER LYS VAL PHE GLU ALA 1LPM 217
SEQRES 9 549 VAL SER PRO SER SER GLU ASP CYS LEU THR ILE ASN VAL 1LPM 218
SEQRES 10 549 VAL ARG PRO PRO GLY THR LYS ALA GLY ALA ASN LEU PRO 1LPM 219
SEQRES 11 549 VAL MET LEU TRP ILE PHE GLY GLY PHE GLU VAL GLY 1LPM 220
SEQRES 12 549 GLY THR SER THR PHE PRO PRO ALA GLN MET ILE THR LYS 1LPM 221
SEQRES 13 549 SER ILE ALA MET GLY LYS PRO ILE ILE HIS VAL SER VAL 1LPM 222
SEQRES 14 549 ASN TYR ARG VAL SER SER TRP GLY PHE LEU ALA GLY ASP 1LPM 223
SEQRES 15 549 GLU ILE LYS ALA GLU GLY SER ALA ASN ALA GLY LEU LYS 1LPM 224
SEQRES 16 549 ASP GLN ARG LEU GLY MET GLN TRP VAL ALA ASP ASN ILE 1LPM 225
SEQRES 17 549 ALA ALA PHE GLY GLY ASP PRO THR LYS VAL THR ILE PHE 1LPM 226
SEQRES 18 549 GLY GLU SER ALA GLY SER MET SER VAL MET CYS HIS ILE 1LPM 227
SEQRES 19 549 LEU TRP ASN ASP GLY ASP ASN THR TYR LYS GLY LYS PRO 1LPM 228
SEQRES 20 549 LEU PHE ARG ALA GLY ILE MET GLN SER GLY ALA MET VAL 1LPM 229
SEQRES 21 549 PRO SER ASP ALA VAL ASP GLY ILE TYR GLY ASN GLU ILE 1LPM 230
SEQRES 22 549 PHE ASP LEU LEU ALA SER ASN ALA GLY CYS GLY SER ALA 1LPM 231
SEQRES 23 549 SER ASP LYS LEU ALA CYS LEU ARG GLY VAL SER SER ASP 1LPM 232
SEQRES 24 549 THR LEU GLU ASP ALA THR ASN ASN THR PRO GLY PHE LEU 1LPM 233
SEQRES 25 549 ALA TYR SER SER LEU ARG LEU SER TYR LEU PRO ARG PRO 1LPM 234
SEQRES 26 549 ASP GLY VAL ASN ILE THR ASP ASP MET TYR ALA LEU VAL 1LPM 235
SEQRES 27 549 ARG GLU GLY LYS TYR ALA ASN ILE PRO VAL ILE ILE GLY 1LPM 236
SEQRES 28 549 ASP GLN ASN ASP GLU GLY THR PHE PHE GLY THR SER SER 1LPM 237
SEQRES 29 549 LEU ASN VAL THR THR ASP ALA GLN ALA ARG GLU TYR PHE 1LPM 238
SEQRES 30 549 LYS GLN SER PHE VAL HIS ALA SER ASP ALA GLU ILE ASP 1LPM 239
SEQRES 31 549 THR LEU MET THR ALA TYR PRO GLY ASP ILE THR GLN GLY 1LPM 240
SEQRES 32 549 SER PRO PHE ASP THR GLY ILE LEU ASN ALA LEU THR PRO 1LPM 241
SEQRES 33 549 GLN PHE LYS ARG ILE SER ALA VAL LEU GLY ASP LEU GLY 1LPM 242
SEQRES 34 549 PHE THR LEU ALA ARG ARG TYR PHE LEU ASN HIS TYR THR 1LPM 243
SEQRES 35 549 GLY GLY THR LYS TYR SER PHE LEU SER LYS GLN LEU SER 1LPM 244
SEQRES 36 549 GLY LEU PRO VAL LEU GLY THR PHE HIS SER ASN ASP ILE 1LPM 245
SEQRES 37 549 VAL PHE GLN ASP TYR LEU LEU GLY SER GLY SER LEU ILE 1LPM 246
SEQRES 38 549 TYR ASN ASN ALA PHE ILE ALA PHE ALA THR ASP LEU ASP 1LPM 247
SEQRES 39 549 PRO ASN THR ALA GLY LEU LEU VAL LYS TRP PRO GLU TYR 1LPM 248
SEQRES 40 549 THR SER SER SER GLN SER GLY ASN ASN LEU MET MET ILE 1LPM 249
SEQRES 41 549 ASN ALA LEU GLY LEU TYR THR GLY LYS ASP ASN PHE ARG 1LPM 250
SEQRES 42 549 THR ALA GLY TYR ASP ALA LEU PHE SER ASN PRO PRO SER 1LPM 251
SEQRES 43 549 PHE PHE VAL 1LPM 252
FTNOTE 1 1LPM 253
FTNOTE 1 CIS PROLINE - PRO 390 1LPM 254
HET MPA 560 19 (1R)-MENTHYL HEXYL PHOSPHONATE 1LPM 255
HET CA 589 1 CALCIUM ION 1LPM 256
HET CA 590 1 CALCIUM ION 1LPM 257
HET NAG 991 14 N-ACETYL-D-GLUCOSAMINE 1LPM 258
HET NAG 992 14 N-ACETYL-D-GLUCOSAMINE 1LPM 259
HET NAG 994 14 N-ACETYL-D-GLUCOSAMINE 1LPM 260

```





ATOM	3980	N	PRO	530	53.888	64.882	-28.148	1.00	14.93	LLPM4290
ATOM	3981	CA	PRO	530	54.447	66.079	-27.511	1.00	15.89	LLPM4291
ATOM	3982	C	PRO	530	53.651	66.672	-26.355	1.00	14.09	LLPM4292
ATOM	3983	O	PRO	530	54.137	67.574	-25.687	1.00	15.33	LLPM4293
ATOM	3984	CB	PRO	530	54.553	67.074	-28.670	1.00	13.27	LLPM4294
ATOM	3985	CG	PRO	530	54.723	66.206	-29.847	1.00	18.78	LLPM4295
ATOM	3986	CD	PRO	530	53.721	65.115	-29.594	1.00	16.59	LLPM4296
ATOM	3987	N	SER	531	52.426	66.207	-26.145	1.00	17.39	LLPM4297
ATOM	3988	CA	SER	531	51.606	66.709	-25.049	1.00	20.51	LLPM4298
ATOM	3989	C	SER	531	52.136	66.169	-23.736	1.00	18.33	LLPM4299
ATOM	3990	O	SER	531	51.840	66.717	-22.670	1.00	15.66	LLPM4300
ATOM	3991	CB	SER	531	50.156	66.264	-25.218	1.00	24.52	LLPM4301
ATOM	3992	OG	SER	531	49.528	66.979	-26.264	1.00	33.31	LLPM4302
ATOM	3993	N	PHE	532	52.913	65.089	-23.846	1.00	15.44	LLPM4303
ATOM	3994	CA	PHE	532	53.499	64.395	-22.712	1.00	16.36	LLPM4304
ATOM	3995	C	PHE	532	55.030	64.421	-22.604	1.00	16.59	LLPM4305
ATOM	3996	O	PHE	532	55.619	63.575	-21.940	1.00	19.95	LLPM4306
ATOM	3997	CB	PHE	532	52.982	62.956	-22.703	1.00	16.21	LLPM4307
ATOM	3998	CG	PHE	532	51.521	62.863	-22.407	1.00	17.21	LLPM4308
ATOM	3999	CD1	PHE	532	51.061	62.953	-21.087	1.00	13.60	LLPM4309
ATOM	4000	CD2	PHE	532	50.594	62.815	-23.440	1.00	15.22	LLPM4310
ATOM	4001	CE1	PHE	532	49.706	63.011	-20.803	1.00	10.85	LLPM4311
ATOM	4002	CE2	PHE	532	49.226	62.876	-23.157	1.00	15.19	LLPM4312
ATOM	4003	CZ	PHE	532	48.788	62.977	-21.834	1.00	10.97	LLPM4313
ATOM	4004	N	PHE	533	55.664	65.402	-23.240	1.00	15.56	LLPM4314
ATOM	4005	CA	PHE	533	57.117	65.547	-23.205	1.00	11.42	LLPM4315
ATOM	4006	C	PHE	533	57.536	66.347	-21.994	1.00	12.49	LLPM4316
ATOM	4007	O	PHE	533	56.811	67.240	-21.540	1.00	11.28	LLPM4317
ATOM	4008	CB	PHE	533	57.636	66.279	-24.449	1.00	8.47	LLPM4318
ATOM	4009	CG	PHE	533	57.680	65.437	-25.694	1.00	6.38	LLPM4319
ATOM	4010	CD1	PHE	533	57.258	64.110	-25.682	1.00	4.45	LLPM4320
ATOM	4011	CD2	PHE	533	58.144	65.981	-26.884	1.00	7.40	LLPM4321
ATOM	4012	CE1	PHE	533	57.302	63.344	-26.837	1.00	9.76	LLPM4322
ATOM	4013	CE2	PHE	533	58.189	65.220	-28.050	1.00	6.48	LLPM4323
ATOM	4014	CZ	PHE	533	57.772	63.910	-28.028	1.00	6.76	LLPM4324
ATOM	4015	N	VAL	534	58.742	66.063	-21.525	1.00	11.22	LLPM4325
ATOM	4016	CA	VAL	534	59.326	66.745	-20.378	1.00	15.19	LLPM4326
ATOM	4017	C	VAL	534	60.498	67.633	-20.804	1.00	15.66	LLPM4327
ATOM	4018	O	VAL	534	60.763	68.616	-20.088	1.00	21.21	LLPM4328
ATOM	4019	CB	VAL	534	59.793	65.748	-19.276	1.00	13.73	LLPM4329
ATOM	4020	CG1	VAL	534	58.595	64.980	-18.739	1.00	15.41	LLPM4330
ATOM	4021	CG2	VAL	534	60.865	64.795	-19.808	1.00	12.82	LLPM4331
ATOM	4022	OXT	VAL	534	61.102	67.384	-21.869	1.00	17.63	LLPM4332
TER	4023		VAL	534						LLPM4333
HETATM	4024	C1	MPA	560	65.798	55.043	-16.026	1.00	13.03	LLPM4334
HETATM	4025	C2	MPA	560	65.627	55.959	-17.255	1.00	11.39	LLPM4335
HETATM	4026	C3	MPA	560	64.571	57.124	-17.048	1.00	13.35	LLPM4336
HETATM	4027	C4	MPA	560	63.922	57.787	-18.372	1.00	17.30	LLPM4337
HETATM	4028	C5	MPA	560	62.913	58.995	-18.258	1.00	15.04	LLPM4338
HETATM	4029	C6	MPA	560	62.623	59.730	-19.553	1.00	14.17	LLPM4339
HETATM	4030	C7	MPA	560	67.973	52.605	-13.943	1.00	15.72	LLPM4340
HETATM	4031	C8	MPA	560	68.743	51.433	-14.430	1.00	20.25	LLPM4341
HETATM	4032	C9	MPA	560	69.810	51.057	-13.389	1.00	20.78	LLPM4342
HETATM	4033	C10	MPA	560	69.188	50.884	-11.965	1.00	18.95	LLPM4343
HETATM	4034	C11	MPA	560	68.239	52.010	-11.495	1.00	14.81	LLPM4344
HETATM	4035	C12	MPA	560	67.288	52.442	-12.571	1.00	17.17	LLPM4345
HETATM	4036	C13	MPA	560	70.517	49.796	-13.891	1.00	24.06	LLPM4346
HETATM	4037	C14	MPA	560	66.540	53.805	-12.329	1.00	18.80	LLPM4347
HETATM	4038	C15	MPA	560	65.785	53.887	-11.013	1.00	17.76	LLPM4348
HETATM	4039	C16	MPA	560	67.452	55.043	-12.547	1.00	21.52	LLPM4349
HETATM	4040	O1	MPA	560	66.925	52.892	-14.862	1.00	13.70	LLPM4350
HETATM	4041	O2	MPA	560	68.437	54.261	-16.496	1.00	18.55	LLPM4351
HETATM	4042	P1	MPA	560	67.120	53.790	-16.192	1.00	12.82	LLPM4352
HETATM	4043	CA	CA	589	68.380	81.327	-18.575	1.00	54.48	LLPM4353
HETATM	4044	CA	CA	590	65.200	56.805	-44.075	1.00	14.15	LLPM4354
HETATM	4045	C1	NAG	991	76.768	66.745	-35.311	0.60	11.07	LLPM4355
HETATM	4046	C2	NAG	991	77.875	65.765	-35.652	0.60	10.48	LLPM4356
HETATM	4047	C3	NAG	991	78.944	66.476	-36.517	0.60	13.37	LLPM4357

```

.
.
.
HETATM 4084 O5 NAG 994 56.271 71.193 -2.103 1.00 37.50 1LPM4394
HETATM 4085 O6 NAG 994 55.520 72.100 0.318 1.00 49.13 1LPM4395
HETATM 4086 O7 NAG 994 57.451 70.075 -6.771 1.00 29.51 1LPM4396
HETATM 4087 O HOH 601 64.372 44.835 -20.429 1.00 12.60 1LPM4397
HETATM 4088 O HOH 602 56.325 59.188 -9.129 1.00 13.22 1LPM4398
HETATM 4089 O HOH 603 54.327 49.638 -14.598 1.00 4.76 1LPM4399
.
.
.
HETATM 4345 O HOH 859 100.339 58.865 -22.355 1.00 48.45 1LPM4655
HETATM 4346 O HOH 860 62.591 79.133 -21.449 1.00 50.68 1LPM4656
HETATM 4347 O HOH 861 59.180 55.274 -40.591 1.00 37.36 1LPM4657
CONNECT 438 437 721 1LPM4658
CONNECT 721 438 720 1LPM4659
CONNECT 1547 1546 4042 1LPM4660
CONNECT 1978 1977 2035 1LPM4661
CONNECT 2035 1978 2034 1LPM4662
CONNECT 2316 2314 4045 1LPM4663
CONNECT 2411 2410 4044 1LPM4664
CONNECT 2601 2599 4059 1LPM4665
CONNECT 4024 4025 4042 1LPM4666
CONNECT 4025 4024 4026 1LPM4667
CONNECT 4026 4025 4027 1LPM4668
CONNECT 4027 4026 4028 1LPM4669
CONNECT 4028 4027 4029 1LPM4670
CONNECT 4029 4028 1LPM4671
CONNECT 4030 4031 4035 4040 1LPM4672
CONNECT 4031 4030 4032 1LPM4673
CONNECT 4032 4031 4033 4036 1LPM4674
CONNECT 4033 4032 4034 1LPM4675
CONNECT 4034 4033 4035 1LPM4676
CONNECT 4035 4030 4034 4037 1LPM4677
CONNECT 4036 4032 1LPM4678
CONNECT 4037 4035 4038 4039 1LPM4679
CONNECT 4038 4037 1LPM4680
CONNECT 4039 4037 1LPM4681
CONNECT 4040 4030 4042 1LPM4682
CONNECT 4041 4042 1LPM4683
CONNECT 4042 1547 4024 4040 4041 1LPM4684
CONNECT 4043 4153 1LPM4685
CONNECT 4044 2411 4320 1LPM4686
CONNECT 4045 2316 4046 4056 1LPM4687
CONNECT 4046 4045 4047 4053 1LPM4688
CONNECT 4047 4046 4048 4054 1LPM4689
CONNECT 4048 4047 4049 4055 1LPM4690
CONNECT 4049 4048 4050 4056 1LPM4691
CONNECT 4050 4049 4057 1LPM4692
CONNECT 4051 4052 4053 4058 1LPM4693
CONNECT 4052 4051 1LPM4694
CONNECT 4053 4046 4051 1LPM4695
CONNECT 4054 4047 1LPM4696
CONNECT 4055 4048 1LPM4697
CONNECT 4056 4045 4049 1LPM4698
CONNECT 4057 4050 1LPM4699
CONNECT 4058 4051 1LPM4700
CONNECT 4059 2601 4060 4070 1LPM4701
CONNECT 4060 4059 4061 4067 1LPM4702
CONNECT 4061 4060 4062 4068 1LPM4703
CONNECT 4062 4061 4063 4069 1LPM4704
CONNECT 4063 4062 4064 4070 1LPM4705
CONNECT 4064 4063 4071 1LPM4706
CONNECT 4065 4066 4067 4072 1LPM4707
CONNECT 4066 4065 1LPM4708
CONNECT 4067 4060 4065 1LPM4709
CONNECT 4068 4061 1LPM4710
CONNECT 4069 4062 4073 1LPM4711
CONNECT 4070 4059 4063 1LPM4712

```

```
CONNECT 4071 4064 1LPM4713
CONNECT 4072 4065 1LPM4714
CONNECT 4073 4069 4074 4084 1LPM4715
CONNECT 4074 4073 4075 4081 1LPM4716
CONNECT 4075 4074 4076 4082 1LPM4717
CONNECT 4076 4075 4077 4083 1LPM4718
CONNECT 4077 4076 4078 4084 1LPM4719
CONNECT 4078 4077 4085 1LPM4720
CONNECT 4079 4080 4081 4086 1LPM4721
CONNECT 4080 4079 1LPM4722
CONNECT 4081 4074 4079 1LPM4723
CONNECT 4082 4075 1LPM4724
CONNECT 4083 4076 1LPM4725
CONNECT 4084 4073 4077 1LPM4726
CONNECT 4085 4078 1LPM4727
CONNECT 4086 4079 1LPM4728
CONNECT 4153 4043 1LPM4729
CONNECT 4320 4044 1LPM4730
MASTER 196 2 6 25 12 0 0 6 4346 1 73 43 1LPM4731
END 1LPM4732
```

## 8.2. COORDINATE FILE IN GROMOS96 FORMAT (LPMCOORD6.DAT)

TITLE

\$Id: iemlpm10.dat 15/05/97  
1LPM aus PDB, 43A1 force field,  
in SPC water, trunc. oct. box, ions,  
solute restrained,  
EM from lpmcoord5.dat to lpmcoord6.dat  
END

POSITION

# first 24 chars ignored

1	ALA	H1	1	3.561213903	5.641323162	1.756004436
1	ALA	H2	2	3.708338410	5.575928634	1.734334492
1	ALA	N	3	3.657285195	5.646645138	1.783250447
1	ALA	H3	4	3.664295607	5.629649568	1.881542624
1	ALA	CA	5	3.712228203	5.779254738	1.751545971
1	ALA	CB	6	3.623570168	5.890389921	1.808122597
1	ALA	C	7	3.859101243	5.793633756	1.791940131
1	ALA	O	8	3.941340059	5.809926482	1.701931411
2	PRO	N	9	3.895588093	5.791095967	1.919825049
2	PRO	CA	10	4.038723686	5.799229289	1.952342852
2	PRO	CB	11	4.043863597	5.802379237	2.105218370
2	PRO	CG	12	3.914893881	5.877675386	2.138450202
2	PRO	CD	13	3.818376575	5.805692653	2.044061879
2	PRO	C	14	4.107314976	5.673753301	1.897974212
2	PRO	O	15	4.048109702	5.565954395	1.898838361
3	THR	N	16	4.231933939	5.688868270	1.854048742
3	THR	H	17	4.279341860	5.776801156	1.858548451
3	THR	CA	18	4.302733321	5.574441270	1.794831409
3	THR	CB	19	4.276769023	5.570645866	1.644087919
3	THR	OG1	20	4.140188962	5.535745981	1.620079608
3	THR	HG1	21	4.123155700	5.531759864	1.521621787
3	THR	CG2	22	4.367961804	5.472590697	1.570077362
3	THR	C	23	4.452024991	5.573348931	1.828251008
3	THR	O	24	4.514386225	5.677955798	1.845497555
.						
.						
.						
530	PRO	N	5069	6.304928832	4.372624144	6.250268559
530	PRO	CA	5070	6.255416729	4.235054417	6.234901995
530	PRO	CB	5071	6.379854486	4.150653889	6.206641402
530	PRO	CG	5072	6.471727155	4.250726129	6.136277600
530	PRO	CD	5073	6.449536291	4.374208438	6.223826359
530	PRO	C	5074	6.181063105	4.177437335	6.355580945
530	PRO	O	5075	6.122543350	4.069598649	6.346926161
531	SER	N	5076	6.189047127	4.244778214	6.469979958
531	SER	H	5077	6.238658594	4.331392959	6.476167543
531	SER	CA	5078	6.117105857	4.199937285	6.590082349
531	SER	CB	5079	6.163123737	4.276932463	6.714017965
531	SER	OG	5080	6.294713617	4.232773184	6.748403389
531	SER	HG	5081	6.321528287	4.285921803	6.828763810
531	SER	C	5082	5.966408684	4.220444186	6.573449489
531	SER	O	5083	5.886795251	4.158275011	6.643629491
532	PHE	N	5084	5.933652845	4.308890917	6.479695997
532	PHE	H	5085	6.005663043	4.353713222	6.426715493
532	PHE	CA	5086	5.795193250	4.347611437	6.449030783
532	PHE	CB	5087	5.780377444	4.498076038	6.472517842
532	PHE	CG	5088	5.791806522	4.533608067	6.620883741
532	PHE	CD1	5089	5.682412642	4.515255721	6.704635582
532	PHE	HD1	5090	5.586272952	4.485145268	6.663036632
532	PHE	CD2	5091	5.914236799	4.573500359	6.673225905
532	PHE	HD2	5092	5.999356472	4.589631197	6.607075217
532	PHE	CE1	5093	5.695202628	4.534674368	6.841676906
532	PHE	HE1	5094	5.609339000	4.519842447	6.907161538
532	PHE	CE2	5095	5.926772067	4.592799160	6.810299131
532	PHE	HE2	5096	6.022765334	4.623593039	6.851749773

532	PHE	CZ	5097	5.817867393	4.573234227	6.894437059
532	PHE	HZ	5098	5.828054770	4.587875825	7.001968826
532	PHE	C	5099	5.744000073	4.311052162	6.309553493
532	PHE	O	5100	5.647320320	4.369708948	6.261153256
533	PHE	N	5101	5.807709876	4.212486542	6.247001328
533	PHE	H	5102	5.884541876	4.165079172	6.289999004
533	PHE	CA	5103	5.766513637	4.164639039	6.114236898
533	PHE	CB	5104	5.882563339	4.100533297	6.037886028
533	PHE	CG	5105	5.981837166	4.201760171	5.980403895
533	PHE	CD1	5106	5.964512527	4.338400546	5.999147456
533	PHE	HD1	5107	5.878970883	4.375711385	6.055447937
533	PHE	CD2	5108	6.091083668	4.155081415	5.908254330
533	PHE	HD2	5109	6.104495803	4.047933479	5.893382051
533	PHE	CE1	5110	6.056247447	4.428318131	5.946055663
533	PHE	HE1	5111	6.041653059	4.535268407	5.961140112
533	PHE	CE2	5112	6.183109188	4.244765779	5.855262724
533	PHE	HE2	5113	6.269163543	4.208181743	5.799248255
533	PHE	CZ	5114	6.165571484	4.381333017	5.874232477
533	PHE	HZ	5115	6.238170768	4.451030500	5.832372330
533	PHE	C	5116	5.656021589	4.059520691	6.126362294
533	PHE	O	5117	5.652941427	3.983347026	6.222878597
534	VAL	N	5118	5.572690928	4.056310740	6.022757518
534	VAL	H	5119	5.585576864	4.119327246	5.946189874
534	VAL	CA	5120	5.461615485	3.960437955	6.013738694
534	VAL	CB	5121	5.327624684	4.030288445	5.989704870
534	VAL	CG1	5122	5.293188149	4.122605187	6.106769357
534	VAL	CG2	5123	5.325573256	4.107672193	5.857721805
534	VAL	C	5124	5.489640528	3.854783494	5.906663561
534	VAL	O1	5125	5.431557982	3.744704967	5.918176481
534	VAL	O2	5126	5.565796701	3.882733024	5.811554855
535	NA+	NA	5127	4.871452795	5.964626580	5.188640606
536	NA+	NA	5128	3.250329596	4.016433140	4.143931720
537	NA+	NA	5129	4.225369819	4.582503880	6.037663018
538	NA+	NA	5130	5.550492691	3.762371425	7.090195042
539	NA+	NA	5131	3.239464139	3.308178947	4.892187100
540	NA+	NA	5132	5.210982627	4.600049179	2.140117801
541	NA+	NA	5133	6.329812200	3.980860486	6.908602608
542	NA+	NA	5134	6.401820878	3.784670020	5.507314288
543	NA+	NA	5135	3.724276068	3.880971542	3.055108551
544	NA+	NA	5136	6.118609898	2.549264949	4.985139104
545	NA+	NA	5137	4.827412807	2.629891029	6.035621008
546	NA+	NA	5138	7.150620896	5.139831558	3.982724322
547	NA+	NA	5139	4.568159797	3.627397291	6.692673298
548	NA+	NA	5140	5.667224981	2.441194450	5.634335741
549	NA+	NA	5141	3.033897613	3.364380915	5.917040754
550	NA+	NA	5142	3.181194072	3.123445559	4.678371936
551	NA+	NA	5143	4.386980183	3.586445193	1.906021415
552	H2O	OW	5144	4.340642666	4.588272800	6.527109556
552	H2O	HW1	5145	4.261060158	4.563379150	6.471899841
552	H2O	HW2	5146	4.408180048	4.514628496	6.523314951
553	H2O	OW	5147	4.706103942	5.632894651	6.387288932
553	H2O	HW1	5148	4.628733948	5.609722762	6.328334071
553	H2O	HW2	5149	4.745881615	5.719689911	6.357547082
554	H2O	OW	5150	6.422503432	4.812401830	4.074029796
554	H2O	HW1	5151	6.391683078	4.822304492	4.168655452
554	H2O	HW2	5152	6.493784682	4.742407317	4.069366136
.						
.						
.						
793	H2O	OW	5867	4.340417216	3.855671125	1.991655642
793	H2O	HW1	5868	4.262446423	3.842205426	1.930491184
793	H2O	HW2	5869	4.307337424	3.875721288	2.083880410
794	H2O	OW	5870	5.730474050	2.707130635	5.874866275
794	H2O	HW1	5871	5.651863963	2.682969510	5.817985546
794	H2O	HW2	5872	5.799883043	2.635474771	5.868026184
795	H2O	OW	5873	7.126666934	5.368167434	5.206460250
795	H2O	HW1	5874	7.049092550	5.342427687	5.148858232
795	H2O	HW2	5875	7.162914367	5.456296251	5.176161108
1	SOLV	CCh1	5876	2.130284091	2.900437649	2.768500287
1	SOLV	HCh1	5877	2.234100342	2.865539417	2.758626969

1	SOLV	CLCh1	5878	2.111056082	2.964475581	2.931095221
1	SOLV	CLCh2	5879	2.104435522	3.025133411	2.647314096
1	SOLV	CLCh3	5880	2.024971099	2.762311291	2.741429970
2	SOLV	CCh1	5881	2.744351049	2.670505030	2.243706438
2	SOLV	HCh1	5882	2.837664517	2.624988169	2.280105304
2	SOLV	CLCh1	5883	2.610568011	2.581557118	2.315055583
2	SOLV	CLCh2	5884	2.743822450	2.838654877	2.294996132
2	SOLV	CLCh3	5885	2.743688743	2.657175470	2.068427535
3	SOLV	CCh1	5886	1.772506967	3.041674399	2.589787417
3	SOLV	HCh1	5887	1.851730161	3.089199241	2.649525735
3	SOLV	CLCh1	5888	1.849469683	2.962602616	2.452934851
3	SOLV	CLCh2	5889	1.690718357	2.925297423	2.693077966
3	SOLV	CLCh3	5890	1.662731249	3.168364488	2.536862130
.						
.						
.						
2287	SOLV	CCh1	17306	9.565781418	6.654859392	4.393319471
2287	SOLV	HCh1	17307	9.490297160	6.706658615	4.454329520
2287	SOLV	CLCh1	17308	9.611449900	6.762945733	4.262429801
2287	SOLV	CLCh2	17309	9.702814475	6.619183547	4.497489994
2287	SOLV	CLCh3	17310	9.492264940	6.507497659	4.331815662
2288	SOLV	CCh1	17311	9.417029119	6.631154294	5.432513915
2288	SOLV	HCh1	17312	9.491954269	6.550611369	5.431366399
2288	SOLV	CLCh1	17313	9.297862684	6.591060953	5.555369972
2288	SOLV	CLCh2	17314	9.500648366	6.780885247	5.471133430
2288	SOLV	CLCh3	17315	9.344110946	6.638053720	5.272703675
2289	SOLV	CCh1	17316	9.179087204	6.409714216	3.910299826
2289	SOLV	HCh1	17317	9.072405544	6.436428957	3.912866070
2289	SOLV	CLCh1	17318	9.197994764	6.277680191	3.795793511
2289	SOLV	CLCh2	17319	9.268219025	6.552229525	3.858817656
2289	SOLV	CLCh3	17320	9.225428828	6.360641822	4.072642524
END						
BOX						
9.583323479			9.583323479		9.583323479	
END						
REFPOSITION						
# first 24 chars ignored						
1	ALA	H1	1	3.560513020	5.640790939	1.755991101
1	ALA	H2	2	3.708401203	5.575164795	1.734097123
1	ALA	N	3	3.656673431	5.645361900	1.783052087
1	ALA	H3	4	3.664319038	5.629738808	1.881527901
1	ALA	CA	5	3.711434841	5.779919624	1.749617338
1	ALA	CB	6	3.624674320	5.890852928	1.811247349
1	ALA	C	7	3.860270500	5.792210579	1.789570570
1	ALA	O	8	3.944236279	5.810335159	1.700924039
2	PRO	N	9	3.894936562	5.789951324	1.921684265
2	PRO	CA	10	4.038403988	5.799990654	1.951897621
2	PRO	CB	11	4.040180206	5.803217888	2.104882479
2	PRO	CG	12	3.916931629	5.876769066	2.136884451
2	PRO	CD	13	3.817605972	5.806612015	2.046393394
2	PRO	C	14	4.108020782	5.674599648	1.896918774
2	PRO	O	15	4.049883366	5.566116333	1.897231579
3	THR	N	16	4.232239723	5.687985420	1.853227735
3	THR	H	17	4.277975082	5.776694298	1.859463453
3	THR	CA	18	4.302445412	5.574079514	1.796170473
3	THR	CB	19	4.277027607	5.570743561	1.643551588
3	THR	OG1	20	4.140268326	5.534572601	1.620137811
3	THR	HG1	21	4.122768402	5.532123566	1.521711349
3	THR	CG2	22	4.368932724	5.472751617	1.573439837
3	THR	C	23	4.452146530	5.571396828	1.827240467
3	THR	O	24	4.515362740	5.676453590	1.845225930
.						
.						
.						
530	PRO	N	5069	6.305693626	4.372111320	6.249258995
530	PRO	CA	5070	6.254941940	4.235119820	6.236300468
530	PRO	CB	5071	6.381126404	4.153870583	6.205945015
530	PRO	CG	5072	6.468871117	4.251329422	6.139019966
530	PRO	CD	5073	6.450753689	4.374536514	6.223132133
530	PRO	C	5074	6.181035042	4.178025246	6.356690407

530	PRO	O	5075	6.123350143	4.070626259	6.346783638
531	SER	N	5076	6.186075211	4.246253967	6.470396996
531	SER	H	5077	6.238455772	4.331346035	6.474337578
531	SER	CA	5078	6.116593361	4.199345589	6.589678764
531	SER	CB	5079	6.163883209	4.276085854	6.712827682
531	SER	OG	5080	6.294261932	4.236040115	6.750176430
531	SER	HG	5081	6.323146820	4.287501335	6.830905914
531	SER	C	5082	5.967523575	4.220680237	6.572717667
531	SER	O	5083	5.887130260	4.158463478	6.642781258
532	PHE	N	5084	5.933859348	4.309777260	6.479172707
532	PHE	H	5085	6.007248878	4.353159904	6.426904678
532	PHE	CA	5086	5.796836853	4.347405434	6.448859215
532	PHE	CB	5087	5.780858040	4.497329712	6.474318504
532	PHE	CG	5088	5.792096615	4.533478260	6.618799210
532	PHE	CD1	5089	5.683053493	4.515266895	6.704816818
532	PHE	HD1	5090	5.586717606	4.485273361	6.663575172
532	PHE	CD2	5091	5.913928032	4.573342800	6.672233582
532	PHE	HD2	5092	5.999481201	4.589471817	6.606647491
532	PHE	CE1	5093	5.695556164	4.534728527	6.841438293
532	PHE	HE1	5094	5.609683990	4.519872665	6.906907082
532	PHE	CE2	5095	5.926949501	4.592810631	6.810087204
532	PHE	HE2	5096	6.022827625	4.623470783	6.851901054
532	PHE	CZ	5097	5.817235947	4.573017597	6.894319534
532	PHE	HZ	5098	5.827700615	4.587805748	7.001803398
532	PHE	C	5099	5.744377613	4.310259819	6.309463501
532	PHE	O	5100	5.648214340	4.369421482	6.261630058
533	PHE	N	5101	5.806448936	4.211257935	6.245950699
533	PHE	H	5102	5.884020329	4.166587353	6.290528297
533	PHE	CA	5103	5.765467167	4.165385723	6.113471031
533	PHE	CB	5104	5.882646084	4.101860046	6.037570953
533	PHE	CG	5105	5.980830193	4.200532436	5.980710983
533	PHE	CD1	5106	5.964215279	4.337551117	5.999182701
533	PHE	HD1	5107	5.878604889	4.374403954	6.055695534
533	PHE	CD2	5108	6.090617180	4.155544281	5.908625603
533	PHE	HD2	5109	6.104708195	4.048535824	5.893406868
533	PHE	CE1	5110	6.055524349	4.427560329	5.946379662
533	PHE	HE1	5111	6.041580200	4.534654140	5.961125374
533	PHE	CE2	5112	6.183032990	4.245211601	5.855463982
533	PHE	HE2	5113	6.268857002	4.208350182	5.799281120
533	PHE	CZ	5114	6.165689468	4.380334854	5.874054909
533	PHE	HZ	5115	6.237764835	4.450730324	5.832453728
533	PHE	C	5116	5.656642914	4.061275482	6.125273705
533	PHE	O	5117	5.652747154	3.984036922	6.221767426
534	VAL	N	5118	5.573053360	4.055747032	6.022644043
534	VAL	H	5119	5.585957527	4.119869232	5.947001457
534	VAL	CA	5120	5.463182449	3.960409164	6.015098572
534	VAL	CB	5121	5.326257706	4.030325413	5.990027428
534	VAL	CG1	5122	5.293644428	4.122398376	6.106614113
534	VAL	CG2	5123	5.326517105	4.107015610	5.857653618
534	VAL	C	5124	5.488585472	3.855677843	5.906368256
534	VAL	O1	5125	5.434253693	3.744523525	5.919948578
534	VAL	O2	5126	5.566412926	3.882370472	5.812343597
535	NA+	NA	5127	4.875833035	5.967102051	5.188457489
536	NA+	NA	5128	3.251719952	4.018607616	4.145293236
537	NA+	NA	5129	4.224418163	4.583529472	6.038466454
538	NA+	NA	5130	5.549729347	3.762169361	7.090925217
539	NA+	NA	5131	3.241190195	3.303741693	4.887248039
540	NA+	NA	5132	5.212962151	4.599943638	2.139769316
541	NA+	NA	5133	6.332628727	3.976588488	6.908881187
542	NA+	NA	5134	6.401489258	3.782540798	5.505774498
543	NA+	NA	5135	3.722269535	3.882233858	3.055072784
544	NA+	NA	5136	6.120596409	2.548722982	4.982964039
545	NA+	NA	5137	4.826287270	2.628887653	6.035641670
546	NA+	NA	5138	7.150632858	5.143043518	3.982505560
547	NA+	NA	5139	4.568508148	3.626051903	6.691980362
548	NA+	NA	5140	5.668888092	2.440378428	5.639416695
549	NA+	NA	5141	3.035711527	3.367045164	5.919903755
550	NA+	NA	5142	3.181775331	3.126857996	4.683610916
551	NA+	NA	5143	4.387071609	3.585877419	1.904066324
552	H2O	OW	5144	4.336902142	4.588841438	6.528038979

552	H2O	HW1	5145	4.259902954	4.562710285	6.469829559
552	H2O	HW2	5146	4.407840729	4.518537521	6.523026466
553	H2O	OW	5147	4.709156036	5.634369850	6.388966560
553	H2O	HW1	5148	4.632156372	5.608239174	6.330757141
553	H2O	HW2	5149	4.746491909	5.721691132	6.357643127
554	H2O	OW	5150	6.424482346	4.810408115	4.077130318
554	H2O	HW1	5151	6.393206596	4.819522858	4.171674728
554	H2O	HW2	5152	6.495421410	4.740104675	4.072117805
.						
.						
793	H2O	OW	5867	4.338065147	3.864952803	1.989468694
793	H2O	HW1	5868	4.261065960	3.838821411	1.931259632
793	H2O	HW2	5869	4.306789398	3.874067307	2.084013939
794	H2O	OW	5870	5.727099895	2.709977150	5.875579834
794	H2O	HW1	5871	5.650100708	2.683845997	5.817370415
794	H2O	HW2	5872	5.798038483	2.639673471	5.870567322
795	H2O	OW	5873	7.126580238	5.368671417	5.207871437
795	H2O	HW1	5874	7.049581528	5.342539787	5.149662971
795	H2O	HW2	5875	7.163916111	5.455991745	5.176548004
1	SOLV	CCh1	5876	2.130000114	2.899999857	2.769000053
1	SOLV	HCh1	5877	2.233999968	2.865999937	2.759000063
1	SOLV	CLCh1	5878	2.111000061	2.964999914	2.930999994
1	SOLV	CLCh2	5879	2.104000092	3.024999857	2.647000074
1	SOLV	CLCh3	5880	2.025000095	2.761999846	2.742000103
2	SOLV	CCh1	5881	2.689000130	2.667999983	2.236000061
2	SOLV	HCh1	5882	2.746000051	2.591999769	2.292000055
2	SOLV	CLCh1	5883	2.518000126	2.635999918	2.259999990
2	SOLV	CLCh2	5884	2.733999968	2.824999809	2.299999952
2	SOLV	CLCh3	5885	2.733999968	2.651999950	2.066999912
3	SOLV	CCh1	5886	1.754000068	3.037999868	2.552999973
3	SOLV	HCh1	5887	1.846000075	3.085999966	2.588999987
3	SOLV	CLCh1	5888	1.792000055	2.954999924	2.403000116
3	SOLV	CLCh2	5889	1.700000048	2.925999880	2.677000046
3	SOLV	CLCh3	5890	1.634999990	3.165999889	2.526999950
.						
.						
2287	SOLV	CCh1	17306	9.573100090	6.652400017	4.368700027
2287	SOLV	HCh1	17307	9.491100311	6.694399834	4.427700043
2287	SOLV	CLCh1	17308	9.621100426	6.774399757	4.250699997
2287	SOLV	CLCh2	17309	9.705100060	6.616399765	4.478700161
2287	SOLV	CLCh3	17310	9.514100075	6.507400036	4.289700031
2288	SOLV	CCh1	17311	9.418100357	6.642399788	5.427700043
2288	SOLV	HCh1	17312	9.488100052	6.557399750	5.415699959
2288	SOLV	CLCh1	17313	9.301099777	6.598400116	5.549699783
2288	SOLV	CLCh2	17314	9.513099670	6.781399727	5.477700233
2288	SOLV	CLCh3	17315	9.341099739	6.669399738	5.271699905
2289	SOLV	CCh1	17316	9.202099800	6.413399696	3.882699966
2289	SOLV	HCh1	17317	9.097100258	6.446399689	3.890699863
2289	SOLV	CLCh1	17318	9.204099655	6.266399860	3.785699844
2289	SOLV	CLCh2	17319	9.292099953	6.542399883	3.803699970
2289	SOLV	CLCh3	17320	9.261099815	6.383399963	4.045700073

END



### 8.3. MOLECULAR TOPOLOGY FOR THE CANDIDA RUGOSA LIPASE

```
# GROMOS TOPOLOGY FILE
# WRTOPO version:
# $Id: wrtopo.f,v 1.19 1996/10/18 14:49:29 wscott Exp $
#
TITLE
MOLECULAR TOPOLOGY, 1LPM (offen) aus PDB, FORCE FIELD 43A1,
END
TOPPHYSCON
# FPEPSI: 1.0/(4.0*PI*EPS0) (EPS0 is the permittivity of vacuum)
  0.1389354E+03
# HBAR: Planck's constant HBAR = H/(2* PI)
  0.6350780E-01
END
TOPVERSION
1.7
END
ATOMTYPENAME
# NRATT: number of van der Waals atom types
  43
# TYPE: atom type names
O
OM
OA
OW
N
NT
NL
NR
NZ
NE
#      10
C
CH1
CH2
CH3
CH4
CR1
HC
H
DUM
S
#      20
CU1+
CU2+
FE
ZN2+
MG2+
CA2+
P,SI
AR
F
CL
#      30
BR
CMET
OMET
NA+
CL-
CCHL
CLCHL
HCHL
SDMSO
CDMSO
#      40
```

```
ODMSO
CCL4
CLCL4
END
RESNAME
# NRAA2: number of residues in a solute molecule
  795
# AANM: residue names
ALA
PRO
THR
ALA
THR
LEU
ALA
ASN
GLY
ASP
#      10
.
.
#      520
GLY
TYR
ASP
ALA
LEU
PHE
SER
ASN
PRO
PRO
#      530
SER
PHE
PHE
VAL
NA+
NA+
NA+
NA+
NA+
NA+
#      540
NA+
NA+
NA+
NA+
NA+
NA+
NA+
NA+
NA+
NA+
#      550
NA+
H2O
H2O
H2O
H2O
H2O
H2O
H2O
H2O
H2O
#      560
.
.
.
```

```

#          790
H2O
H2O
H2O
H2O
H2O
H2O
END
SOLUTEATOM
#   NRP: number of solute atoms
5875
#   ATNM: atom number
#   MRES: residue number
#   PANM: atom name of solute atom
#   IAC: integer (van der Waals) atom type code
#   MASS: mass of solute atom
#   CG: charge of solute atom
#   CGC: charge group code (0 or 1)
#   INE: number of excluded atoms
#   INE14: number of 1-4 interactions
#ATNM MRES  PANM IAC      MASS          CG CGC  INE
#
#          INE14
1      1  H1    18      1.00800    0.24800  0  4    2    3    4    5
          2    6    7
2      1  H2    18      1.00800    0.24800  0  3    3    4    5
          2    6    7
3      1  N     7      14.00670   -0.12900  0  4    4    5    6    7
          2    8    9
4      1  H3    18      1.00800    0.24800  0  1    5
          2    6    7
5      1  CA    12     13.01900    0.12700  1  4    6    7    8    9
          2   10   13
6      1  CB    14     15.03500    0.00000  1  1    7
          2    8    9
7      1  C     11     12.01100    0.38000  0  4    8    9   10   13
          3   11   12   14
8      1  O     1     15.99940   -0.38000  1  1    9
          2   10   13
9      2  N     5     14.00670    0.00000  1  5   10   11   12   13   14
          2   15   16
10     2  CA    12     13.01900    0.00000  0  6   11   12   13   14   15   16
          2   17   18
11     2  CB    13     14.02700    0.00000  1  3   12   13   14
          2   15   16
12     2  CG    13     14.02700    0.00000  0  1   13
          1   14
13     2  CD    13     14.02700    0.00000  1  0
          1   14
14     2  C     11     12.01100    0.38000  0  4   15   16   17   18
          2   19   23
15     2  O     1     15.99940   -0.38000  1  1   16
          2   17   18
16     3  N     5     14.00670   -0.28000  0  4   17   18   19   23
          4   20   22   24   25
17     3  H     18     1.00800    0.28000  1  1   18
          2   19   23
18     3  CA    12     13.01900    0.00000  1  6   19   20   22   23   24   25
          3   21   26   27
19     3  CB    12     13.01900    0.15000  0  4   20   21   22   23
          2   24   25
20     3  OG1   3     15.99940   -0.54800  0  2   21   22
          1   23
21     3  HG1   18     1.00800    0.39800  1  0
          1   22
22     3  CG2   14     15.03500    0.00000  1  0
          1   23
23     3  C     11     12.01100    0.38000  0  4   24   25   26   27
          2   28   29
24     3  O     1     15.99940   -0.38000  1  1   25
          2   26   27
25     4  N     5     14.00670   -0.28000  0  4   26   27   28   29

```





5130	538	NA	34	22.98980	1.00000	1	0		
							0		
5131	539	NA	34	22.98980	1.00000	1	0		
							0		
5132	540	NA	34	22.98980	1.00000	1	0		
							0		
5133	541	NA	34	22.98980	1.00000	1	0		
							0		
5134	542	NA	34	22.98980	1.00000	1	0		
							0		
5135	543	NA	34	22.98980	1.00000	1	0		
							0		
5136	544	NA	34	22.98980	1.00000	1	0		
							0		
5137	545	NA	34	22.98980	1.00000	1	0		
							0		
5138	546	NA	34	22.98980	1.00000	1	0		
							0		
5139	547	NA	34	22.98980	1.00000	1	0		
							0		
5140	548	NA	34	22.98980	1.00000	1	0		
							0		
5141	549	NA	34	22.98980	1.00000	1	0		
							0		
5142	550	NA	34	22.98980	1.00000	1	0		
							0		
5143	551	NA	34	22.98980	1.00000	1	0		
							0		
5144	552	OW	4	15.99940	-0.82000	0	2	5145	5146
							0		
5145	552	HW1	18	1.00800	0.41000	0	1	5146	
							0		
5146	552	HW2	18	1.00800	0.41000	1	0		
							0		
5147	553	OW	4	15.99940	-0.82000	0	2	5148	5149
							0		
5148	553	HW1	18	1.00800	0.41000	0	1	5149	
							0		
5149	553	HW2	18	1.00800	0.41000	1	0		
							0		
5150	554	OW	4	15.99940	-0.82000	0	2	5151	5152
							0		
5151	554	HW1	18	1.00800	0.41000	0	1	5152	
							0		
5152	554	HW2	18	1.00800	0.41000	1	0		
							0		
.									
.									
.									
5867	793	OW	4	15.99940	-0.82000	0	2	5868	5869
							0		
5868	793	HW1	18	1.00800	0.41000	0	1	5869	
							0		
5869	793	HW2	18	1.00800	0.41000	1	0		
							0		
5870	794	OW	4	15.99940	-0.82000	0	2	5871	5872
							0		
5871	794	HW1	18	1.00800	0.41000	0	1	5872	
							0		
5872	794	HW2	18	1.00800	0.41000	1	0		
							0		
5873	795	OW	4	15.99940	-0.82000	0	2	5874	5875
							0		
5874	795	HW1	18	1.00800	0.41000	0	1	5875	
							0		
5875	795	HW2	18	1.00800	0.41000	1	0		
							0		

END  
BONDTYPE  
# NBTY: number of covalent bond types

```

47
# CB: force constant
# B0: bond length at minimum energy
#           CB           B0
0.1570000E+08      0.1000000
0.1870000E+08      0.1000000
0.1230000E+08      0.1090000
0.1660000E+08      0.1230000
0.1340000E+08      0.1250000
0.1200000E+08      0.1320000
0.8870000E+07      0.1330000
0.1060000E+08      0.1330000
0.1180000E+08      0.1330000
0.1050000E+08      0.1340000
#           10
.
.
#           40
0.8710000E+07      0.1632990
0.2680000E+07      0.2338390
0.2980000E+07      0.2902830
0.2390000E+07      0.2804120
0.2190000E+07      0.2929930
0.3970000E+07      0.1988420
0.3040000E+07      0.2874070
END
BONDH
# NBONH: number of bonds involving H atoms in solute
1836
# IBH, JBH: atom sequence numbers of atoms forming a bond
# ICBH: bond type code
# IBH  JBH  ICBH
   1    3    2
   2    3    2
   3    4    2
  16   17    2
  20   21    1
  25   26    2
  31   32    2
  35   36    1
  40   41    2
  49   50    2
#           10
.
.
#           1830
5870 5871  35
5870 5872  35
5871 5872  41
5873 5874  35
5873 5875  35
5874 5875  41
END
BOND
# NBON: number of bonds NOT involving H atoms in solute
4120
# IB, JB: atom sequence numbers of atoms forming a bond
# ICB: bond type code
# IB  JB  ICB
   3    5  20
   5    7  26
   7    8   4
   7    9   9
   5    6  26
   9   10  20
  10   14  26
  14   15   4
  14   16   9

```

```

  10  11  26
#      10
.
.
#      4110
5108 5112  15
5110 5114  15
5112 5114  15
5118 5120  20
5120 5124  26
5124 5125   5
5124 5126   5
5120 5121  26
5121 5122  26
5121 5123  26
#      4120
END
BONDANGLETYPE
# NTTY: number of bond angle types
  46
# CT: force constant
# T0: bond angle at minimum energy in degrees
#      CT      T0
0.4200000E+03   90.0000000
0.4050000E+03   96.0000000
0.4750000E+03  100.0000000
0.4200000E+03  103.0000000
0.4900000E+03  104.0000000
0.4650000E+03  108.0000000
0.2850000E+03  109.5000000
0.3200000E+03  109.5000000
0.3800000E+03  109.5000000
0.4250000E+03  109.5000000
#      10
.
.
#      40
0.4840000E+03  107.5699997
0.6320000E+03  111.3000031
0.4690000E+03   97.4000015
0.5030000E+03  106.7500000
0.4430000E+03  108.5299988
0.6180000E+03  109.5000000
END
BONDANGLEH
# NTHEH: number of bond angles involving H atoms in solute
 2030
# ITH, JTH, KTH: atom sequence numbers
#   of atoms forming a bond angle in solute
# ICTH: bond angle type code
# ITH  JTH  KTH  ICTH
   1    3    2    9
   1    3    4    9
   1    3    5   10
   2    3    4    9
   2    3    5   10
   4    3    5   10
  14   16   17   31
  17   16   18   17
  19   20   21   11
  23   25   26   31
#      10
.
.
#      2020
5105 5108 5109  24
5109 5108 5112  24
```



```
5106 5110 5111 24
5111 5110 5114 24
5108 5112 5113 24
5113 5112 5114 24
5110 5114 5115 24
5112 5114 5115 24
5116 5118 5119 31
5119 5118 5120 17
# 2030
END
BONDANGLE
# NTHE: number of bond angles NOT
# involving H atoms in solute
5607
# IT, JT, KT: atom sequence numbers of atoms
# forming a bond angle
# ICT: bond angle type code
# IT JT KT ICT
# 3 5 7 12
# 5 7 9 18
# 5 7 8 29
# 8 7 9 32
# 3 5 6 12
# 7 5 6 12
# 7 9 10 30
# 9 10 14 12
# 10 14 16 18
# 10 14 15 29
# 10
.
.
.
# 5600
5120 5124 5125 21
5125 5124 5126 37
5118 5120 5121 12
5124 5120 5121 12
5120 5121 5122 14
5120 5121 5123 14
5122 5121 5123 14
END
IMPDIHEDRALTYPE
# NQTY: number of improper dihedrals
3
# CQ: force constant of improper dihedral per degrees square
# Q0: improper dihedral angle at minimum energy in degrees
# CQ Q0
# 0.5100000E-01 0.0000000
# 0.1020000E+00 35.2643890
# 0.2040000E+00 0.0000000
END
IMPDIHEDRALH
# NQHIH: number of improper dihedrals
# involving H atoms in the solute
863
# IQH,JQH,KQH,LQH: atom sequence numbers
# of atoms forming an improper dihedral
# ICQH: improper dihedral type code
# IQH JQH KQH LQH ICQH
# 16 14 18 17 1
# 25 23 27 26 1
# 31 29 33 32 1
# 40 38 42 41 1
# 49 47 51 50 1
# 55 53 57 56 1
# 61 62 63 59 1
# 66 64 68 67 1
# 71 69 73 72 1
# 80 78 82 81 1
# 10
```

```

.
.
#
#           860
5112 5114 5108 5113    1
5114 5110 5112 5115    1
5118 5116 5120 5119    1
END
IMPDIHEDRAL
# NQHI: number of improper dihedrals NOT
#   involving H atoms in solute
1775
# IQ,JQ,KQ,LQ: atom sequence numbers of atoms
#   forming an improper dihedral
# ICQ: improper dihedral type code
# IQ  JQ  KQ  LQ  ICQ
#   7   5   9   8   1
#   5   3   7   6   2
#   9   7  10  13   1
#  14  10  16  15   1
#  10   9  14  11   2
#  23  18  25  24   1
#  18  16  23  19   2
#  19  20  22  18   2
#  29  27  31  30   1
#  27  25  29  28   2
#           10
.
.
#           1770
5106 5110 5114 5112    1
5108 5112 5114 5110    1
5124 5120 5126 5125    1
5120 5118 5124 5121    2
5121 5123 5122 5120    2
END
DIHEDRALTYPE
# NPTY: number of dihedral types
21
# CP: force constant
# PD: cosine of the phase shift
# NP: multiplicity
#           CP           PD    NP
#   5.86000  -1.00000    2
#   7.11000  -1.00000    2
#  16.70000  -1.00000    2
#  33.50000  -1.00000    2
#  41.80000  -1.00000    2
#   0.00000   1.00000    2
#   0.41800   1.00000    2
#   2.09000   1.00000    2
#   3.14000   1.00000    2
#  16.70000   1.00000    2
#           10
#   1.05000   1.00000    3
#   1.26000   1.00000    3
#   2.93000   1.00000    3
#   3.77000   1.00000    3
#   4.18000   1.00000    3
#   5.44000   1.00000    3
#   5.86000   1.00000    3
#   0.00000   1.00000    4
#   1.00000  -1.00000    6
#   1.00000   1.00000    6
#           20
#   3.77000   1.00000    6
END
DIHEDRALH
# NPHIH: number of dihedrals involving H atoms in solute

```

```

199
# IPH, JPH, KPH, LPH: atom sequence numbers
#   of atoms forming a dihedral
# ICPH: dihedral type code
# IPH  JPH  KPH  LPH  ICPH
#   1   3   5   7   14
#  18  19  20  21  12
#  33  34  35  36  12
#  58  59  61  62   4
#  82  83  84  85  12
# 100 101 102 103  12
# 124 125 127 128   4
# 159 160 162 163   4
# 293 294 296 297   4
# 316 318 319 320   4
#      10
.
.
#      190
4902 4903 4904 4905  14
4922 4923 4925 4926   4
4953 4955 4956 4957   4
4953 4955 4959 4960   4
4966 4967 4968 4969  12
4993 4997 4998 4999   2
5045 5046 5047 5048  12
5054 5055 5057 5058   4
5078 5079 5080 5081  12
END
DIHEDRAL
# NPHI: number of dihedrals NOT involving H atoms in solute
2546
# IP, JP, KP, LP: atom sequence numbers
#   of atoms forming a dihedral
# ICP: dihedral type code
# IP  JP  KP  LP  ICP
#   3   5   7   9  20
#   5   7   9  10   4
#   7   9  10  14  19
#   9  10  14  16  20
#   9  10  11  12  17
#  10  11  12  13  17
#  11  12  13   9  17
#  12  13   9  10  19
#  10  14  16  18   4
#  14  16  18  23  19
#      10
.
.
#      2540
5101 5103 5104 5105  17
5103 5104 5105 5106  20
5103 5116 5118 5120   4
5116 5118 5120 5124  19
5118 5120 5124 5126  20
5118 5120 5121 5122  17
END
LJPARAMETERS
# NRATT2: number of LJ interaction types = NRATT*(NRATT+1)/2
946
# IAC,JAC: integer (van der Waals) atom type code
# C12: r**(-12) term in nonbonded interactions
#   C6: r**(-6) term in nonbonded interactions
# CS12: r**(-12) term in 1-4 nonbonded interactions
#   CS6: r**(-6) term in 1-4 nonbonded interactions
# IAC  JAC      C12      C6      CS12      CS6
#   1   1  0.7414932E-06  0.2261953E-02  0.7414932E-06  0.2261953E-02
#

```

```
1 2 0.7414932E-06 0.2261953E-02 0.7414932E-06 0.2261953E-02
2 2 0.7414932E-06 0.2261953E-02 0.7414932E-06 0.2261953E-02
#
1 3 0.1380375E-05 0.2261953E-02 0.9687375E-06 0.2261953E-02
2 3 0.2258907E-05 0.2261953E-02 0.9687375E-06 0.2261953E-02
3 3 0.1505529E-05 0.2261953E-02 0.1265625E-05 0.2261953E-02
#
1 4 0.1825875E-05 0.2433170E-02 0.1329538E-05 0.2433170E-02
2 4 0.2987943E-05 0.2433170E-02 0.1329538E-05 0.2433170E-02
3 4 0.1991421E-05 0.2433170E-02 0.1737000E-05 0.2433170E-02
4 4 0.2634129E-05 0.2617346E-02 0.2383936E-05 0.2617346E-02
#
1 5 0.2185875E-05 0.2347562E-02 0.1120291E-05 0.2347562E-02
2 5 0.3577063E-05 0.2347562E-02 0.1120291E-05 0.2347562E-02
3 5 0.2384061E-05 0.2347562E-02 0.1463625E-05 0.2347562E-02
4 5 0.3153489E-05 0.2525258E-02 0.2008744E-05 0.2525258E-02
5 5 0.1692601E-05 0.2436409E-02 0.1692601E-05 0.2436409E-02
#
.
.
.
#
1 43 0.3076882E-05 0.4147280E-02 0.3076882E-05 0.4147280E-02
2 43 0.3076882E-05 0.4147280E-02 0.3076882E-05 0.4147280E-02
3 43 0.4019850E-05 0.4147280E-02 0.4019850E-05 0.4147280E-02
4 43 0.5517021E-05 0.4461203E-02 0.5517021E-05 0.4461203E-02
5 43 0.4648733E-05 0.4304241E-02 0.4648733E-05 0.4304241E-02
6 43 0.4648733E-05 0.4304241E-02 0.4648733E-05 0.4304241E-02
7 43 0.4648733E-05 0.4304241E-02 0.4648733E-05 0.4304241E-02
8 43 0.4648733E-05 0.4304241E-02 0.4648733E-05 0.4304241E-02
9 43 0.4648733E-05 0.4304241E-02 0.4648733E-05 0.4304241E-02
10 43 0.4648733E-05 0.4304241E-02 0.4648733E-05 0.4304241E-02
11 43 0.6563968E-05 0.4218784E-02 0.6563968E-05 0.4218784E-02
12 43 0.1205240E-04 0.5361117E-02 0.6906996E-05 0.4705366E-02
13 43 0.1814114E-04 0.7350172E-02 0.9529725E-05 0.5993324E-02
14 43 0.2070312E-04 0.8683476E-02 0.1240972E-04 0.7218499E-02
15 43 0.2094610E-04 0.1001067E-01 0.2094610E-04 0.1001067E-01
16 43 0.1389260E-04 0.6474674E-02 0.1031226E-04 0.6483394E-02
17 43 0.4395036E-06 0.8022492E-03 0.4395036E-06 0.8022492E-03
18 43 0.0000000E+00 0.0000000E+00 0.0000000E+00 0.0000000E+00
19 43 0.0000000E+00 0.0000000E+00 0.0000000E+00 0.0000000E+00
20 43 0.1292069E-04 0.8713123E-02 0.1292069E-04 0.8713123E-02
21 43 0.2558054E-06 0.1783260E-02 0.2558054E-06 0.1783260E-02
22 43 0.2558054E-06 0.1783260E-02 0.2558054E-06 0.1783260E-02
23 43 0.0000000E+00 0.0000000E+00 0.0000000E+00 0.0000000E+00
24 43 0.3471721E-06 0.1783260E-02 0.3471721E-06 0.1783260E-02
25 43 0.2086034E-06 0.7045841E-03 0.2086034E-06 0.7045841E-03
26 43 0.2521607E-05 0.2764272E-02 0.2521607E-05 0.2764272E-02
27 43 0.1683334E-04 0.1058620E-01 0.1683334E-04 0.1058620E-01
28 43 0.1121270E-04 0.6901959E-02 0.1121270E-04 0.6901959E-02
29 43 0.3116545E-05 0.2992738E-02 0.3116545E-05 0.2992738E-02
30 43 0.1397479E-04 0.8163758E-02 0.1397479E-04 0.8163758E-02
31 43 0.2891434E-04 0.2994482E-02 0.2891434E-04 0.2994482E-02
32 43 0.1631702E-04 0.8215206E-02 0.1631702E-04 0.8215206E-02
33 43 0.4019850E-05 0.4147280E-02 0.4019850E-05 0.4147280E-02
34 43 0.5181140E-06 0.7402492E-03 0.5181140E-06 0.7402492E-03
35 43 0.3694689E-04 0.1024612E-01 0.3694689E-04 0.1024612E-01
36 43 0.7203571E-05 0.4472713E-02 0.7203571E-05 0.4472713E-02
37 43 0.1325693E-04 0.7947586E-02 0.1325693E-04 0.7947586E-02
38 43 0.2343090E-06 0.5354141E-03 0.2343090E-06 0.5354141E-03
39 43 0.1656750E-04 0.8961647E-02 0.1656750E-04 0.8961647E-02
40 43 0.1666719E-04 0.8296216E-02 0.1666719E-04 0.8296216E-02
41 43 0.3097464E-05 0.4155302E-02 0.3097464E-05 0.4155302E-02
42 43 0.9850598E-05 0.4472713E-02 0.9850598E-05 0.4472713E-02
43 43 0.1276776E-04 0.7604014E-02 0.1276776E-04 0.7604014E-02
#
END
SOLVENTATOM
# NRAM: number of atoms per solvent molecule
5
```

```
#      I: solvent atom sequence number
# IACS: integer (van der Waals) atom type code
# ANMS: atom name of solvent atom
# MASS: mass of solvent atom
# CGS: charge of solvent atom
#      I  ANMS  IACS      MASS      CGS
#      1 CCh1  36   12.01100   0.17900
#      2 HCh1  38    1.00800   0.08200
#      3 CLCh1 37   35.45300  -0.08700
#      4 CLCh2 37   35.45300  -0.08700
#      5 CLCh3 37   35.45300  -0.08700
END
SOLVENTCONSTR
# NCONS: number of constraints
#      9
# ICONS, JCONS: atom sequence numbers forming constraint
#      CONS constraint length
# ICONS JCONS      CONS
#      1      3      0.1758000
#      1      4      0.1758000
#      1      5      0.1758000
#      2      3      0.2338390
#      2      4      0.2338390
#      2      5      0.2338390
#      3      4      0.2902830
#      3      5      0.2902830
#      4      5      0.2902830
END
# end of topology file
```

# Lebenslauf

## Persönliches:

Name: Ulrich Kahlow  
Geburtsdatum: 28.09.1967  
Geburtsort: München  
Nationalität: deutsch

## Schulbildung:

09.1974 - 07.1978 Erich-Kästner-Grundschule in Ratingen  
09.1978 - 07.1984 Dietrich-Bonhöffer-Schule in Ratingen  
09.1984 - 07.1987 Siebold-Gymnasium in Würzburg  
Schulabschluß 1987 Abitur

## Wehrdienst:

07.1987 - 08.1987 Grundausbildung in Hammelburg  
08.1987 - 09.1988 12. Stabskompanie in Veitshöchheim

## Wissenschaftliche Ausbildung:

10.1988 - 02.1989 Berufsakademie Mosbach  
1 Semester Maschinenbau  
10.1989 - 12.1989 Technische Fachhochschule in Berlin im Fachbereich Biotechnologie  
12.1989 - 03.1991 Technische Universität Berlin im Fachbereich Biotechnologie  
04.1991 - 03.1996 Technische Universität Carolo-Wilhelmina zu Braunschweig im Fachbereich Biotechnologie  
09.1994 - 09.1995 Diplomarbeit in Tokyo, Japan, mit dem Titel:  
"Examination of electrochemical properties of a pseudoazurin from *Alcaligenes faecalis* using an artificial, light switchable electrondonator"  
Universitätsabschluß Diplom der Biotechnologie an der Technische Universität Carolo-Wilhelmina zu Braunschweig